Characterization of Bud14 Function in Yeast Centrosome Size Maintenance

by

Sevilay Münire GİRGİN

A Dissertation Submitted to the
Graduate School of Sciences and Engineering
in Partial Fulfillment of the Requirements for
the Degree of
Master of Science
in
Molecular Biology and Genetics

KOÇ
ÜNİVERSİTESİ

September, 2023

Characterization of Bud14 Function in Yeast Centrosome Size Maintenance

Koç University

Graduate School of Sciences and Engineering

This is to certify that I have examined this copy of a master's thesis by

Sevilay Münire GİRGİN

and have found that it is complete and satisfactory in all respects,
and that any and all revisions required by the final
examining committee have been made.

Committee Members:

Asst. Prof. Dr. Ayşe Koca Çaydaşı (Advisor-Koç University)

Prof. Dr. Tamer Önder (Koç University)

Prof. Dr. Ayşe Elif Erson Bensan (Middle East Technical University)

Date: 15/09/2023

To my dear grandmother Naciye Sevim DAĞLI

ABSTRACT

The cell cycle is an extensively conserved process that governs DNA duplication and chromosome segregation. Eukaryotic cells distribute their chromosomes into daughter cells by the mitotic spindle, formed between spindle poles named centrosome. The Spindle Pole Body (SPB) is a functional equivalent of mammalian centrosome in *S. cerevisiae*. SPB consists of distinct structural layers and is embedded into a nuclear envelope throughout its life cycle, thereby nucleating cytoplasmic and nuclear microtubules. The yeast centrosome size changes throughout the cell cycle. In addition, cell cycle arrest conditions have various effects on SPB size. Recent studies illustrated that SPB undergoes growth and exchange cycles, thus portraying a dynamic yeast centrosome to an extent that was not anticipated previously.

In this study, we have identified a novel role for Bud14 in SPB size maintenance. Through microscopy-based quantification of relative and exact amounts of SPB structural proteins, we showed that cells lacking Bud14 had more Spc72, Nud1, Spc97, Spc42, Spc29, and Spc110 at their SPBs. Bud14 is also a regulatory subunit of the Protein Phosphatase 1 Glc7. We indicated that Bud14 function in Spc29, Spc97, Spc110, and Spc42 size maintenance depends on its interaction with Glc7.

We elucidated Spc110 and Spc72 dynamics by measuring their molecule numbers throughout the cell cycle. This dynamic nature might be integral to the mitotic spindle formation and presents a mechanism for reacting to changes in cellular conditions.

Furthermore, this research established that functional Cdc14 phosphatase is required for Spc72 and Spc110 size maintenance in cells lacking Bud14. Forceful localization of Cdc28 to SPB outer plaque disclosed that phosphorylation of SPB structural proteins causes their enlargement at the SPB. This research determined that Bud14 regulates SPB size primarily via its interaction with Glc7. Cdc14 also functions in the SPB size maintenance network.

ÖZKAYNAKÇA

Hücre döngüsü, DNA çoğalmasını ve kromozom ayrılmasını yöneten, kapsamlı bir şekilde korunmuş bir süreçtir. Ökaryotik hücreler, kromozomlarını sentrozom adı verilen mil kutupları arasında oluşan mitotik iğ aracılığıyla yavru hücrelere dağıtır. Mil Kutup Gövdesi (SPB), S. cerevisiae'deki memeli sentrozomunun işlevsel bir eşdeğeridir. SPB, farklı yapısal katmanlardan oluşur ve yaşam döngüsü boyunca nükleer bir zarfın içine gömülür, böylece sitoplazmik ve nükleer mikrotübülleri çekirdeklendirir. Maya sentrozomunun boyutu hücre döngüsü boyunca değişir. Ayrıca hücre döngüsü durdurma koşullarının SPB boyutu üzerinde çeşitli etkileri vardır. Son çalışmalar, SPB'nin büyüme ve değişim döngülerinden geçtiğini, dolayısıyla daha önce beklenmeyen bir ölçüde dinamik bir maya sentrozomunu tasvir ettiğini gösterdi.

Bu çalışmada Bud14'ün SPB boyutunun korunmasında yeni bir rolünü belirledik. SPB yapısal proteinlerinin göreceli ve kesin miktarlarının mikroskopi bazlı miktarının belirlenmesi yoluyla, Bud14 içermeyen hücrelerin SPB'lerinde daha fazla Spc72, Nud1, Spc97, Spc42, Spc29 ve Spc110'a sahip olduğunu gösterdik. Bud14 aynı zamanda Protein Fosfataz 1 Glc7'nin düzenleyici bir alt birimidir. Spc29, Spc97, Spc110 ve Spc42 boyut kontrolünde Bud14 fonksiyonunun Glc7 ile etkileşimine bağlı olduğunu belirttik.

Hücre döngüsü boyunca molekül sayılarını ölçerek Spc110 ve Spc72 dinamiklerini açıkladık. Bu dinamik doğa, mitotik iğ oluşumunun ayrılmaz bir parçası olabilir ve hücresel koşullardaki değişikliklere tepki vermek için bir mekanizma sunar.

Ayrıca bu araştırma, Bud14 içermeyen hücrelerde Spc72 ve Spc110 boyutunun korunması için fonksiyonel Cdc14 fosfatazın gerekli olduğunu ortaya koydu. Cdc28'in SPB dış plakasına kuvvetli lokalizasyonu, SPB yapısal proteinlerinin fosforilasyonunun bunların SPB'de genişlemesine neden olduğunu ortaya çıkardı. Bu araştırma Bud14'ün SPB boyutunu öncelikle Glc7 ile etkileşimi yoluyla düzenlediğini belirledi. Cdc14 ayrıca SPB boyutu kontrol ağında çalışır (Sonuç 3.8 ve 3.9).

ACKNOWLEDGEMENTS

I would like to thank my advisor, Dr. Ayşe Koca Çaydaşı, who made possible this research with her supervision. She is always available for her students, even during nights and vacations. Knowing that I could reach my supervisor was great motivation for me. I admire her intelligence and scientific integrity. She always asks great questions that you are surprised and amazed by them. She has an excellent eye; she can catch misaligned pixels in Photoshop. In addition, she is one of the most hardworking people I have met.

I also thank Deniz Çaydaşı because she is such a bundle of joy. Playing with her and getting a good night hug were highlights of last New Year's Eve dinner. Hearing about Deniz's kindergarten adventures from her is always a pleasure.

I am grateful for the current and former AKC Lab members Mariam, Şeyma, Cansu, and İdil. Each one of you taught me laboratory techniques with patience. We shared the same frustration about the lost mCherry-Tub signal. You listened to me when I complained about my failed time-lapse experiments. I always enjoyed having tea/coffee breaks in the kitchen. Each of you is very bright and kind, and I am lucky to meet you. I also thank Ata Mert for conducting many transformations for me while enduring my so-called mobbing.

I present my deepest gratitude to my grandmother. She never had a chance to learn reading and writing. It still breaks my heart that she could not have everyday joys like reading a fine book. Your whole presence and stories made up a home for me, independent from any land. Your death was the most challenging thing I have ever encountered. I finally understood what you told me çiçeğim. I still miss you every day. I would choose you to be my grandmother in every parallel universe. I will cherish you till the last days of my life.

I would like to thank my mother, Narin Dağlı. You are the strength that resides at the core of my existence. I could not be here if I had not had a mother like you. You taught me to be persistent and hardworking by your behaviors. You taught me to be compassionate about other people. Your acts have always been a great example of honesty and integrity. You made me start kindergarten at the age of 4, and thanks to you, I have been educated for 22 years. Lastly, thank you for listening to 5-year-old me and gifting me with my brother.

I thank my brother Ceyhun Utku. You are the rock of my life. You are the best gift that my family ever gave me. Your presence always heales my soul. Nothing can break my heart like seeing you unhappy. I would choose to be your big sister in every lifetime. Your importance to me is incomparable with anything. I hope I will always make you proud, baby brother. Your health and success are the great wishes of my life.

I also thank my father, Fatih Girgin. He always trusts me to make the right choice and behave. My father took me to the park and fed rabbits with grasses, which is my oldest memory. He used to cool down my pillow and blanket cause I liked to sleep on cold bed when I was a child. I love my father deeply. I know he loves his kids more than anything, which helps me continue even in the worst days.

Elifsu, İlkkanım, I cannot thank you enough. You have seen my worst but still stand beside me. We had many absurd things that made us think that the writer was really lazy. We even adopted a dog together and decided to throw a house party on the same day. Your commedarie was the best flower I grew during my master years. We had great nights imagining and talking about insane scenarios. By the way, my movie idea will be trendy. We experienced a snow blizzer together and almost got hit by a car. Even though you choose the wrong horse sometimes, your opinions are always valuable to me. Your friendship will hold a special place in my heart whatever happens years after now. Nothing can change all the important things you have done for me.

I am also very grateful for my Mona Lisa, Esra Çevikbaş. She understands me and counts on me even in times I doubt myself. It is always so fun being with her. We share a deep enthusiasm for wine and for partying so hard that it made Elifsu almost cry to go back home. I had one of my best birthdays with you. No, it was not because we were in Belgium. It was awesome cause you were there and genuinely celebrated my existence. Together, we laughed so hard that we ended up in tears. I can trust you because you have a very kind heart and a beautiful soul.

Lastly, I thank myself for carrying on even after the long and dreadful nights. I am grateful for each lesson I learned in the last two years because they will illuminate my way. And I want to conclude this part with great lines of Birhan Keskin: “Buraya, bir inanç bir inat koydum. Tut ki unuttun, tekrar bak, o inat neyse, sen osun. Buraya umutlu günler koydum. Şimdilik uzak gibi görünüyor, ama kimbilir, birazdan uzanıp dokunursun.”

TABLE OF CONTENTS

LIST OF TABLES

LIST OF FIGURES

ABBREVIATIONS

CDK: Cyclin Dependent Kinase

MEN: Mitotic Exit Network

SPOC: Spindle Position Checkpoint

SAC: Spindle Assembly Checkpoint

MT: Microtubule

MTOC: Microtubule Organizing Center

SPB: Spindle Pole Body

SPOC: Spindle Position Checkpoint

FI: Fluorescence Intensity

SAC: Spindle Assembly Checkpoint

CIN: Chromosome Instability

OP: Outer Plaque

IP: Inner Plaque

CP: Central Plaque

IL: Inner Layer

HB: Half Bridge

EM: Electron Microscopy

PP1: Protein Phosphatase 1

TCA: Trichlorocacetic acid

APS: Ammonium Persulfate

PFA: Paraformaldehyde

Chapter 1: INTRODUCTION

1.1 Saccharomyces cerevisiae as A Model Organism in Cell Biology Research

Yeast is an extensively utilized model organism in applied and fundamental research (Mager & Winderickx, 2005). *Saccharomyces cerevisiae* is commonly studied to understand molecular and cellular biology of eukaryotes. This model organism's division and growth can be maintained effectively via controlling environmental conditions. In addition, the budding yeast's whole genome has been completely sequenced; thus, it is genetically well-defined organism. Its genome can be efficiently manipulated by modifications like gene marking, mutation, and gene disruption (Mager & Winderickx, 2005). Due to its many advantages, the yeast has been a popular choice for medicinal research. For instance, research on *S. cerevisiae* greatly contributed to our knowledge about cell cycle, thus, elucidated cancer related disturbances in the cells. Recent studies depicted regulator pathway of apoptosis in the yeast. Therefore, *S. cerevisiae* has been employed to discover novel networks as well as further elucidate shared pathways with mammalian cells (Mager & Winderickx, 2005). Yeast has various bacterial like features such as growth simplicity and rapidity. In addition, being suitable for genetic and biochemical manipulations allow application of diverse molecular genetic technologies in the yeast research. The success of *S. cerevisiae* as a model organism is due to extensive conservation of several cellular processes between human and yeast like heat shock, protein folding, protein secretion, and autophagy (Nielsen, 2019). High degree conservation is also present in the genome level. 47% of 414 fundamental yeast genes can be recovered by its human orthologs. Furthermore, several signal transduction modes are also conserved between human and yeast. Therefore, diverse array of regulation hierarchies, protein-protein interactions and signal cross-talks are also conserved. For instance, Sirtuin2 that is crucial metabolic state sensor is first defined in the yeast. Conservation of many regulators and their effectors from yeast to human renders yeast research indispensable to elucidate essential cell biology principles that can be utilizable in human pathology studies (Nielsen, 2019).

1.2 Life Cycle of Budding Yeast

S. cerevisiae grows by producing an ellipsoidal daughter cell from a mother cell. This process is named as a budding (Trans et al., 1996)(Herskowitz, 1988). Yeast cells can halt their proliferation mode due to environmental conditions. For instance, if nutrient shortage occurs, cells are arrested at G1 phase where they can continue to survive and resume growth if

conditions favor it. The other parameter that can interfere with proliferation mode is presence of another yeast in proximity which it can mate (Herskowitz, 1988). When cells with different mating type are together, these partners can arrest each other in G1 and undergo cell fusion. Even though *S. cerevisiae* is a unicellular, it can exist in three different cell types: haploid form with a mating type haploid form with mating type and the a/α diploid form (Figure 1.1). Each one of cell types bears crucial and distinctive roles in the life cycle and can undergo mitotic division. Cells with a and α mating type can mate with each other efficiently. Due to nuclear and cellular fusion mating results in a/α diploid cell (Herskowitz, 1988). Mating product with distinctive shape called as zygote and generates daughter diploid cells by budding. The a/α diploid cell is not able to mate with any of a and α cells but can sporulate under nutritional starvation. Sporulation occurs through meiosis, which produces 4 haploid meiotic progenies (spores), encased by a spore coat. All four spores are wrapped up in a sac called the ascus (Herskowitz, 1988). Research displayed that a and α cells generate particular signaling molecules and their receptors systems aid the mating. Mating factor, a secreted peptide, of each haploid type prepares cells for the mating. Since these molecules facilitate communication between organisms, mating factors are termed as pheromones (Herskowitz, 1988). α cells secrete α-factor, length in 13 amino acids, whereas a type cells make a-factor, length in 12 amino acids. The mating factor system synchronizes the cell cycle of the partners, halting their cell cycle progression before DNA synthesis (Herskowitz, 1988). Due to this cell cycle arrest, cells start mating with exactly one chromosome copy; thus ensuring that the progeny will be diploid.

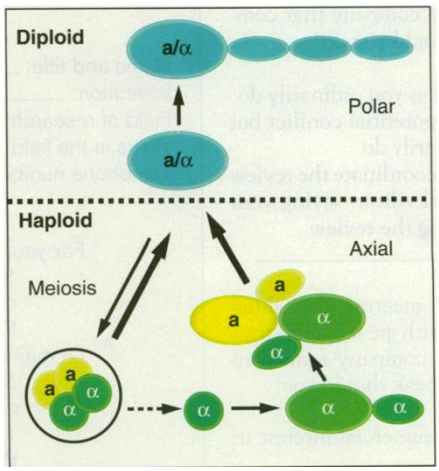

Figure 1.1: Life Cycle of the S. cerevisiae.

The budding yeast life cycle is drawn based on MAT locus they carry (Gimeno & Fink, 1992).

1.3 The Cell Cycle

Eukaryotic cells divide through a process named as the cell cycle. In essence, cell cycle is a collection of events that are responsible for (1) -DNA replication and (2) partitioning of chromosomes to the daughter cells- two crucial steps of the cell cycle that are conserved to all cell cycles with few exceptions (Nurse, 2000). Special mechanisms are required for the precise DNA replication and chromosome partition since chromosomes have low copy number. Cells replicate their DNA in a restricted phase part named as the S phase. First, in yeast, chromatin associated origin recognition complexes (ORCs) were identified. ORCs act like a landing pad for the DNA replication complexes (Bell & Stillman, 1992). Cdc6p/Cdc18p initiator protein loads Mcm proteins onto chromatin to license DNA replication. Licensing mechanisms secure that DNA is only replicated for once in each cell cycle (Diffley, 1996). The pre-replication complex formation in the budding yeast correlates to the origin being in a licensed state. The complex production and maintenance are dependent on the function of the CDC6 gene. CDC6 is fundamental for the DNA replication initiation. Protein levels of Cdc6 are periodic in the cell cycle, as the gene is only expressed in G1anna late mitosis (Diffley, 1996).

Cells partition their chromosomes to the daughter cells in M-phase by the mitotic spindle apparatus (Nurse, 2000). The mitotic spindle is consisted of microtubules which oscillate between shrinking and growing states, dynamic instability process. Microtubular organizing centers (MTOCs) locates at spindle poles to seed micro tubular growth. Kinetochores capture and stabilize microtubules. Microtubular motor proteins and tubulin turnover move chromosomes towards the spindle poles (Boleti et al., 1996). Motor proteins also function in mitotic spindle formation by organizing and bundling microtubules (Boleti et al., 1996).

Chromosomes composed of two sister chromatids become condensed in the beginning of the M-phase. Each chromatid carries a kinetochore at its centromere that capture spindle microtubules. A steady chromosome configuration can be reached when one sister chromatid's kinetochore attached to microtubules of one pole and the other sister chromatid's kinetochore attached to microtubules of the other pole- a states known as bipolar attachment (Nicklas, 1997). Only, when all the chromosomes are bipolarly attached (metaphase), sister chromatids can be separated.

This is an extremely crucial step of mitosis since when this is the only way by which chromosomes can be equally partitioned to opposite cell poles (Uhlmann et al., 1999). At this point, cohesion between sister chromatids is lost, chromatids move apart to spindle poles to make two nuclei. Cytokinesis separates two nuclei (Uhlmann et al., 1999).

The cell cycle is an extremely controlled phenomenon (Nurse, 2000). Cell cycle control systems modulate onset of events like S phase and mitosis and assure that distinct events occur in an exact sequence. The cell cycle can be viewed as a temporally organized sequence of incidences analogous to basic developmental systems.

At various points of the cell cycle, the cell confirms that an earlier event like S phase has been executed properly before carrying on with a later event like mitosis. The checkpoints also govern other situations like blocking mitosis after DNA damage occur until it is repaired, a mechanism that provides faithful genomic transmission.

The spindle checkpoint halts mitosis if the spindle is not formed correctly, or if chromosomes are not correctly oriented and securely attached to the spindle. The spindle checkpoint operates by monitoring proper association of kinetochores and microtubules (Trans et al., 1996). If they are not properly attached, the cohesion of sister chromatids remains and microtubules cannot shorten; thus, sister chromatids do not segregate to the cell poles (Trans et al., 1996).

Checkpoints are fundamental for maintaining genomic stability (Nurse, 2000). Checkpoint failures enable cells to divide when DNA is incompletely replicated or when chromosomes are falsely partitioned compromising genetic fidelity. This is frequently observed in cancer generation proven by the observation that to block S phase upon DNA damage, p53 is needed (Nurse, 2000).

Cyclin dependent kinases (CDKs) consisted of a cyclin subunit and a catalytic protein kinase, function as a the major cell cycle regulator conserved from yeast to mammals (Morgan, 1995). Murray and Hunt defined CDKs as a cell cycle engine proceeding cell through the cell cycle. Different CDKs regulate the S and M phase onsets. CDK activity is modulated by diverse mechanisms like association with CKI inhibitors and cyclin availability (Morgan, 1995).

In metazoans, CDKs function in early G1 to induce E2F-dependent transcription of S phase. CDKs act in late G1 to trigger S Phase start and in G2 to initiate mitosis (Fisher & Nurse, 1996). In budding yeast, CDKs range is highly limited having only one, Cdc28 (see 1.3.1 for detailed explanation).

Other significant regulatory processes for cell cycle progression are transcription and proteolysis (Uhlmann et al., 1999). Proteolysis mediates cyclin levels thereby regulating CDK activity. In addition, proteolysis functions in different cell cycle events like the changes in cohesion of sister-chromatids. Proteolysis also mediates irreversibility of cell cycle transitions (Uhlmann et al., 1999).

1.3.1 Cdc28 as a Single Cdk in The Budding Yeast

In Saccharomyces cerevisiae, Cdc28 (equivalent of Cdk1) mediates the cell cycle through association with various cyclins (Bloom & Cross, 2007). Cyclin specificity of yeast cell cycle engine employs different mechanisms: the degradation of cyclins, transcriptional activation of cyclins, cyclin localization, inhibition of cyclin-Cdk by several Cdk inhibitors. Ubiquitin-mediated proteolysis controls cyclin levels. Cyclins tagged with ubiquitin molecules are send to 26S proteosome for degradation (Bloom & Cross, 2007). In addition, cyclins' specificity varies among different ubiquitin ligases impose another layer of regulation. For instance, Cln1 and Cln2 are ubiquitinylated and degraded by SCF complex. Nonetheless, APC targets other B-type cyclins for degradation (Shirayama et al., 1999). In metaphase, APC^{Cdc20} induce degradation of Clb5 and mitotic B type cyclins. It is proceeded by APC^{Cdh1}completes mitotic B type cyclins' degradation. Cdc28 modulated phosphorylation differentially controls APC^{Cdh1} and APC^{Cdc20}. During the cell cycle, G1 and B type cyclins transcription levels changes. For example, Cln3 transcription peaks in late M-early G1, whereas Cln1 transcription reaches its highest level in G1-S phase (Bloom & Cross, 2007). SBF, heterodimeric transcription factor, controls early expressed cyclins. Clb5 and Clb6 expression is mediated by MBF transcription factor (Schwob & Nasmyth, 1993). Throughout the cell cycle, cyclins localize to various subcellular sites. Cln3, G1 cyclin, is primarily nuclear, whereas Cln2 is mainly cytoplasmic and found in the polarized growth sites (Bloom & Cross, 2007). Different localization patterns of Cln2 and Cln3 enable them to regulate distinct substrates. Clb1-4 mainly reside at nucleus and associate with the SPB. In addition, Clb2 is the only cyclin that localizes to bud neck. Cyclin Dependent Kinase Inhibitors (CKI) can negatively regulate several cyclin-Cdk complexes via binding (Figure 1.2). For instance, CKI Sic1 binding inhibits Clb-Cdc28 complexes in the budding yeast, and therefore help mitotic exit (Verma et al., 1997). Cdc28 inhibition is eminent for other cell cycle events like pheromone mediated cell-cycle arrest and budding. α-Factor binding to its receptor Ste2 induces mitogen-activated protein kinase cascade (MAPK) (Breitkreutz & Tyers, 2002). This cascade leads MAPK Fus3 phosphorylation; thus, regulate Far1, Cdk inhibitor. Fus3 phosphorylated Far1 inhibits Cln2-Cdc28 and Cln3-Cdc28 activity (Figure 3.1). Far1 modulated G1 cyclin-Cdc28 inhibition promotes G1 specific mating-factor arrest (Breitkreutz & Tyers, 2002). G1 cyclin activation is associated with pre-bud site assembly since this complex induce actin polymerization at the bud site. *cln1*Δ and *cln2*Δ are associated with delayed bud emergence (Bloom & Cross, 2007).

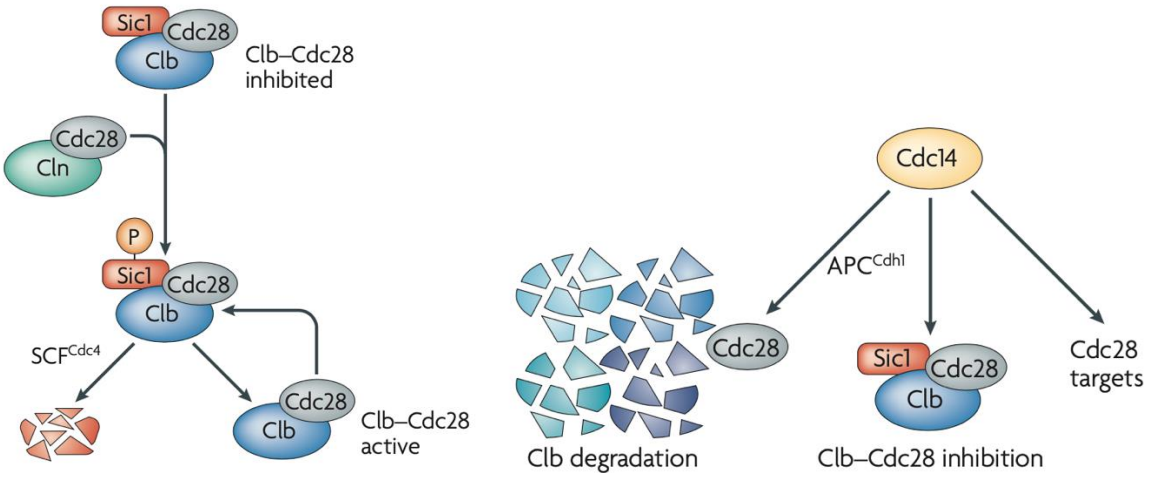

Figure 1.2: Cdc28 inhibition mechanisms in the budding yeast.

In budding yeast, cyclin specificity is achieved via different mechanisms. Left panel depicts how Sic1, Cdk inhibitor, inactivates Clb-Cdc28 complex. Right panel displays how Cdc14 regulates Clb-Cdc28 complex activity. Cdc14 phosphatase exploit ubiquitin mediated cyclin degradation and Cdk1inhibitor Sic1 (Bloom & Cross, 2007).

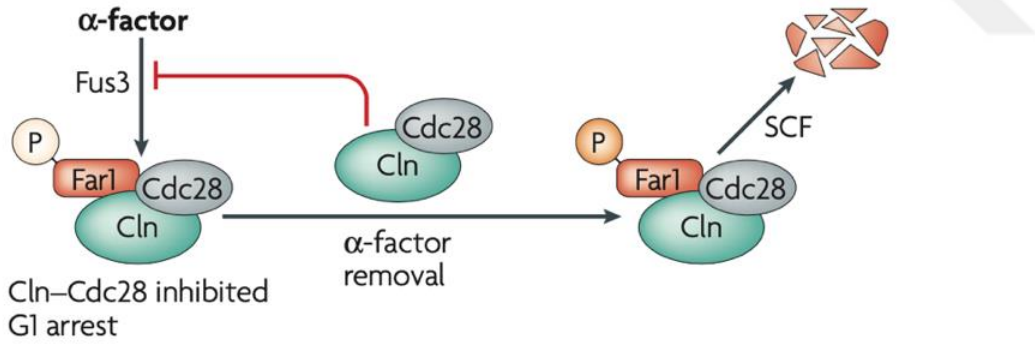

Figure 1.3: α-Factor mediated Cdc28 inhibition.

α-Factor treatment causes yeast cells arrest in G1. The scheme depicts a mode of action on how this pheromone inactivates Cln2-Cdc28 complex (Bloom & Cross, 2007).

1.4 Microtubule Organizing Center in Yeast: Spindle Pole Body

The cell cycle is extensively conserved process that governs chromosome replication and segregation (Chen et al., 2020). In eukaryotic cells, chromosomes are distributed into daughter

cells by the mitotic spindle which is a microtubule network formed in between of two spindle poles named as centrosome in metazoans (Chen et al., 2020). Functional equivalent of mammalian centrosome in Saccharomyces cerevisiae is spindle pole body (SPB) (Greenland et al., 2010). SPB is microtubule organizing center and responsible for chromosome segregation during mitosis and meiosis. SPB of haploid wild-type yeast can nucleate and 2 to 4 pole-to-pole and 16 kinetochore microtubules (Greenland et al., 2010).

1.4.1. Molecular Structure of Spindle Pole Body

SPBs of S. cerevisiae are incorporated into the nuclear envelope throughout its life cycle; thus, SPBs nucleate both cytoplasmic and nuclear microtubules (Jaspersen & Winey, 2004). Due to SPB's location in membrane, its small size and all the involved genes being essential, make SPB study is challenging. Nonetheless, SPB is one of the well characterized MTOC. Electron microscopy (EM) is extensively used to analyze its structure. The yeast centrosome is a cylindrical organelle consists of three plaques of darkly staining material: inner plaque faces nucleoplasm, outer plaque faces the cytoplasm and responsible for cytoplasmic microtubule nucleation while central plaque spans nuclear membrane (Jaspersen & Winey, 2004). Further cryo-EM studies revealed that SPB contains many interconnected layers (Figure 1.4).

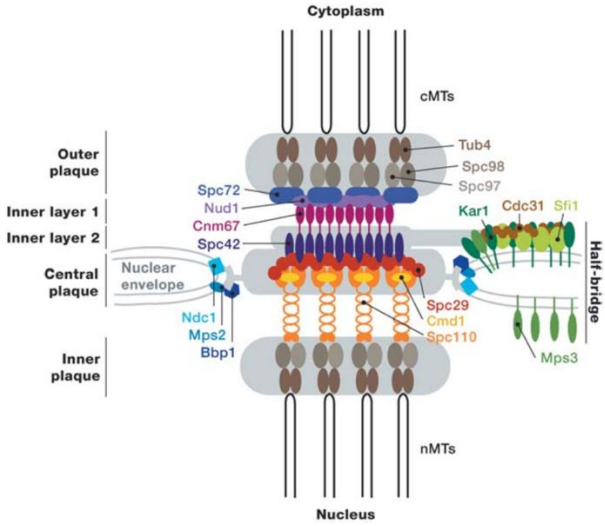

Figure 1.4: Detailed drawing of Spindle Pole Body.

The SPB proteins positions within the organelle are displayed along with cytoplasmic and nuclear and microtubulesp. Detailed explanation of how those proteins interact is stated in the text above. Features of studied SPB proteins by this research are listed in the Table 1.

Studies identified 17 components of mitotic SPB (Table 1.1). SPB component can be defined as a structural protein that makes up spindle pole body (Jaspersen & Winey, 2004). Mutation or deletion of those identified SPB components drive drastic defects in centrosome function and structure. Spc42 is a coiled coil essential protein that forms SPB central plaque. Spc42's N terminus associates with Spc42 and Spc110 which are also coiled coil proteins reside at inner plaque (Jaspersen & Winey, 2004). Spc110's C terminus localizes to CP and it binds to Calmodulin (Cmd1) and Spc29 via unique and partially overlapping binding sites. It has been proposed that Cmd1 regulates Spc110 binding to Spc29. Since Spc29 binds both Spc110 and Spc42, it functions as a linker between two distinct plaque: inner and central. Spc110 N terminus resides in IP and directly binds to Spc98, γ -tubulin binding protein responsible for microtubule nucleation. Spc42' C terminus faces cytoplasm and binds to Cnm67 C terminus. Coiled-coil region of Cnm67 mediates its dimerization and works a spacer between IL1 and IL2. Cnm67's N terminus is attached to OP component Nud1, required for mitotic exit. Spc72, coiled- coil OP component, bind to C terminus of Nud1. N terminus of Spc72 is attached to the γ -tubulin complex. Surprisingly, Cnm67 and Spc72 are not essential for cell viability even though spc72Δ and cnm67Δ cells are frequently multinucleated (Jaspersen & Winey, 2004). In addition, spc72Δ and cnm67Δ cells are heavily defected in microtubule-dependent processes.
Half-bridge (HB) presents site for assembly of new SPB. HB has role in cytoplasmic microtubule nucleation in G1. Despite similar EM appearance of half-bridge' both sides, these sites are not equivalent since the satellite, works as a SPB precursor, forms particularly on the cytoplasmic tip (Jaspersen & Winey, 2004). Mutations in coiled-coil regions of several SPB core proteins causes lethal or temperature-sensitive alleles illuminates significance of coiled-coil domains in SPB structure maintenance.

Table 1.1: Features of studied SPB components are listed.

Protein Name	SPB Localization [b]	Role in SPB Function	Regulation[c]	Deletion	MT Defects[d]	Human Homolog
Nud1	OP, Satellite	MEN Function	Phosphorylation	Lethal	NP, Signaling	Centriolin
Spc72[e]	OP, HB	γ-tubulin binding protein	MCB, Phosphorylation	Slow[f]	NP, K	TACC[g]
Spc42[e]	CP, IL2, Satellite	Structural SPB Core	MCB, Phosphorylation	Lethal	K	
Spc29[e]	CP, Satellite	Structural SPB Core	MCB, Phosphorylation	Lethal		
Spc110[e]	IP	Spacer, γ-tubulin binding protein	MCB, Phosphorylation	Lethal	S, K	Pericentrin
Spc97	γ-tubulin complex	MT Nucleation		Lethal	NP, S, K	TUBGCP 2
Spc98[e]	γ-tubulin complex	MT Nucleation	Phosphorylation	Lethal	NP, S, K	TUBGCP 3
Sfi1	HB	SPB Duplication	Phosphorylation	Lethal	K	HSfi1

[b]OP, outer plaque; IP, inner plaque; CP, central plaque.

[c] MCB, MluI-cell cycle box leading to G1 transcription; P, phosphorylation.

[d] NP, nuclear positioning; S, spindle formation and function; K, karyogamy.

[e]coiled-coil protein structure.

[f]deletion causes MT abnormalities, slow growth, reduced viability, and increased ploidy.

[g]Functional homolog of Spc72 in human.

1.4.2. SPB duplication

The yeast cell couples SPB duplication with cell cycle such that mitotic cells have exactly two poles to form a bipolar spindle (Chen et al., 2020). Centrosome duplication error can drive monopolar or multipolar spindle formation (Chen et al., 2020).

The HF is connected to the central plaque's one site (Rüthnick & Schiebel, 2018). Half-bridge localizes to the top of cytoplasmic and nuclear sites of the NE. during late mitosis, HF doubles its length to grow into the bridge structure (Rüthnick & Schiebel, 2018). In G1, the bridge's distal end assembles the dSPB precursor, the satellite. The satellite is consists of Sfi1, Cdc31 and Spc42 proteins in G1. Upon increased Cdk1 activity, the satellite expands and becomes embedded in the nuclear envelope (Rüthnick & Schiebel, 2018).

SPB duplication final stage is the insertion of duplication plaque into NE (Jaspersen & Winey, 2004). Then Cmd1, Spc110 and γ -tubulin complex assembles onto newly made SPB. Spc110 is not essential for NE insertion however cells without functional Spc110 lacks IP and nuclear microtubules. Yeast preferentially segregate the old SPB into the bud because it is the first one able to nucleate cytoplasmic microtubules (Jaspersen & Winey, 2004). The cytoplasmic microtubule nucleation capacity is important for nuclear positioning and move towards to the bud. Microtubule depolymerization abolish difference between old and new SPB which results in randomized SPB segregation (Jaspersen & Winey, 2004).

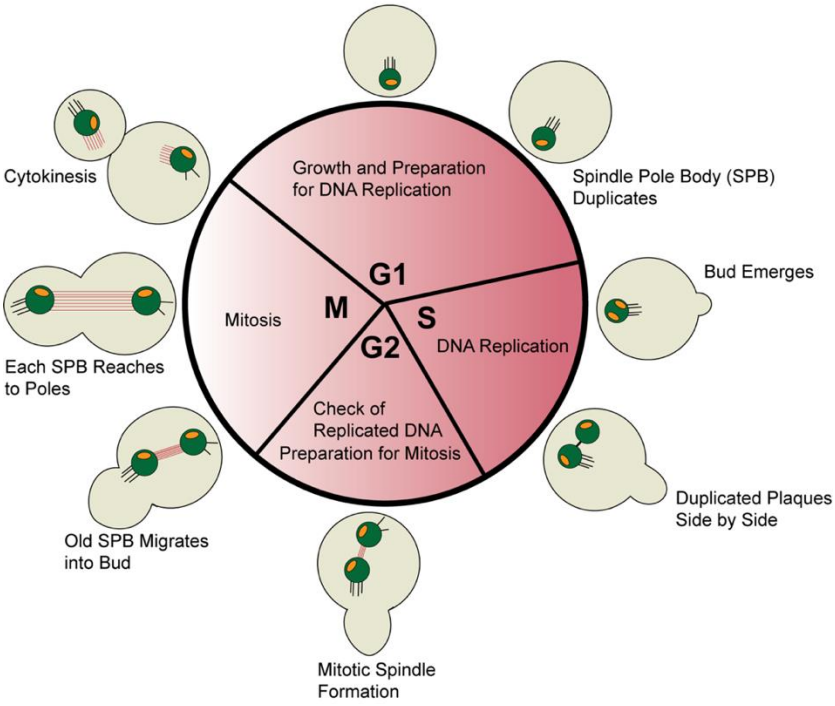

Figure 1.5: Yeast cells couples SPB duplication to the cell cycle.

Schematic representation of changes yeast centrosome undergoes throughout the cell cycle. Black lines represent astral microtubules while red color indicates MTs.

1.4.3. SPB Size

In haploid cells, the yeast centrosome grows in diameter. In G1 it starts approximately with 80 nm and reaches 110nm in mitosis, but its height stays constant, approximately 150nm (Jaspersen & Winey, 2004). DNA content is another parameter effects SPB size. For instance, in diploid cells, SPB diameter is160nm (Jaspersen & Winey, 2004). Enlarged SPB diameter elevates capacity of microtubule nucleation which is vital for chromosome segregation. Yet, the regulation of SPB size has not been depicted.

Although during SPB duplication a new SPB forms next to the old one giving a conservative appearance to SPB duplication, not all components behave the same. For example, Spc110 was shown to be dynamically associating with the SPBs which does not fit to the conservative or disperse models of duplication (Yoder T.J, Pearson C., Bloomn K., Dvis TN 2003 MBoC). Indeed, the yeast centrosome frequently undergoes growth and exchange cycles. SPB growth can be defined as adding novel components, whereas exchange is replacing old components by the new ones (Greenland et al., 2010). These changes are concomitant with the cell cycle. Growth usually occurs late in the cell cycle while exchange is observed during SPB duplication, G1/S, resulting in that parent SPB has mixture of the new and old components (Greenland et al., 2010). In addition, cell cycle arrests have varied effects on this dynamic phenomenon of SPB (Greenland et al., 2010). α-Factor assisted G1 arrest usually cause dramatic decrease in SPB core size. In contrast, metaphase arrest cause enlarged SPB core. For instance, Mps1 kinase overexpression leads doubled SPB size (Greenland et al., 2010). Since SPB size undergoes diverse changes due to cell cycle progression and checkpoint activation, the processes underlying these changes are significant for the SPB maintenance; thus, spindle assembly (Greenland et al., 2010).

1.5 The Mitotic Spindle of S. cerevisiae and Spc110 as a γ-TuCR

The spindle microtubules should have access to the nucleoplasm throughout mitosis for daughter genome segregation (Niepel et al., 2005). This can be achieved by two ways: nuclear envelope (NE) breakdown (open mitosis) or spindle assembly in the nucleus, closed mitosis. In yeast, mitosis is closed and SPBs assemble the mitotic spindle. The spindle also ensures nuclear

division and migration happens in concert with the bud formation and DNA replication (Niepel et al., 2005).

Even though individual components of microtubules can self-assemble, it happens very slowly; thus, cells utilize other components to speed up this event. In yeast, the Spc110 recruits gamma-tubulin to the SPB where Spc110 associates with two other molecules to establish γ-tubulin small complex (γ-TuSC). Several γ-TuSCs join each other to produce a ring which presents a platform where microtubules can grow from.

Gamma-tubulin complex receptors, γ-TuCRs, are essential for targeting γ-Tubulins to MTOCs. γ-TuCRs can be grouped into two: one has both SPM and CM1 motif and the other has only CM1. The Spc110 belongs to SPM-CM1 group whereas Spc72 only carries CM1 motif (Lin et al., 2014). Centrosomin motif 1(CM1) enables γ-TuSC interaction with γ-tubulin complexes' GCP subunits (Lin et al., 2014).

Spc110 can mediate microtubule formation by controlling γ-TuSCs binding to each other. Therefore, Spc110 is a regulator of microtubule nucleation (Lin et al., 2014). Nonetheless, Spc110 should be activated to perform this specific role. Its activation depends on cell cycle progression and is regulated by its N-terminus phosphorylation. Spc110 phosphorylation emerges at S phase, accumulates through mitosis, and disappears at the anaphase onset (Lin et al., 2014). Lack of phosphorylation mediated Spc110 regulation results in disruptions which are compensated by SAC induced cell cycle delay (Lin et al., 2014).

The duplication plaque is inserted into NE in G1/S. This enables Spc110-calmodulin-Spc29 binding to the nuclear Spc29-Spc42 layer of duplication plaque (Lin et al., 2014). In this cell cycle stage, Cdc28-Clb5 phosphorylate five residues of Spc110 N terminus. Consistently, this is the time window for Cdc28-Clb5 association with the SPB. Lin et al. suggests that Cdc28-Clb5 and Mps1 coordinate MT nucleation time via Spc110 phosphorylation.

Spc110 T18 site is phosphorylated in M phase. T18A, T18E, T18D and T18V mutations of Spc110 causes similar phenotypes in vivo and vitro (Lin et al., 2014). All these mutations inactivate major SPM motif which T18 resides in. In vivo, Spc110 T18 site phosphorylation occurs in mitosis but not in S stage. Therefore, T18 is different Cdk1 site than other two sites: S36 and S91, which are S phase Cdk1 subunits. Cdk1-Clb2 phosphorylation of $Spc110^{T18}$ limits the SPB's MT nucleation activity (Lin et al., 2014).

All in all, Spc110's MT nucleation activity requires the SPM motif and stimulatory phosphorylation. Cdc28 and Mps1 phosphorylation mediates Spc110 interaction with γ-TuSC and MT nucleation (Lin et al., 2014).

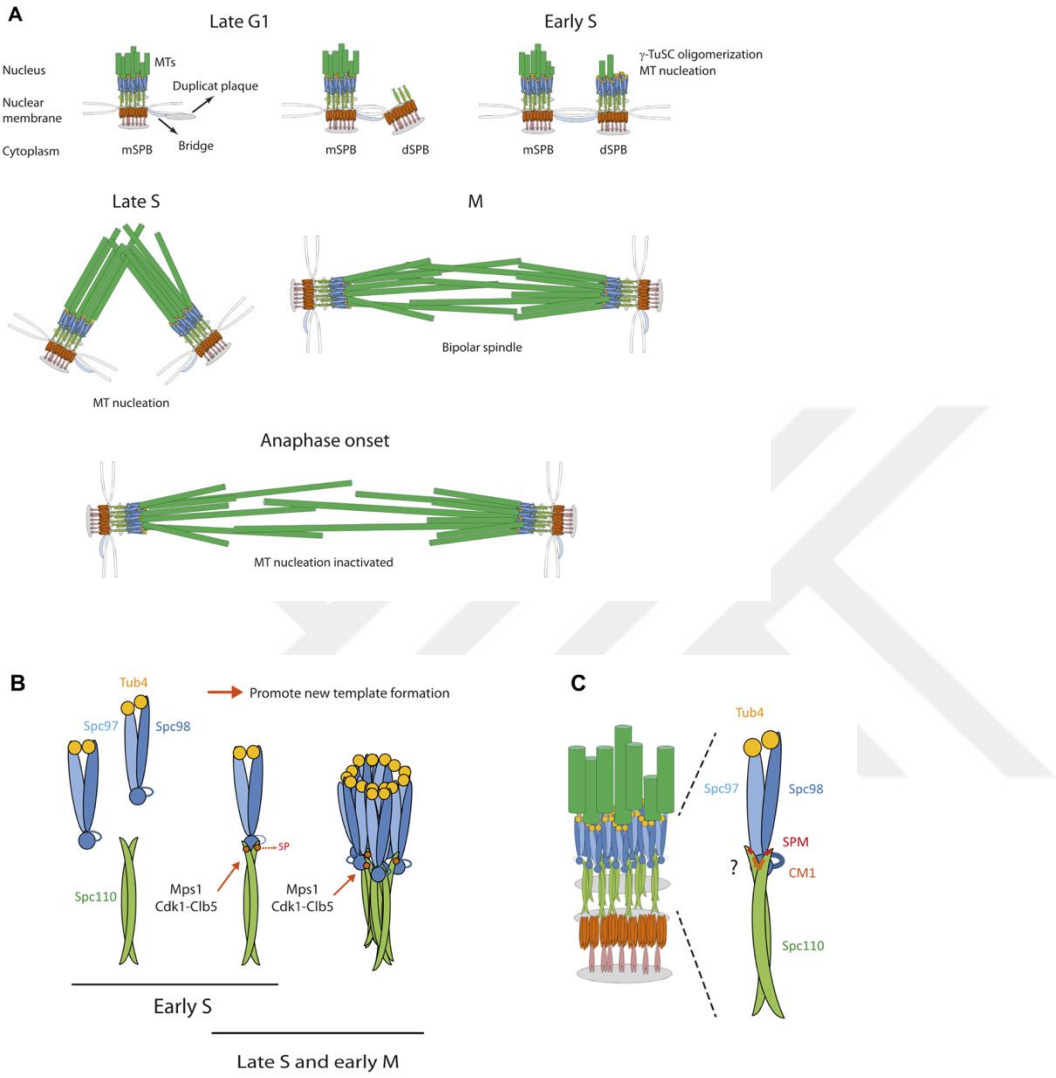

Figure 1.6: Spc110 phosphorylation role during SBP duplication.

Fig.5A demonstrates microtubule nucleation during the cell cycle. Part B displays Mps1 and Cdk1-Clb5 mediated stimulatory Spc110 phosphorylation. Fig.5C draws Spc110 interaction with γ-TuSC. Dimer of Spc110 uses its CM1 and SPM motifs to interact with Spc98 N-terminus (Lin et al., 2014).

1.6 Novel Paradigm on Spindle Pole Body Dynamics

In vitro, it is observed that the SPB core is strongly resistant to disruptions (Niepel et al., 2005). Nonetheless, various recent studies advocates that these macromolecules are dynamic in vivo. Both old and newly synthesized SPB experience size growth from G2 to telophase. Furthermore, the mother SPB (novel one) regularly undergoes Spc110 exchange (Niepel et al., 2005).

Dynamic characteristic of SPB, shown by recent studies, are not consistent with the conservative-dispersive theory of SPB duplication since this model assumes that duplicated biological entities are static (Yoder et al., 2003). Yoder et al. suggests that duplication and assembly can be well defined by analyzing growth and exchange. Application of this methodology to other inherited cell structures can indicate unique and universal features of macromolecule assembly (Yoder et al., 2003).

Ectopic expression of several SPB components induce their incorporation into pre-existing yeast centrosome, including nonduplicating centrosome in S phase and mitosis (Jaspersen & Winey, 2004). Moreover, FRAP experiment demonstrated that approximately half of Spc110 within a yeast centrosome is exchanged with newly made Spc110 during G1 and S whereas no exchange could be observed in cells with short spindles (Jaspersen & Winey, 2004). Several evidence imply that SPB duplication can be depicted as a continuous growth and exchange period rather than a strict conserved process. Protein incorporation into existing SPBs can be significant for their structural maintenance and functional integrity (Jaspersen & Winey, 2004). SPB duplication occurs only once in each cell cycle like DNA duplication. Meselson and Stahl established that DNA replication is semiconservative which nucleotides are incorporated into only new strand. Their study presents a paradigm that issues cell cycle modulated macromolecular structure assembly (Jaspersen & Winey, 2004).

The conservative assembly model explains that only novel entities utilize new components whereas old structure continues with old components. In contrast, the dispersive assembly model advocates that both old and new structures are consists of mixture of old and new components. Centrioles duplicate conservatively and a centriole pair constitutes a centrosome. Only the daughter centriole integrates newly labeled tubulin. Pereira et al. demonstrate that Spc42 assembles conservatively (Jaspersen & Winey, 2004). However, studies of Yoder et al. displayed that neither dispersive nor conservative assembly models can explain Spc110

dynamics. Accumulation of recent studies portray a dynamic SPB in an extend that was not appreciated previously.

1.7 Roles of Cdc28 and Cdc14 in the SPB Cycle

Cdc28 governs yeast cell cycle in association with G1, S phase and mitotic cyclins. Genome wide studies on Cdc28 substrates discovered several SPB components: Mps2, Spc29, Spc42, and Sfi1 (Jaspersen & Winey, 2004). In addition, multiple Cdc28 consensus sites are identified in other SPB proteins like Cnm 67 and Spc110. The function of Cdc28 phosphorylation on SPB duplication is not elucidated except for Spc42. Cdc28 phosphorylation of Spc42's N terminal sites enable its packaging into high order. In addition, this phosphorylation enhances the Mps1 phosphorylation of Spc42 on additional sites. Cdc28 prevents SPB reduplication in later stage of cell cycle via poorly known process (Jaspersen & Winey, 2004). Involvement of Mps1 in SPB duplication is known; however, it is not clear whether Mps1 phosphorylate multiple centrosome components or sequentially phosphorylate just one component. Mps1 does not have consensus phosphorylation sequence and only three SPB components, Spc110, Spc42 and Spc98, has been established as Mps1 substrate (Jaspersen & Winey, 2004).

Phosphorylation and dephosphorylation patterns govern SPB duplication (Elserafy et al., 2014). Cdc28 activity can promote or inhibit the yeast centrosome duplication regarding the cell cycle phase. Cdc28-G1 cyclins (Cln1-Cln2) induces novel SPB formation via expanding the satellite into complete SPB (Elserafy et al., 2014). Cdc28-S cyclins (Clb5-Clb6) stimulates separation of two connected SPBs via APC^{Cdh1} inhibition. In mitosis, Cdc28-Clb1 or Clb4 prevents SPB reduplication (Elserafy et al., 2014).

Upon mitotic exit, Cdc14 counteracts mitotic Cdc28 activity by promoting Clb2 degradation and dephosphorylating several Cdc28 substrates (Elserafy et al., 2014). Sfi1 phosphorylation by Cdc28 blocks SPB duplication; therefore, these modifications should be abolished before entrance to the G1. Sfi1 dephosphorylation by Cdc14 prepares this component for half-bridge elongation which marks the new cell cycle. Surprisingly, four Cdc28 sites of the Sfi1 C terminus are also consensus Cdc14 dephosphorylation sequence, which is SPxK/R.

Elserafy et al. identified several SPB components as Cdc14 binding partner via Cdc14-TAP pull down assay. These components includes Bub2, Spc42, Nud1, Spc110 and Sfi1 which this

finding is consistent with the known SPB binding of Cdc14. Sic1 expression inactivates mitotic Cdc28 activity and drives cells into G1. In early S phase, Cdc28-Clb4 associates with SPB cytoplasmic side. Therefore, it can phosphorylate C-Sfi1 and induce SPB separation (Elserafy et al., 2014).

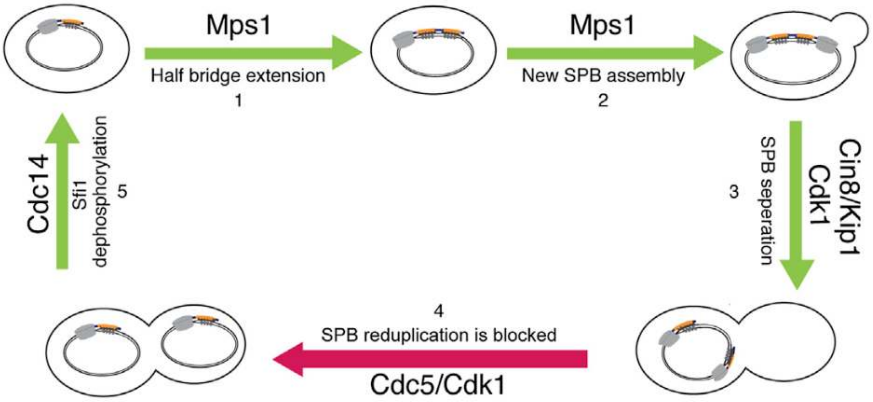

Figure 1.7: Counteracting actions of Cdc28 and Cdc14.

Schematic model of counteracting actions of Cdc14 and Cdc28 on SPB are depicted (Elserafy et al., 2014).

1.9 Diverse Functions of Bud14-Glc7 Complex

Protein phosphatases perform several functions to control the cell cycle (Kocakaplan et al., 2021). In animal cells, PP1, along with PP2A, counteracts CDK activity to execute mitotic exit. In addition, PP1 also mediates centrosome splitting by counteracting the Nek2 kinase activity in human cells. From yeast to mammals, the PP1 is fundamental for suppressing the spindle assembly checkpoint (SAC) (Kocakaplan et al., 2021). Bud14 is known regulatory subunit of Glc7, member of PP1 family. Previous research demonstrated that Bud14 interacts with Glc7 to regulate dynein-dependent microtubule sliding at the cortex of bud; thus, mediates nuclear migration (Chesarone et al., 2009).

Deletion of *BUD14* causes poorly understood elongated bud phenotype. Bud14 overexpression is conditionally lethal and intensified by bni1Δ suggest that Bud14 might have role in actin-based cell morphogenesis. Bud14 directly governs formin activity to control actin cable function and architecture. Bud14 is a multifaceted cytoskeletal protein that coordinates actin and microtubule-based functions (Chesarone et al., 2009). At the bud cortex, Bud14 directly recruits Glc7 which regulates dynein activity for positioning of mitotic spindle (Gould et al., 2014).

S. cerevisiae chooses nonrandom bud site based on mating-type status (Cannon, 2010) (Figure 1.1). Bud14-Glc7 holoenzyme governs this bud site selection since mutants of *BUD14* display random budding patterns. Overexpression of Glc7 causes noticeable elongated bud phenotype even though no aberrant bud-site selection is observed. Overexpression of Bud14 results in cell cycle arrest after DNA replication with large buds (Cannon, 2010). This observed phenotype can be related to the Clb2 stabilization driven by Glc7 overexpression. In many Bud14 overexpressing cells, metaphase mitotic spindle was pulled into bud. Usually, the mitotic spindle is distributed equally between mother and bud. The Bud14-Glc7 complex stabilizes attachments of microtubule to the cell cortex (Cannon, 2010).

Bud14 is low abundance Glc7 regulator and Bud14 overexpression dislocates Glc7 from the nucleus. The Bud14 protein has affinity for Kel1 and Kel2, cell cortex proteins; thus, positions Bud14-Glc7 at the cell cortex to maintain microtubule attachment. Nuclear Glc7 activity also governs microtubule attachment to kinetochores. This is proven by that Glc7 dephosphorylates many kinetochore proteins (Cannon, 2010).

Spindle position checkpoint (SPOC) is activated by spindle mispositioning; and inhibits mitotic exit (Kocakaplan et al., 2021). Bfa1, the most downstream protein of the SPOC, is strictly regulated with respect to the spindle orientation via phosphorylation by Cdc5 and Kin4 in antagonistic manner. Even though Bfa1 mediating kinases are elucidated, little is known about phosphatases that counteracts the activity of those kinases. Kocakaplan et al. established that Bud14-Glc7 complex is a SPOC component that induces dephosphorylation of Bfa1 that is hyperphosphorylated by Cdc5 in anaphase. Bud14-Glc7 activates Bfa1-Bub2 complex in a parallel way to Kin4 (Kocakaplan et al., 2021). Due to spindle misalignment, Bfa1 is phosphorylated by Kin4 which leads its disassociation from the SPBs. Bud14-Glc7 dephosphorylates Bfa1 to abolish the inhibitory phosphorylation. Therefore, Bud14-Glc7 is a novel SPOC component which prevents mitotic exit when spindle is mispositioned. (Kocakaplan et al., 2021). Moreover, absence of BUD14 causes increased Bfa1 and Tem1 localization at daughter SPB which elevates their asymmetric localization. Therefore, it is plausible to assume that Bud14-Glc7might have other targets at the SPB which lowers SPB docking sites of Bfa1-Bub2.

Absence of *BUD14* does not prematurely activate MEN which is proven by Mob1 localization analysis. Therefore, Kocakaplan et al. advocates that Bud14-Glc7 inhibits mitotic exit via

activating Bfa1-Bub2 GAP complex. It performs this function by removing the inhibitory Bfa1 phosphorylation rather than altering its localization level at the SPB (Kocakaplan et al., 2021).

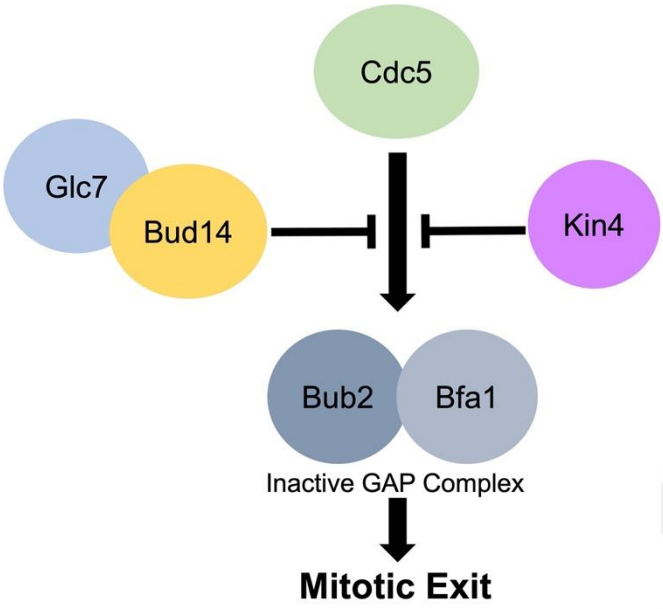

Figure 1.8: Proposed model on Bud14-Glc7 action in SPOC.

Bud14-Glc7 prevents inhibitory phosphorylation of Bub2-Bfa1 GAP complex. Kin4 functions like Bud14-Glc7 in a parallel pathway.

1.9.1 520kDa Formin Regulatory Complex: Kelch Proteins and Bud14

In vivo, formins function in actin assembly and organization. Formin activity is also tightly regulated to maintain functioning actin structures. Polarity axis establishment and maintenance is required for yeast cells to grow a bud and divide (Gould et al., 2014). Formation of polarity axis requires actin cable assembly which act as tracks for myosin V-based organelles and secretory vesicles transport to the bud (Gould et al., 2014). Bud14 is a formin regulator which target specifically FH2 domain of Bnr1 which results in displacement of Bnr1 from growing ends. Therefore, Bud14 prevents actin polymerization. In many organisms Kelch proteins are crucial for cell morphogenesis and polarity. In budding yeast, Bud14, Kel1, and Kel2 assembles 520kDa complex with stoichiometry of 2:2:1 (Gould et al., 2014). Absence of any component of this complex causes hyper-stable, bent, and long actin cables which causes defects in septum formation during cytokinesis and secretory vesicle traffic. Bud14-Kel1-Kel2 complex localizes to bud neck where Bnr1 is stably anchored via septins. Kel1directs the complex to the bud site while Kel2 maintains Bud14-Bnr1 activity. Therefore, kel1Δ phenotype is less drastic than either of bud14Δ and kel2Δ phenotypes (Gould et al., 2014).

Chapter 2: MATERIALS AND METHODS

2.1 Saccharomyces cerevisiae Techniques

S288C isogenic yeast strains are employed in this research and are listed in Table X. cassette PCR and yeast competent cell transformations were commonly performed to gene tagging and manipulations. All used plasmids are listed in Table 6.3. The components and descriptions of utilized buffers, media and agents are listed in the Table 6.4.

2.1.1 Yeast Growth

The strains were grown in a medium regarding the selection marker and cell type. D-(+)-Glucose (NeoFroxx) is utilized as the carbon source. YPAD media is employed for general cell culture. 20g per Liter Agar (Carl Roth #5210.2) is used for apar plates. Autoclave and filter sterilization methos are employed for all used media and agar plates.

The wild-type yeast strains are grown at the 30 °C, and in autoclaved YPAD media or on YPAD plates if not stated otherwise. Filter sterilized synthetic complete (SC) media which lacks the specific auxotrophic nutrients are exploited for growth of plasmid carrying strains. Filter sterilized SC media is sole media used for microscopy experiments. Regarding the temperature sensitive status of the strains, cells are cultured at an appropriate temperature.

To obtain logarithmically growing yeast cultures: Cells grown on specific agar plates prior the experiments. Then, grown cells inoculated into liquid medium and grown are overnight (12-18h) so culture reaches stationary phase. In the morning, optical density (OD) of the culture is measured at 600nm utilizing a spectrophotometer (PG Instrument, T60 Visible Spectrophotometer). According to their OD value, the culture is diluted to 0.15-0.2 value in a fresh medium and incubated until their OD-600 of 0.8-1.0 to have a logarithmically growing culture.

2.1.2 Yeast Competent Cell Preparation and Transformation

Yeast competent cells are prepared by Lithium acetate and PEG mediated chemical method. 10 ml stationary culture is prepared by overnight inoculation. The stationary culture is brought to OD600 0.15-0.2 in 50mL fresh media. The culture is incubated until cells reach to log phase. Then, the log-phase culture is centrifugated at 3200 rpm for 2 minutes. All centrifugations are done at room temperature. After centrifuge, supernatant is removed. The pellet is resuspended with 40 mL autoclaved double-distilled water. Resuspended cells are centrifugated for 2

minutes at 3200 rpm. The supernatant is removed. 20mL LiSORB is used to resuspend the pellet. The resuspended culture is centrifugated as stated before which followed by supernatant removal. This time, the pellet is centrifugated again to remove LiSORB remaining. At last step, for initial 50mL culture of OD600 1.0, the pellet is resuspended with 50 µl denaturated salmon sperm DNA and 300 µl LiSORB. To denaturate salmon sperm DNA, it is boiled at 95 °C for 5 minutes proceeded by 5 minutes incubation on ice. Resuspended culture is aliquoted into 100µL and stored at -80 °C.

Competent cells are transformed with plasmids or PCR products. In general, 1µl circular plasmid, 5 µl of PCR product or integration plasmid are used for transformations.

For transformation of yeast, firstly, competent cells are thawed at bench. DNA of interest is mixed with the cells. Tubes are incubated for 20 minutes at room temperature. 300 µl LiPEG is added to the tube and resuspension is reached by vortex. It is followed by 20 minutes incubation at room temperature.

35 µl DMSO (Fisher Scientific #BP231-1) is added to the tube, vortexed and incubated for 15 minutes at 42°C water bath (for *ts* mutants incubation is done for 12 minutes). Then the cells are centrifugated for 2 minutes at 3200 rpm at room temperature. The supernatant is removed by aspiration. If cells are transformed with DNA carrying an auxotrophic marker, the cell pellet is resuspended in 150µl 1X sterile PBS and directly plated out onto corresponding selective agar plate. If the selective marker is an antibiotic, the cells are recovered by overnight inoculation in YPAD. After recovery, the cells are plated out onto antibiotic containing agar plate. Then, the plates are incubated at respective degree.

2.2. PCR-based Techniques

Casette PCR based genome editing technique is employed for C- or N- terminus tagging and gene deletions. Yeast cells are confirmed according to gene manipulation type. Gene deletion is confirmed by either yeast colony or yeast chromosomal DNA PCR.

2.2.1 Casette PCR

All PCR reactions are performed via Biometra TAdvenced Twin Analytik Jena PCR machine.

For C' terminus tagging S2/S3 primer pair; for N' terminus tagging S1/S4 primer pair; for gene deletion S1/S2 primers are employed.

To produce 50µl cassette PCR reaction; 3.2µL from each primer (10µM), 5µL template plasmid (20ng/µL), 8.75µL dNTPs (100nM), 5µL 10X PCR Buffer 1, 0.6 µL enzyme mix consists of 1X Vent polymerase (2U/ µL, NEB #M0254S) + 2X Taq polymerase (NEB #M0273L) and 24.25µL double distilled water is mixed.
The PCR cycles are indicated in Table X. 0.8% agarose gel electrophoresis is performed to verify the cassette.

2.2.2 Yeast Colony PCR

By the sterile micropipette tip, small amount of yeast cells is taken from agar plates into 50µL Sarkosyl solution (0.01% Sarkosyl in 0.02 NaOH). The mixture is vigorously vortexed.
Then it is boiled for 20 minutes at 95 °C. Then it is directly placed into -20 °C for approximately 20 minutes. Proper amount usage of freshly grown yeast cells increases the efficiency of colony PCR. See Table X for PCR conditions.
0.8 % agarose gel electrophoreses is used to analyze PCR results. WT PCR product is loaded onto gel as a control.

2.2.3 Chromosomal DNA PCR

The yeast cells are inoculated overnight in 2ml sterile YPAD media. In the morning, the culture is pelleted at 14000 rpm for 1 minute. The supernatant is decanted. Pellet is resuspended in 300 µl %6 SET buffer by vortexing. The mixture is incubated in 65°C heat block for 15 minutes with 400 rpm shake and then placed on ice for 5 minutes. 150µL cold P3 is added to the tube and the tube is inverted several times to mix which followed by 15 min incubation on ice. The sample is centrifuged at 14000 rpm for 10 minutes. The supernatant is transformed into new eppendorf which contains 550µL isopropanol. The sample is mixed by inverting and rotating which proceeded by 2 min centrifugation at 14000 rpm. The supernatant is discarded. 200µL ice cold 70% analysis EtOH is added onto the pellet. Vortex should be avoided. The sample is 1 min centrifuged at 14000 rpm. The supernatant is removed by decant. The pellet is left on tissue paper for air dry for 30 minutes. Then the tube is placed at 65°C heat block with open lid for approximately 50 minutes. 30µL preheated ddH_2O is used for resuspension of the pellet. 1µL RNaseA (1mg/mL) is added to the resuspension. The tube is incubated at 37°C for 15 minutes. The chromosomal DNA can be stored at -20°C or can be used directly for downstream experiments.

Table 2.1: Cycling Conditions of Cassette PCR.

Step	Temperature (°C)	Duration	Go To
1	94	2 min	
2	94	20 sec	
3	52	30 sec	
4	68	1 min per 1000 kb	10x Step 2
5	94	30 sec	
6	52	30 sec	
7	68	1 min per 1000 kb	20x Step 5
8	4	∞	

Table 2.2: Cycling Conditions of Yeast Colony PCR.

Step	Temperature (°C)	Duration	Go To
1	94	5 min	
2	94	30 sec	
3	53	30 sec	
4	68	1 min per 1000 kb	35x Step 2
5	68	3 min	
6	4	∞	

2.3 Molecular Biology Techniques

2.3.1 Plasmid Isolation by Manual Method

E. coli colony from the agar plate is added to the respective antibiotic involving TY media. Tubes are placed to 37°C shaker for overnight (12-16h). Next morning overnight culture is transferred to 2mL eppendorfs. These tubes are centrifuged for 5 minutes at 6000 rpm (all centrifuges are performed at 23-25°C). The supernatant removed via vacuum-aspiration. The pellet is resuspended by 300µl P1 buffer. Right after, 300µl P2 buffer added onto tubes and mixed by invert/rotate method. This is proceeded by addition of 300µL P3 buffer. Mixing is done by careful rotating and inverting. Vortex should be avoided. Tubes are centrifuged for 10 minutes at 14000 rpm. The supernatant is carefully transferred to the new tubes containing 500µL Isopropanol (ACS #0312.2500). It is followed by 20 min centrifugation at 14000 rpm. The supernatant is removed by decanting. 500µl 70% molecular EtOH is added onto the pellet. The tubes are centrifuged for 10 minutes at 14000 rpm. The supernatant is removed. The pellet

containing tubes are left for air-dry on tissue paper for at least 30 minutes till all liquid remaining evaporates. 20µL pre-heated double-distilled water is used to resuspend the pellet. This eluted plasmid DNA can be stored at -20 °C.

2.3.2 Molecular Cloning of Endogenous Bud14

Bud14 gene is amplified by PCR using Bud14-P-fw and Bud14-T-rv primers. PCR product is cut by XhoI (Thermo Scentific #ER0691 Lot: 00524815) and BglII (Thermo Scentific #ER0082 Lot:00521747). Insert is eluted from agarose gel by employing NucleoSpin® Gel and PCR Clean-up Kit (Lot: 1907/006). Backbone pRS405 cut with BamHI (Thermo Scentific #ER0051 Lot: 00509047) and XhoI since BamHI produces same sticky end like BglII. Cut backbone is eluted from agarose gel by procedure of NucleoSpin® Gel and PCR Clean-up Kit Manual (Lot: 1907/006). Ligation reaction is set as follows: 0.5µL T4 ligase, 1µL T4 ligase Buffer, 5µl eluted backbone, 2µL insert and 1.5µL ddH_2O. Reaction is incubated at room temperature for 30 mins. DH5α is transformed with ligation product. Isolated plasmid is confirmed by PCR with Bud14-P-fw and Bud14-T-rv primers. Furthermore, confirmed plasmids are cut with XhoI and StuI and run on 8% agarose gel. Endogenous Bud 14 functionality is established by SPOC analysis.

2.3.3 Site-Directed Mutagenesis via Phusion DNA Polymerase

To introduce specific mutation into plasmid DNA, site directed mutagenesis is utilized. To construct 50 µL mutagenesis PCR reaction; 5 µL freshly opened 2mM dNTPs (NEB #N0446S), 2.5µL forward primer (10µM), 2.5µL reverse primer (10µM), 1µL template plasmid (130 ng/µL), 0.5µL Phusion DNA Polymerase (X), 10µL 5X High Fidelity Buffer and 28.5 µL ddH2O are mixed. As a reaction control 0.6µL template plasmid, 4µL 5X HF Buffer and 15.4µL ddH2O is prepared. The PCR conditions and cycles are described in Table X.

After completion of cycle, PCR products are cut by 2µL DpnI (Thermo Fisher Scientific #ER1705). This digestion reaction is placed at 37°C for overnight. After the digestion, DH5α competent cells is transformed with 1µL product. Transformed colonies are inoculated for plasmid isolation. Isolated plasmids are verified by sequencing.

Table 2.3: Site Directed Mutagenesis PCR Cycles

Step	Temperature (°C)	Duration	Go To
1	98	30 sec	
2	98	10 sec	
3	64.1	20 sec	
4	72	2 min 15 sec	25x Step 2
5	72	8 min	
6	4	∞	

2.4 Biochemical Methods

2.4.1 TCA Total Cell Protein Extraction

Yeast cells on agar plate are inoculated into 1mL YPAD for overnight. At morning, according to its OD600 value, the culture is diluted to 0.2 to reach logarithmically growing phase. When log phase is reached, the cell culture is collected into Eppendorf and centrifuged at 140000 rpm for 90 seconds. The supernatant is aspirated. The pellet is placed onto ice and rest of the procedure is carried out on the ice. 800µl ice-cold ddH2O is added onto the pellet. 150µL 1.85M NaOH (Merck, #106498) is immediately added onto the tube. The mixture is vortexed vigorously. The tube is incubated on ice for maximum 5 minutes. 150µL 55% (w/w) TCA (Trichloroacetic acid, Merck #100807) is added into the tube. The mixture is vortexed well. The tube is incubated for 10 minutes on ice. It is followed by centrifugation at 14000 rpm for 20 minutes at 4°C. Then the supernatant is aspirated. The pellet is centrifuged at 14000 rpm for 90 seconds at room temperature. After the centrifuge, rest of experiment is performed in room temperature. HU-DTT is used to reach resuspension. Volume of added HU-DTT is determined based on protein abundance. For abundant proteins, 150µL HU-DTT is added onto the pellet derived from 1mL culture with OD600 1.0. Less abundant proteins, 75µL HU-DTT is used for addition. HU-DTT resuspension of the pellet is reached by vortexing. If mixture gets a yellowish color, 2 µL 2M Tris-HCI addition is used for pH neutralization. The protein sample is placed to 65 °C heat block with 400rpm shake for 15 minutes.

2.4.2 SDS- PAGE and Western Blotting

SDS-PAGE technique is exploited for protein separation. SDS-PAGE gels were prepared manually based on Mini-Protean II gel system. The prepared separating gel percentages and

contents are stated in Table X. In this research, only 4% stacking gel is prepared which its content stated in Table X. For all gel preparations, addition starts with water and follows order of decreasing amount. Nevertheless, 10% APS always added last to the mixture.

Table 2.4: Description of used SDS-PAGE gels in this research are listed.

SEPARATING GEL (4 gels)	6%	8%	10%
Polyacrylamide mixture (30%: 0.8% (w/v) Acrylamide:Bisacrylamide, Carl Roth, #3029.1)	4 mL	5.2 mL	6.7 mL
ddH_2O	10.72 mL	9.52 mL	8.1 mL
1.5M Tris-HCl with pH 8.8	5 mL	5 mL	5 mL
10% (w/v) SDS Solution	200 µL	200 µL	200 µL
10% (w/v) APS Solution (APS, Sigma #A3678)	100 µL	100 µL	100 µL
TEMED (Sigma, #T7024)	10 µL	10 µL	10 µL

Table 2.5: Description of stacking gel of every SDS-PAGE used in this research is listed.

STACKING GEL (4 gels)	4%
Polyacrylamide mixture (30%: 0.8% (w/v) Acrylamide:Bisacrylamide, Carl Roth, #3029.1)	1.3 mL
ddH_2O	6.2 mL
0.5M Tris-HCl with pH 6.8	2.5 mL
10% (w/v) SDS Solution	100 µL
10% (w/v) APS Solution (APS, Sigma #A3678)	50 µL
TEMED (Sigma, #T7024)	10 µL

After gels are polymerized, comb is removed, and the gel is placed to the tank filled with 1X Running Buffer. Reagents descriptions and buffer components used in WB are listed in Table

X. Empty wells loaded with HU-DTT. As a protein marker, OPTI Protein Ladder (BRAND) is loaded. Constant 20mA per loaded gel is used. After completion of the run, the protein samples transferred from SDS-PAGE gel to nitrocellulose membrane (Merck, GE1060000 2). For semi-dry transfer is applied. The SDS-PAGE, nitrocellulose membrane, and 8 watmann paper are soaked in 1X blotting buffer. 4 watmann papers are placed to the cassette, top of it membrane and the SDS-PAGE gel is placed. The sandwich is closed with 4 watmann papers. Excess buffer is removed by a roller and tissue paper. For the blotting Bio-Rad Mini-Trans-Blot transfer machine is employed. For one gel; 0.1A 25W is applied for 90 minutes. the transfer efficiency is verified by Ponceau S staining. To remove dye, 1X PBS-T is used. For blocking of membrane 5% non-fat dried milk (AppliChem, # A0830) in 1X PBS-T is used. Blocking can be done 1 hour at room temperature or overnight at 4 °C on the shaker. For antibody blotting, primary antibody is prepared in 3mL 3% non-fat dried milk solution according to its required dilution (see Table X). The membrane is incubated at room temperature for 1h in primary antibody solution. Rotator is employed so antibody solution can reach every membrane site. The membrane is 5 minutes washed with 1X PBS-T for 3 times on the shaker. The membrane is 1 hour blotted by the secondary antibody which diluted to 1:1000 in 3mL 3 % non-fat dried milk solution (see Table X for used antibodies). After completion of antibody blotting, membrane is 1 minute incubated with homemade ECL. Then the experiment is visualized via Chemidoc (BioRad) machine.

Table 2.6: Description of used antibodies in this research.

Name of Primary Antibodies	Antibody Origin	Dilution Ratio
α-HA	Mouse	1:50 in 3% milk solution with PBS-T (0.02% Tween-20)
α-Tubulin	Rabbit	1:50000 in 3% milk solution with PBS-T (0.02% Tween-20)

2.5 Linking Protein Location to Its Function: GBP-GFP System

GFP-binding protein (GBP) is derived from a llama heavy chain antibody (Y. hui Chen et al., 2017). This 13kDa soluble protein has been exploited for protein targeting in vivo. GBP has high binding affinity to GFP with a stoichiometric ratio of 1:1. Therefore, GBP containing plasmid (see Table 7.3) is amplified with primer pair specific to the destination protein. Then protein which targeted to the destination is tagged with GFP C-terminally. Finally, protein of

interest is tagged C-terminally with monomeric mCherry (see Table 7.3). For the control sample, no protein is tagged with GFP whereas GBP tagging is preserved in the strain to eliminate any interference caused by GBP tagging. The strains are proceeded with alive cell imaging by fluorescence microscopy.

2.6 Fluorescence Microscopy Experiments

For the fluorescence microscopy, fixed and alive imaging are utilized in this research.

2.6.1 Fixed-cell Imaging

The yeast cells are always fixed by freshly prepared 8% PFA (Merck, 30525-89-4) solution (table X). 700µL yeast culture is mixed with 700µL 8% PFA. The tube is incubated at bench for 10 minutes. It is centrifugated for 2 minutes at 6000 rpm. The supernatant is decanted. The cell pellet is resuspended with 1 mL sterile 1X PBS. The samples can be store at 4 °C for only 1 day. Before taking images, the samples are centrifuged for 3 min at 3200 rpm. Most of the supernatant is removed by micropipette. Remaining 1X PBS is used to resuspend cell pellet. 2µL sample is used for slide preparation.

For DAPI staining, the cells are fixed by EtOH. 700µL pure molecular Ethanol is mixed with 300µL yeast culture. The samples should be stored at 4°C until experiment. Before DAPI addition, ethanol fixated yeast cells are centrifugated at 3200 rpm for 3 min. The supernatant is aspirated. To remove all EtOH residue, stated centrifugation and aspiration steps are performed again. The cell pellet is resuspended with 10µl of DAPI solution (1mg/mL in 1X PBS; 1:10000 dilution)

2.6.2 Image Analysis

Image J is employed for the analysis of all microscopy images. Graphs and statistical test are done via GraphPad Prism 8.0.1 (GraphPad, Le Jolla, Ca) software. Asterisk used in the presented graphs of this research have following p-values: **** $P < 0.0001$, ***$P < 0.001$, **$P < 0.01$, *$P < 0.05$.

2.6.3 Fluorescence Intensity Quantifications of Protein of Interests

In microscopy experiments, mCherry-Tub1 tagging is exploited as a cell cycle marker. Each still image consisted of 13 z-stacks in 0.30µm thickness. For every channel 2x2 binning and

100X magnification is applied. For GFP channel 20% with 100µsec is used for each experiment. In SPB component measurements, area of 0.494µm^2 (24 pixels) is selected and mean fluorescence intensity (FI) is measured using ImageJ measure tool. As a background signal, mean FI of cellular area free from SPBs (usually in between of two SPBs) is measured. Background FI is extracted from FI of the region of interest (ROI) for correction.

$FI_{SPB\_corrected}=FI_{SPB}-FI_{background}$

For establishing SPB component molecule numbers, Nuf2-sfGFP is used as a reference. It has been previously reported that 352 Nuf2 molecules is present at each anaphase pole (Caydasi et al., 2012). Acordingly, log phase culture of the Nuf2-sfGFP is mixed with the sample of interest in 1/3 ratio right before imaging. Same size of ROI (24 pixels) is measured for Nuf2 in anaphase poles. Cytoplasmic FI is also measured as background and subtracted from ROI measurement.

$FI_{Nuf2\_corrected}=FI_{Nuf2}-FI_{background}$

Median of $FI_{Nuf2\_corrected}$ value was considered as 352 molecules of Nuf2-sfGFP and the number of molecules of corresponding SPB protein at the SPBs were calculated accordingly:

# of Molecules of SPB protein= ($FI_{SPB\_corrected}$ x 352)/ $FI_{Nuf2\_corrected\_MEDIAN}$

2.7 SPOC Functionality Assay

To confirm functionality of endogenous Bud14 clone, SPOC functional assay is performed. WT and bud14Δ+BUD14 strains are fixated by ethanol then DAPI staining is conducted. Images of stained samples are taken via DAPI filter. For the analysis, in each image, cell number, misaligned and aligned nuclei are counted. Then misaligned percentage is calculated by the following formula: (#of cells with misaligned nuclei/total number of cells) X 10. Functionality of endogenous Bud14 clone is assessed by the calculated value.

Chapter 3: RESULTS

3.1 Bud14 is required for SPB size maintenance

Previously, Kocakaplan et al. showed that Bfa1, Bub2, and Tem1 protein levels at the Spindle Pole Bodies (SPBs) increased in *BUD14* knock-out cells (*bud14*Δ). To understand whether this phenotype results from a global change in the levels of the SPB core components, we measured mean fluorescence intensity of SPB structural proteins that belong to the inner plaque (IP: Spc29 and Spc110), central plaque (CP: Scp42), outer plaque (OP: Spc72 and Nud1) and half-bridge (HB: Sfi1) of the SPB (Figure 3.1.1 and 3.1.2). In addition, Spc97 was measured as a protein that is present at both inner and outer plaque through its interaction with both Spc72 and Spc110, which are γ-Tubulin receptors (Lin et al., 2014). Each of the selected proteins were tagged with super-folding GFP (sfGFP) at their C-terminus at their endogenous loci. The mean fluorescence intensity of each selected components was measured in wild type and *bud14*Δ cells that contained mcherry-TUB1 as a mitotic marker (see Materials and Methods for details). sfGFP fluorophore was chosen for its short maturation time.

Absence of Bud14 significantly increased FI of seven SPB proteins except Sfi1 in anaphase (Figure 3.1.1). Nonetheless, in no budded cells, presence of the phenotype *bud14*Δ varies among SPB proteins (Figure 3.1.2). Levels of IP and HF components did change due to absence of *BUD14*. Similar to the cells *bud14*Δ in anaphase, OP components Spc72, Nud1 and Spc97 FI levels were significantly elevated in no budded *bud14*Δ cells. Surprisingly, Spc42 levels were significantly decreased in no budded *bud14*Δ cells (Figure 3.1.2).

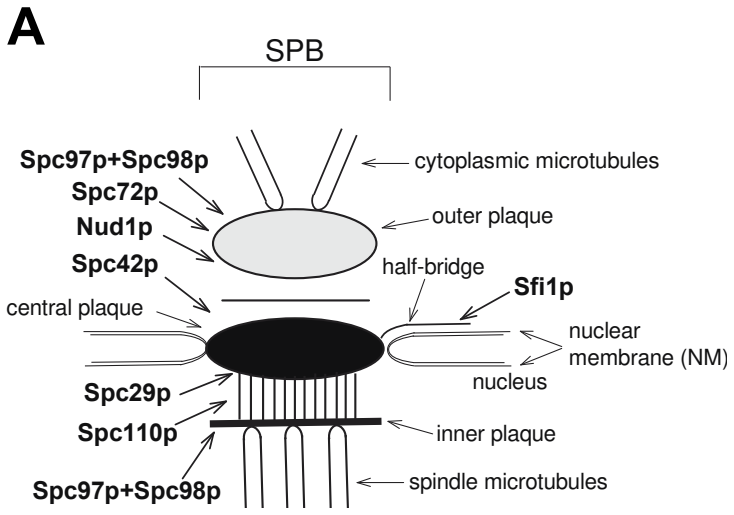

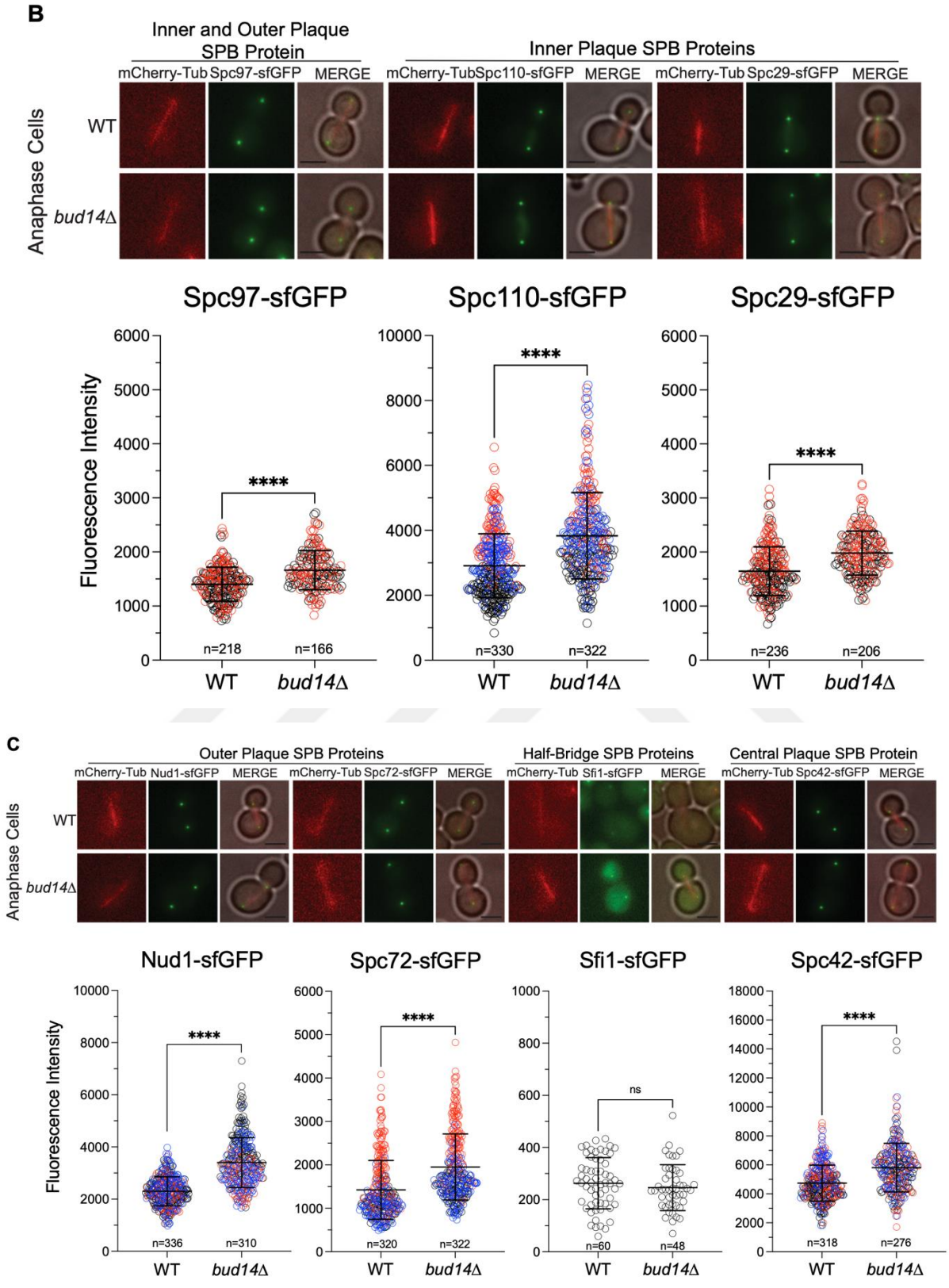

Figure 3.1.1: *BUD14* absence causes enlargement of SPB structural proteins in anaphase.

A. is representative drawing of the Spindle Pole Body (SPB). Analyzed SPB proteins were written in bold and indicated by an arrow. B. Mean fluorescence intensity of SPB-bound Spc97,

Spc110, and Spc29 in wild type (strains are SGY032, SGY026, and SGY028, respectively) and Bud14 knock out (SGY039, SGY037, and SGY038, respectively) anaphase cells (tubulin length≥3μ) were measured, and their graphs are presented. C. Mean fluorescence intensity of SPB bound Nud1, Spc72, Sfi1, and Spc42 were measured in wild type (SGY027, SGY025, SGY046, and SGY024, respectively) and Bud14 knock out (SGY034, SGY050, SGY058, and SGY048, respectively) anaphase cells (tubulin length≥3μ), and their graphs are presented. Representative image of each analyzed SPB proteins is on top of its corresponding graph. Scale bar: 3μ. Independent replicates of the FI measurements are indicated with differently colored symbols in the same graph. Sample numbers of each data set are presented on graphs. t-Test was conducted and p-values: **** P < 0.0001, ***P < 0.001, **P < 0.01, *P < 0.05.

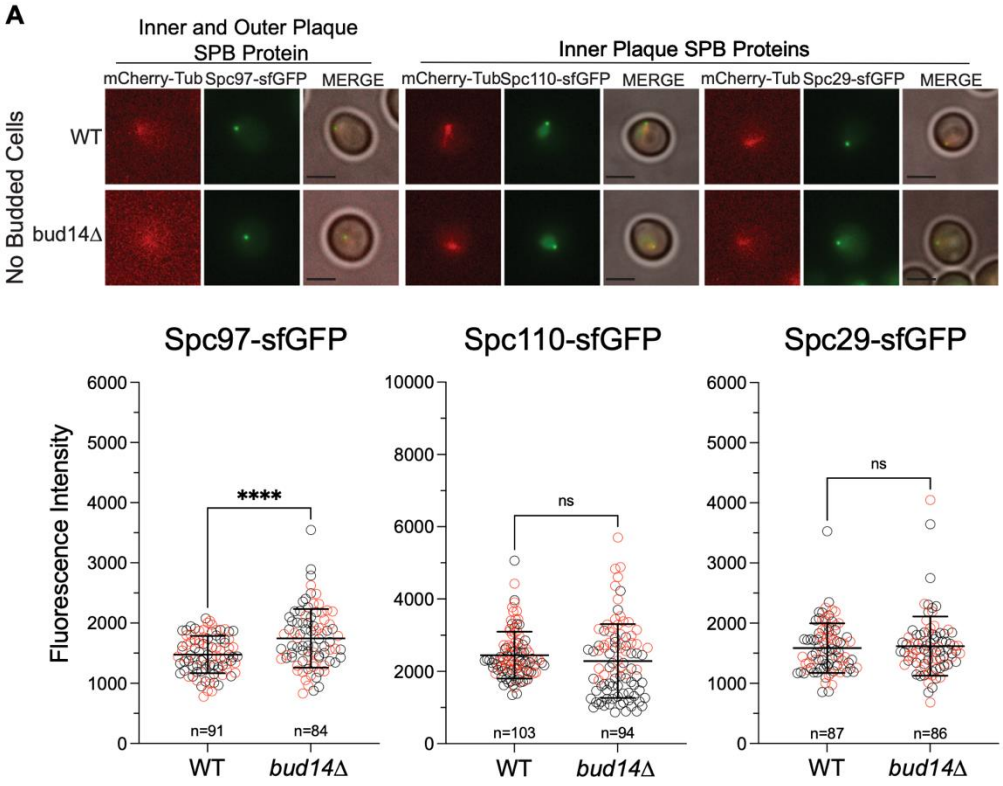

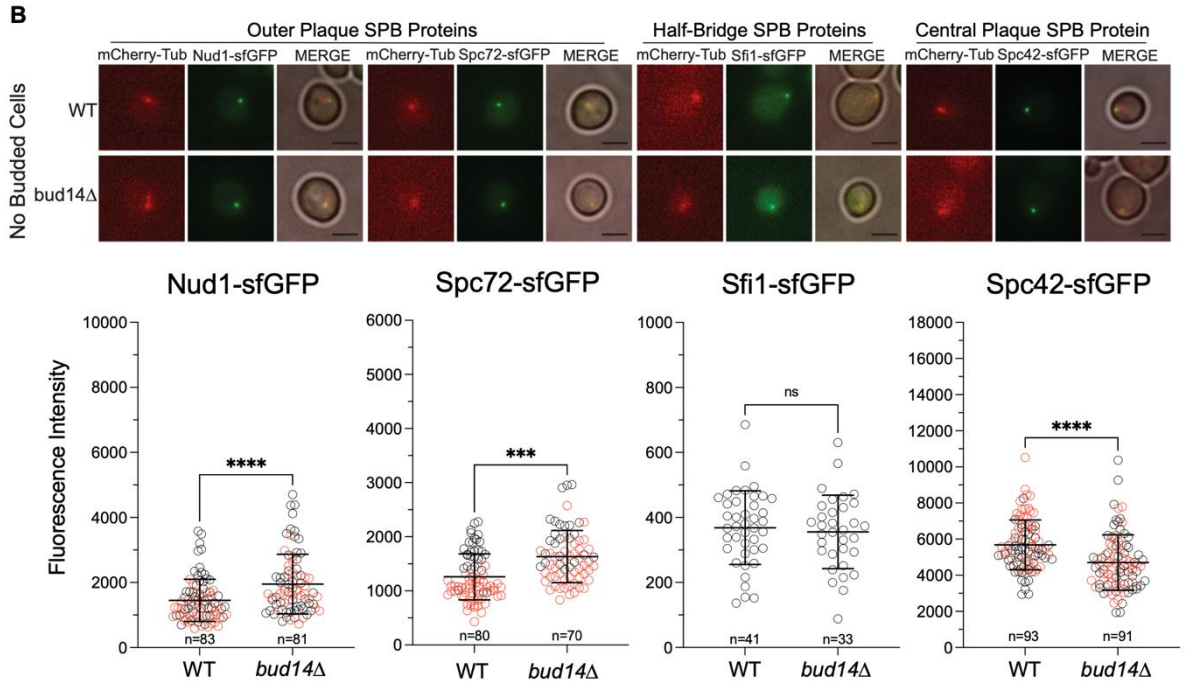

Figure 3.1.2: BUD14 absence increases levels of SPB structural proteins in no budded cells.

A. Mean fluorescence intensity of SPB-bound Spc97, Spc110, and Spc29 in wild type (strains are SGY032, SGY026, and SGY028, respectively) and Bud14 knock out (SGY039, SGY037, and SGY038, respectively) no budded cells were measured, and their graphs are presented. B. Mean fluorescence intensity of SPB-bound Nud1, Spc72, Sfi1, and Spc42 in wild type (SGY027, SGY025, SGY046, and SGY024, respectively) and Bud14 knock out (SGY034, SGY050, SGY058, and SGY048, respectively) no budded cells were measured, and their graphs are displayed. Representative image of each analyzed SPB proteins is shown at top its graph. Scale bar: 3µ. Replicates of the FI measurements are indicated with different colored circles. Sample numbers of each data set are presented on graphs. t-Test was conducted and p-values: **** $P < 0.0001$, ***$P < 0.001$, **$P < 0.01$, *$P < 0.05$.

3.2 Absence of BUD14 induces more tubulin nucleation

γ-Tubulin receptors are essential for targeting γ-Tubulins to MTOCs (Lin et al., 2014). Both γ-TuR components, Spc72, Spc110 and Spc97 demonstrated increased FI levels in *bud14*Δ anaphase cells (Figure 3.1.1). In addition, Spc72-sfGFP and Spc97 levels were significantly higher in no budded cells of the *bud14*Δ strain as well (Figure 3.1.2). Therefore, it was plausible to think microtubule nucleation capacity of SPBs also increases in *bud14*Δ cells. To verify this,

a copy of TUB1 N terminally tagged with GFP under its native promoter was integrated into the yeast genome. To observe tubulin density of the metaphase mitotic spindle, GFP-Tub1 mean FI were measured on the metaphase mitotic spindle in wild-type and *bud14*Δ strains. Same measurement was done around the spindle poles of no budded cells to observe the astral microtubule density and around SPBs of anaphase cells to observe the microtubule density emanating from the anaphase SPBs. In all cases, GFP-Tub1 mean FI were significantly higher in the *bud14*Δ then in wild type cells, supporting elevated tubulin nucleation activity of SPBs in *bud14*Δ cells. This is in line with the increased levels of Spc72, Spc110 and Spc97 observed in *bud14*Δ cells.

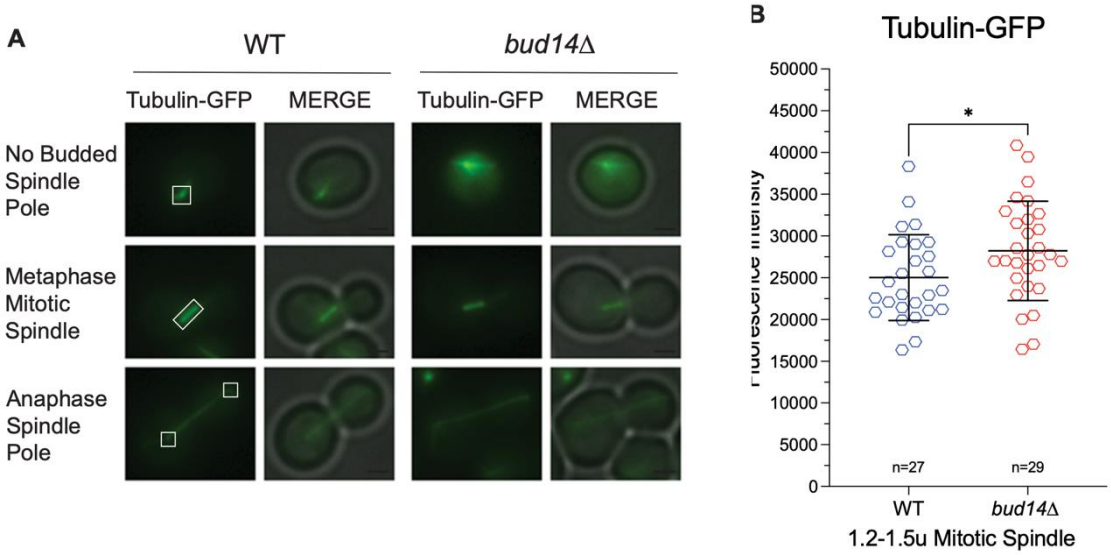

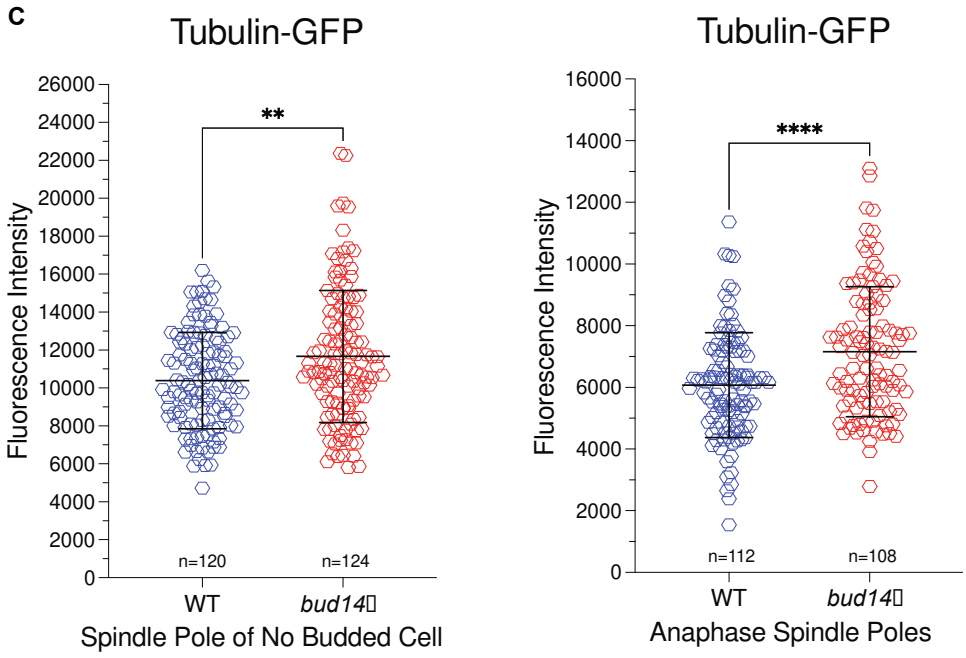

Figure 3.2.1: More tubulin is nucleated in the cells lacking Bud14.

A. Representative images of Tubulin-GFP intensity measurement experiment are shown. Cellular areas where mean fluorescence measurement of Tubulin-GFP are indicated by white rectangular boxes. Scale bar:3µ. B. Graph belongs to tubulin intensity measurement of the mitotic spindle (1.2-1.5µ length). C. Left panel shows the graph derived from tubulin intensity measurement at the pole of no budded in wild type and *bud14*Δ cells. Right panel displays tubulin intensity measurement at the anaphase poles in wild type and *bud14*Δ cells. Sample numbers of each data set are presented on graphs. For each measurement, t-Test was conducted and p-values: **** $P < 0.0001$, ***$P < 0.001$, **$P < 0.01$, *$P < 0.05$.

3.3 Bud14 exerts its effect on SPB mostly via its interaction with Glc7

Next, we asked whether Bud14 exerts its effect on SPB via its role in Glc7 regulation. To address this question, endogenous BUD14 and *bud14-F379A* mutant which cannot interact with Glc7 (Kocakaplan et al., 2021) were integrated into bud14Δ cells. Wild type and *bud14*Δ cells were also added to experimental set up for comparison. In each strain, SPB bound levels of SPB structural proteins were determined. For this purpose, endogenous *BUD14* is cloned into a genome integrating backbone, pRS405. After successfully cloning endogenous *BUD14* under its native promoter, F379A mutation is introduced into this construct (pSMG02). Expression of endogenous Bud14, wild type, and the mutant Bud14 was confirmed by western blotting after tagging Bud14 with 6HA epitope at the C-terminal (Figure 3.3.1 and 3.3.2). In Spc29, Spc42 and Spc97 tagged strains, Bud14 levels were comparable with each other. Nonetheless, F379A-Bud14 expression was lower compared to wild-type and endogenous Bud14 expressing cell lines of Spc72-sfGFP, Nud1-sfGFP and Spc110-sfGFP. Therefore, first comparable Bud14 expression levels were reached then these SPB components were individually tagged (Figure 3.3). After successfully producing 4 strains of each studied SBP protein, the experiments were performed.

SPB bound levels of Spc29, Spc42, Spc97, Spc110, Nud1 and Spc72 were measured in anaphase cells using ImageJ FI measurement tool as described previously. Different from previous measurements, a reference strain (Nuf2-sfGFP) was included in experiments (see Methods 2.4). More specifically, prior to the microscope experiment, logarithmically growing culture of each strain was individually mixed with the log phase culture of Nuf2-sfGFP containing strain to serve as a reference. Images contained reference strain and strain of interest

in the same field were acquired. Given that Nuf2-sfGFP signal at the single anaphase SPB pole corresponds to 352 Nuf2 molecule, number of molecules that corresponds to the fluorescence signal of the SPB structural proteins were calculated in a ratio metric manner (see Methods 2.4). Fluorescence ratio method is conducted in the analysis to generate more full-bodied conclusions among several SPB components. In addition, this approach provided continuity between diverse experimental set-ups.

This experimental collection displayed that wild type Bud14 expression rescued the increased levels phenotype of all seven SPB proteins in *bud14*Δ cells (Figure 3.3.1 and 3.3.2). This result supports our previous finding that Bud14 absence induces increase in the levels of measured SPB proteins.

Furthermore, expression of Bud14-F379A mutant in the *bud14*Δ cells phenocopied bud14Δ for Spc42, Spc97 and Nud1 levels at the SPBs (Figure 3.3.1 and 3.3.2). For Spc110 and Spc29, Bud14-F379A mutant expression in bud14Δ cells caused only a partial rescue phenotype.

Therefore, Bud14-Glc7 interaction is an important parameter for the size of these components: Spc29, Spc110, Spc97, Spc42 and Nud1.

Spc72 however behaved differently. Expression of endogenous and mutant Bud14 in the *bud14*Δ strains, caused similar levels of SPB bound Spc72 suggesting that Bud14 works independently from Glc7 for its effect on Spc72. These experiments altogether show that Bud14 effect on SPB structural proteins occur mostly via Glc7, except for Spc72.

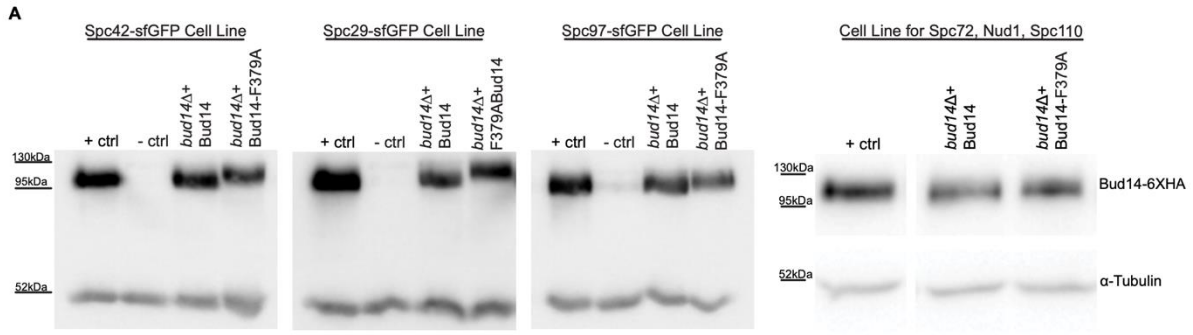

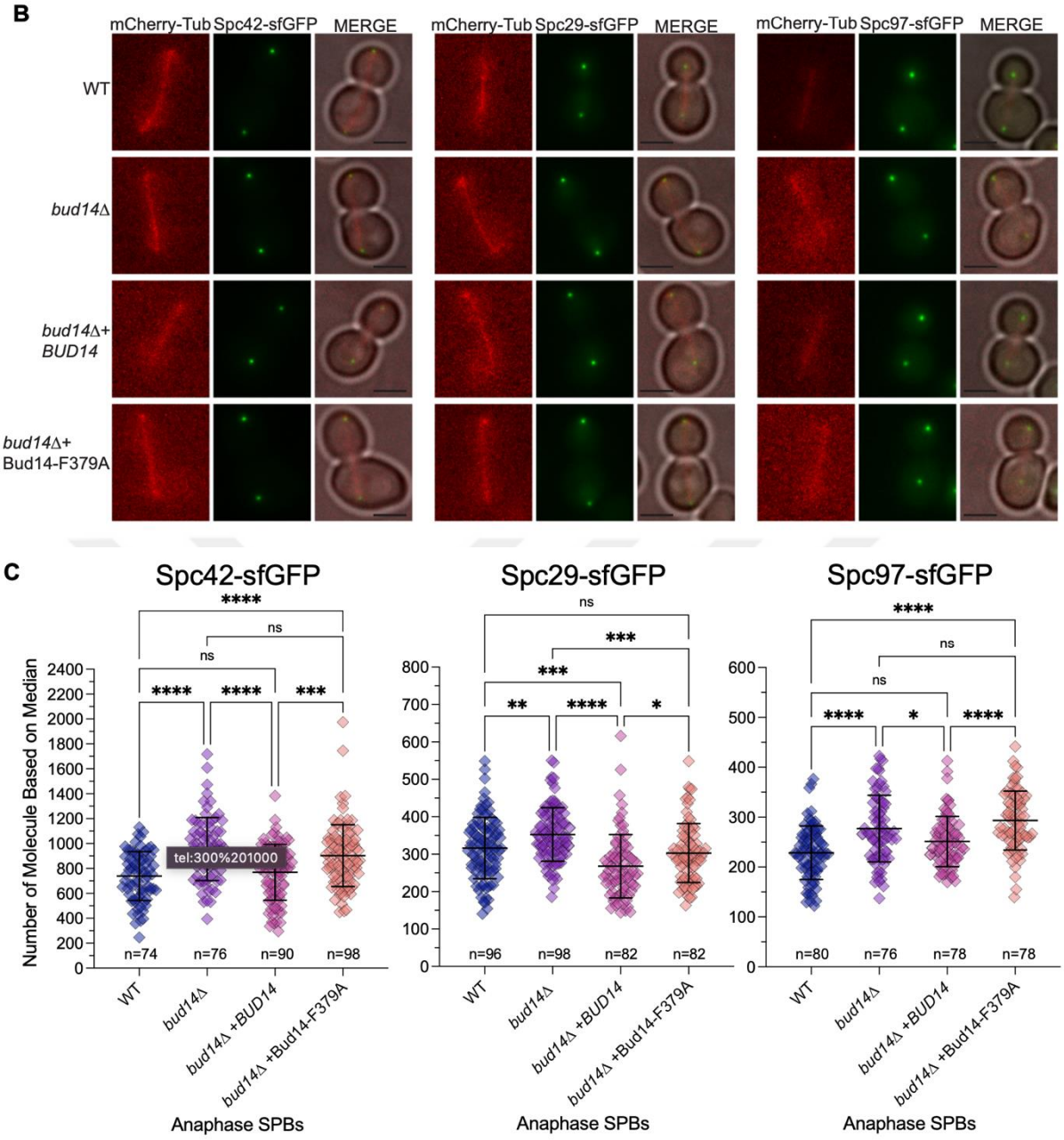
B
mCherry-Tub Spc42-sfGFP MERGE
mCherry-Tub Spc29-sfGFP MERGE
mCherry-Tub Spc97-sfGFP MERGE
WT
bud14Δ
bud14Δ+ BUD14
bud14Δ+ Bud14-F379A
C
Spc42-sfGFP
Spc29-sfGFP
Spc97-sfGFP
Number of Molecule Based on Median
tel:300%201000
n=74
n=76
n=90
n=98
n=96
n=98
n=82
n=82
n=80
n=76
n=78
n=78
WT
bud14Δ
bud14Δ +BUD14
bud14Δ +Bud14-F379A
Anaphase SPBs

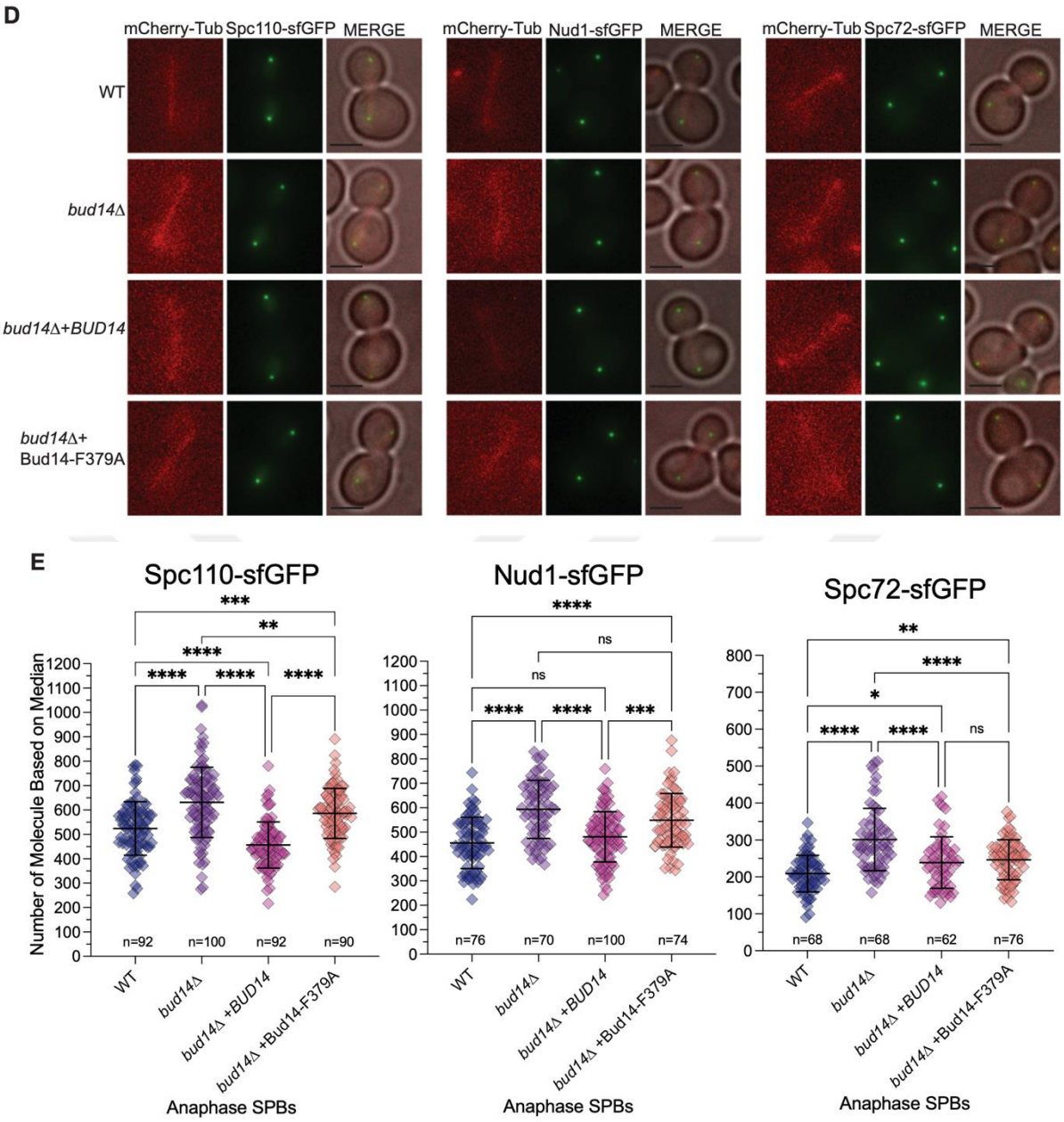

Figure 3.3.1: Bud14 exerts its effect on SPB structural proteins partly via Glc7, except for Spc72.

A. Western blotting results of endogenous Bud14 and Bud14-F379A protein levels in *bud14*Δ cells were shown. For comparison purpose, wild type Bud14 level is also shown as + control. – control is also used as experimental control. B. Representative images of fluorescence imaging of Spc42, Spc97, and Spc29. Scale bar:3μ. C. SPB bound molecule numbers of Spc42, Spc97, and Spc29 in anaphase cells (tubulin length≥3μ) of WT, *bud14*Δ, *BUD14*+*bud14*Δ, and *Bud14*-F379A+*bud14*Δ. One-way ANOVA was conducted and p-values: **** $P < 0.0001$, ***$P < 0.001$, **$P < 0.01$, *$P < 0.05$. D. Representative images of fluorescence imaging of Spc110, Nud1, and Spc72. Scale bar:3μ. E. SPB bound molecule numbers of Spc42, Spc97, and Spc29 in anaphase cells (tubulin length≥3μ) of WT, *bud14*Δ, *BUD14*+*bud14*Δ, and Bud14-

F379A+*bud14*Δ. Sample numbers of each data set are presented on graphs. One-way ANOVA was conducted and p-values: **** P < 0.0001, ***P < 0.001, **P < 0.01, *P < 0.05.

3.4 The SPB phenotype of bud14Δ is not dependent on a prolonged cell cycle phase

It has been showed that cell cycle arrest can cause size change in SPB (Jaspersen & Winey, 2004). To exclude the possibility of SPB size differences that can stem from difference between cell cycle progression of WT and *bud14*Δ cells, SPB core proteins' levels were analyzed upon cell cycle arrests. For this purpose, we exploited two different arrest condition. (1) arrest in G1 upon α-Factor treatment and (2) arrest at metaphase upon nocodazole treatment.

α-Factor is a pheromone which arrests cells in G1 to prepare them for the mating event (Bloom & Cross, 2007). Spc42, Nud1, Spc72 and Spc110 molecule numbers were measured in both α-factor arrested wild-type and *bud14*Δ populations. α-Factor mediated G1 arrest equalized Spc42, Spc72 and Nud1 molecule numbers in WT and *bud14*Δ strains. Nonetheless, α-factor treatment significantly lowered Spc110 molecule number.

Nocodazole agent interferes with tubulin polymerization thereby prevents mitotic spindle formation and arrest cells in metaphase (Wang & Burke, 1995). In this arrest state, cells have 2N DNA content and two centrosomes which are not able to make mitotic spindle. In yeast the two SPBs merge due to lack of microtubules that separate them (Wang & Burke, 1995). Nud1, Spc72 and Spc110 molecule numbers were significantly higher in nocodazole arrested *bud14*Δ strain whereas nocodazole treatment equalized Spc42 molecule numbers of wild-type and *bud14*Δ cells. These two distinct arrest phenotypes of wild-type and *bud14*Δ strains exhibits that the SPB phenotype of *bud14*Δ does not occur due to differences in cell cycle progression compared to wild type.

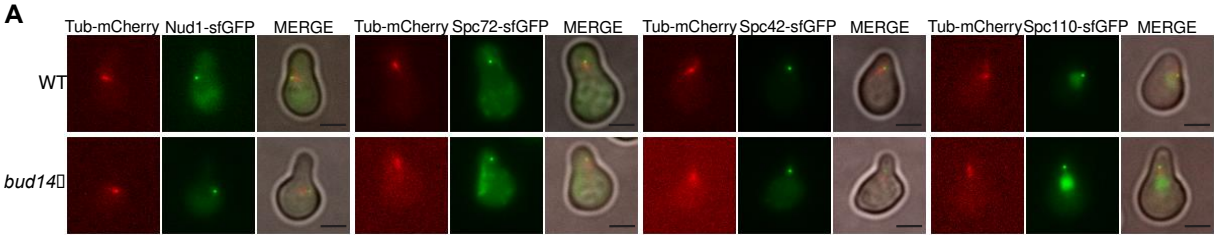

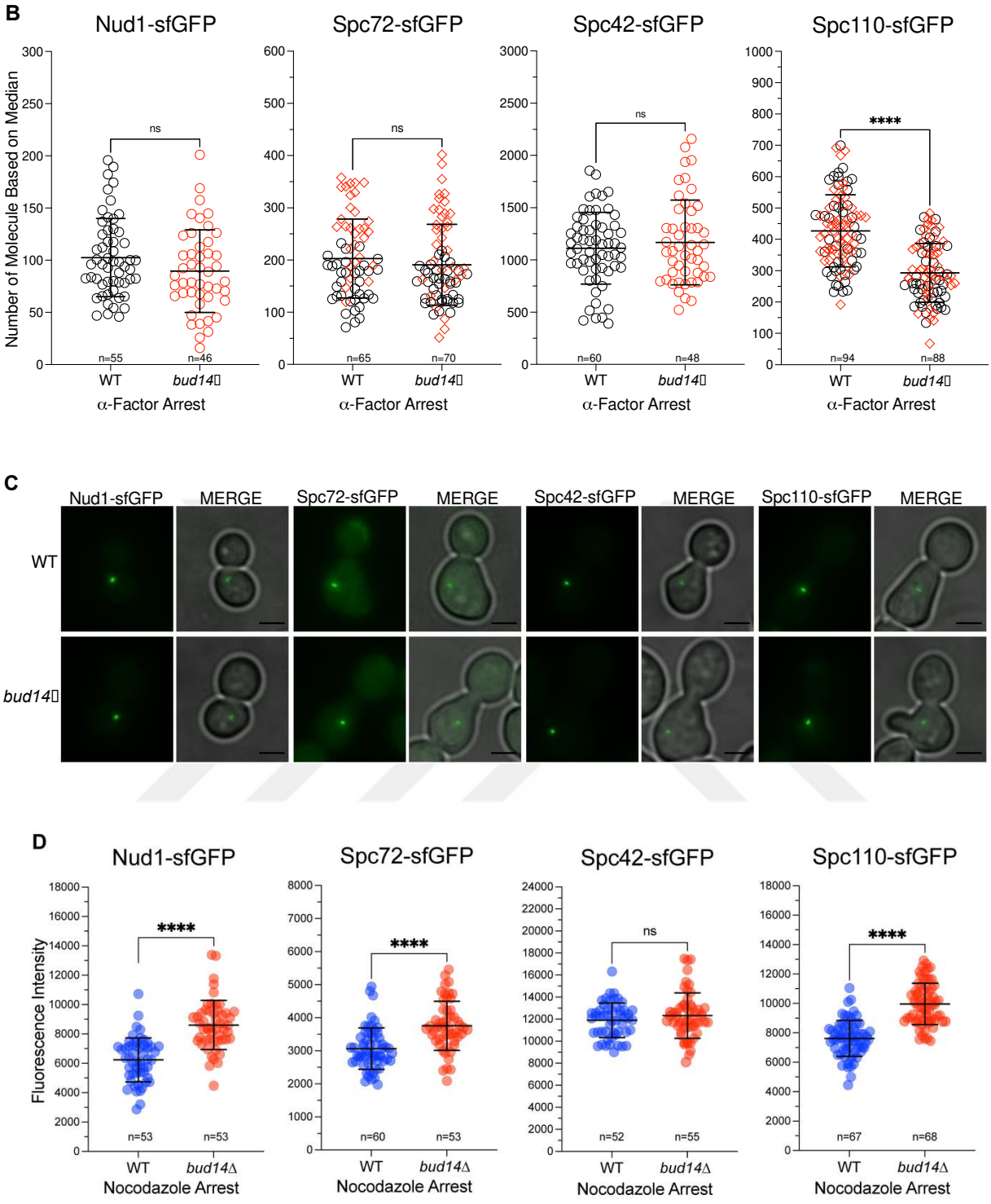

Figure 3.4.1: The SPB phenotype of *bud14*Δ is not dependent on cell cycle arrest.

A. Fluorescence microscopy representative images of each analyzed SPB proteins in α-Factor mediated G1 arrested cells. Scale bar: 3μ. B. SPB bound molecule numbers of Nud1, Spc72, Spc42, and Spc110 in α-Factor mediated G1 arrested cells of wild type and *bud14*Δ strains. C. Fluorescence microscopy representative images of each analyzed SPB proteins in nocodazole

mediated metaphase arrested cells. Scale bar: 3μ. D. SPB bound molecule numbers of Nud1, Spc72, Spc42, and Spc110 in metaphase arrested wild type and *bud14*Δ cells. Sample numbers of each data group are presented on graphs. For each comparison, t-test was conducted and p-values: **** P < 0.0001, ***P < 0.001, **P < 0.01, *P < 0.05.

*3.5 Migration patterns of Nud1, Spc72 and Spc110 on SDS-PAGE are not different in the bud14*Δ

Thus far, this research revealed that *BUD14* expression is required for SPB size maintenance and Bud14 partially employs Glc7 to govern its role. The SPB phenotype of *bud14*Δ is not driven by an cell cycle arrest and/or delay period. Several kinases like Cdc28 and phosphatases as Cdc14 modulate SPB duplication (Elserafy et al., 2014). Given that Glc7 is a phosphatase we wondered whether phosphorylation status of SPB components change in *bud14*Δ cells. To examine it, Spc72, Spc110 and Nud1 are C-terminally tagged with 6HA. Cells first synchronized with α-factor then released into fresh media containing nocodazole to obtain metaphase arrest in WT and *bud14*Δ strains. Samples were collected for total protein extraction. WT and bud14Δ cells were fixated with ethanol and stained with DAPI to calculate single nuclei and large bud percentages. Protein sample concentration was arranged with respect to cell density of each time point. Protein samples were loaded onto SDS-PAGE gel with respect to nocodazole arrest percentage of cell populations. Nevertheless, none of the analyzed proteins showed a readily detectable difference in their migration patterns in the absence or presence of *BUD14* (Figure 3.5.1). There may however be a slight difference in Spc110 migration: Spc110 had a light slow migrating smear in *bud14*Δ but not in *BUD14*, which may indicate differences in posttranslational modifications. It is important to mention that this result does not rule out the possibility of differences in phosphorylation status of other proteins analyzed, nor it clearly supports presence of differences in Spc110. More must be done to compare the phosphorylation status.

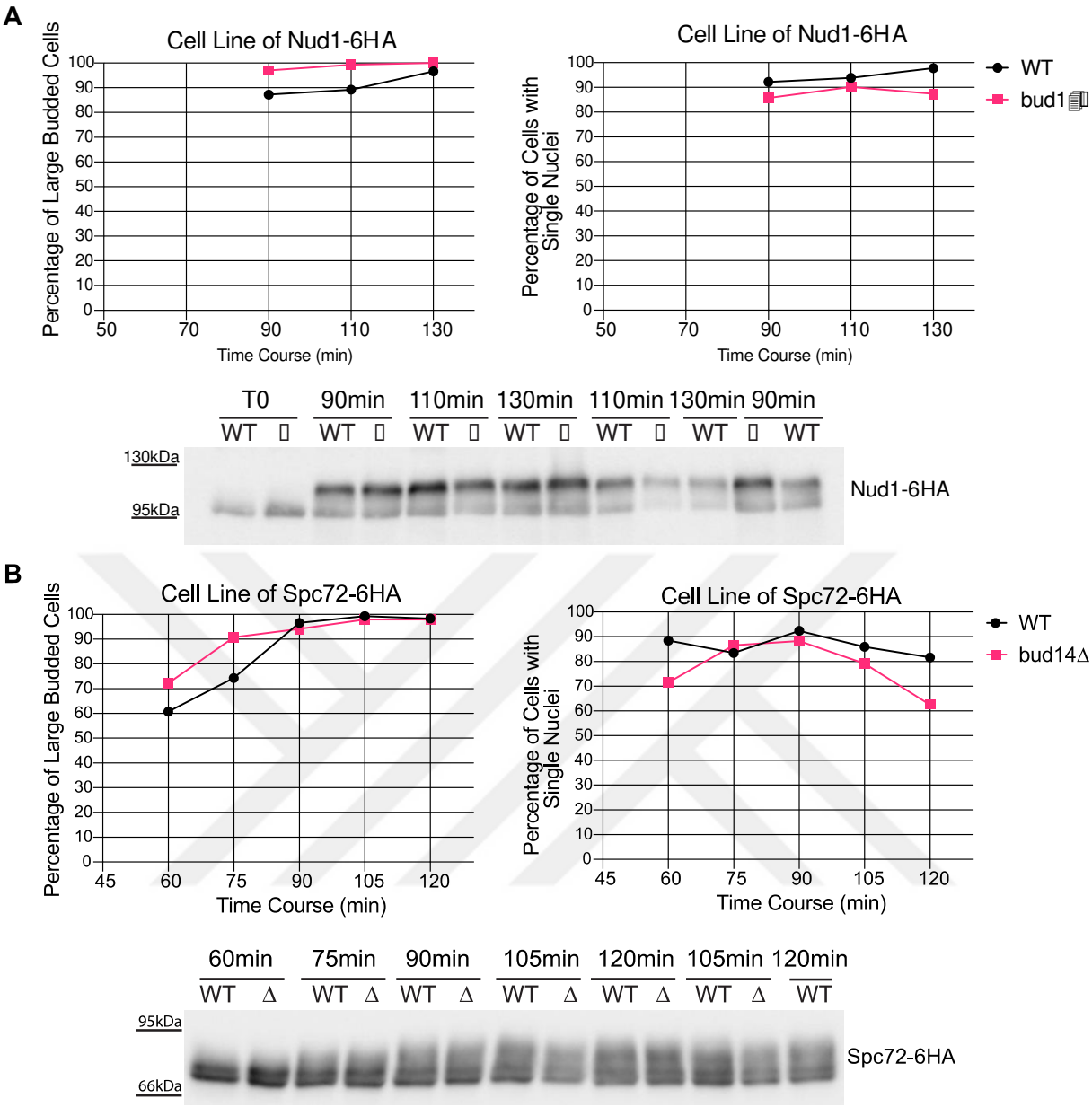
A
Cell Line of Nud1-6HA
Percentage of Large Budded Cells
Time Course (min)
Cell Line of Nud1-6HA
Percentage of Cells with Single Nuclei
Time Course (min)
WT
bud1
T0
90min
110min
130min
110min
130min
90min
WT
130kDa
95kDa
Nud1-6HA
B
Cell Line of Spc72-6HA
Percentage of Large Budded Cells
Time Course (min)
Cell Line of Spc72-6HA
Percentage of Cells with Single Nuclei
Time Course (min)
WT
bud14Δ
60min
75min
90min
105min
120min
105min
120min
WT
Δ
95kDa
66kDa
Spc72-6HA

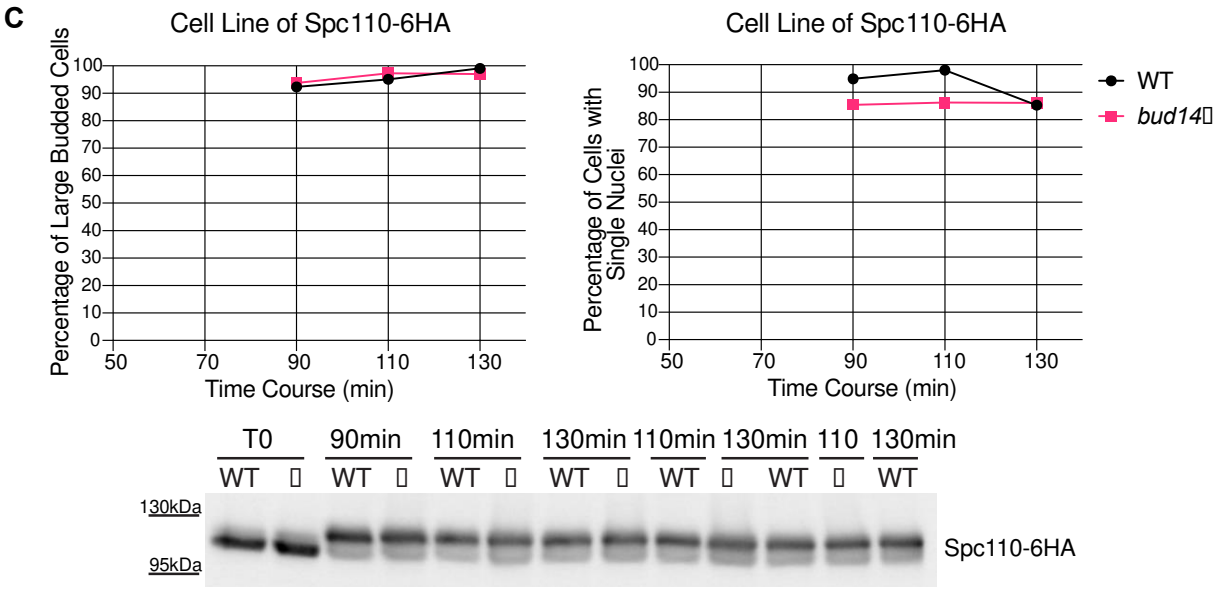

Figure 3.5.1: Spc42, Spc72, and Spc110 did not show readily detectable difference in their migration patterns on SDS-PAGE in the Bud14 absence.

A. Percentage of cells with large bud and percentage of cells with single nuclei, respectively, in wild type and *bud14*Δ. Western blotting of Spc42-6HA on 8% SDS-PAGE is presented at the below. B. Percentage of cells with large bud and percentage of cells with single nuclei, respectively, in wild type and *bud14*Δ. Western blotting of Spc72-6HA on 10% SDS-PAGE is shown at the below. C. Percentage of cells with large bud and percentage of cells with single nuclei, respectively, in wild type and *bud14*Δ. Western blotting of Spc110-6HA on 6% SDS-PAGE is exhibited at the below.

3.6 The Spc110 and Spc72 phenotype of bud14Δ emerges after mitotic spindle formation

It has been demonstrated that *BUD14* absence elevates molecule numbers of six SPB components. To understand when SPB protein level increase in the absence of Bud14, time-course assays was performed for Spc110 and Spc72. These SPB components were selected since they are γ-TuCRs which resides at distinct plaques (Jaspersen & Winey, 2004). First, WT and *bud14*Δ cell populations were arrested by α-factor and then released from G1 arrest to allow synchronious cell cycle progression. Then samples were collected with 15 minutes apart for 2 hours. Collected samples were PFA fixated for fluorescence cell imaging. Tubulin length was used to define cell cycle phases. Three indexes were calculated: budded cell percentage, percentage of cells with separated SPB, and anaphase cell percentage. In both time course assays (Figure 3.6 A and B), the *bud14*Δ strain displayed noticeable delay in anaphase entrance. This might be the time window when the phenotype arises.

In line with our previous result, Spc110 molecule number drastically lowered in both *bud14*Δ and Bud14- F379A expressing strains upon α-mediated G1 arrest (Figure 3.6.1). Nonetheless, in those strains, Spc110 molecule number rose to the wild-type level and exceed it right after SPB duplication and mitotic spindle formation (defined by 0.2-1.2μ length). The increased number of molecules in both strains remained significant throughout the cell division (Figure 3.6.1).

As for Spc72, equalized Spc72 molecule numbers diverged at around the metaphase (1.2-2.5μ length) thus Spc72 phenotype of *bud14*Δ was established at a later cell cycle stage for Spc72 than for Spc110. Increased Spc72 level persisted throughout the cycle and in the next cycle (Figure 3.6.2, no budded cells).

Taken together, Spc72 phenotype aroused later than Spc110 phenotype of *bud14*Δ. The major difference between Spc72 and Spc110 is their subcellular localization; Spc72 localizes at the cytoplasmic face whereas Spc110 localizes at nucleoplasmic face of the SPB. The timing of incorporation of Spc72 and Spc110 at the SPB or the discrepancy in dependency of Spc72 and Spc110 phenotype of bud14Δ cells on Glc7-Bud14 binding may account for this time difference.

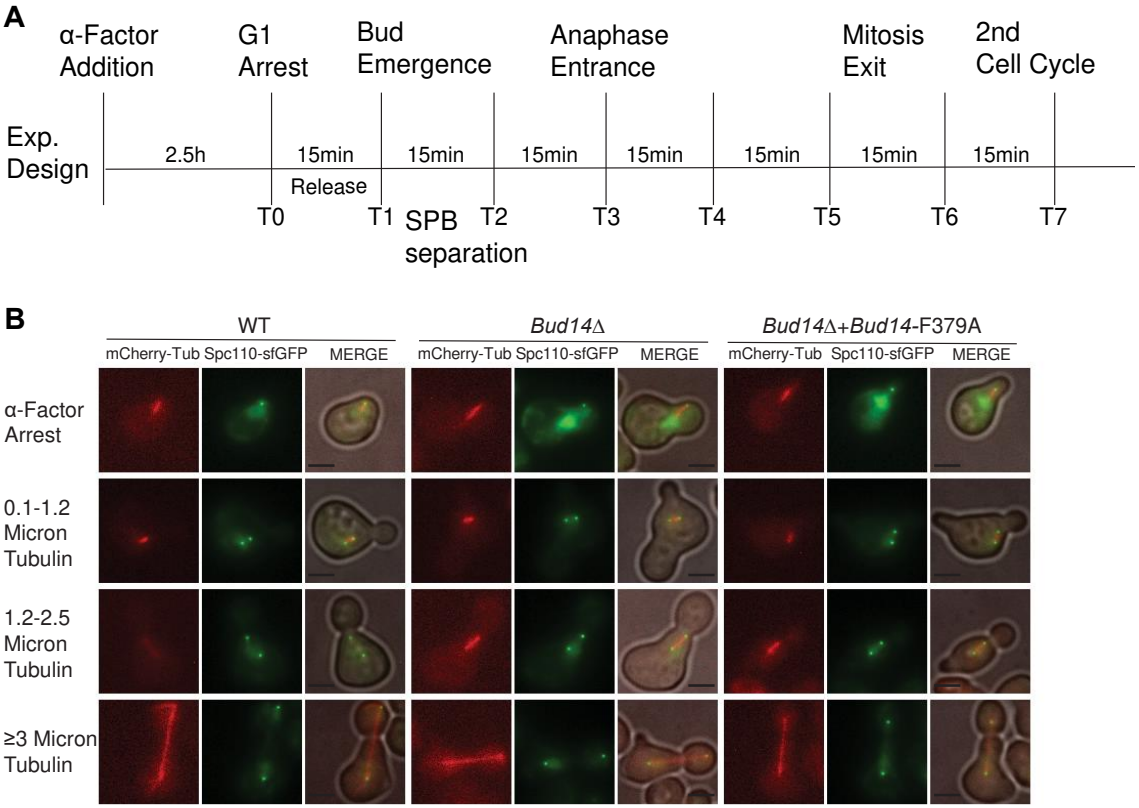

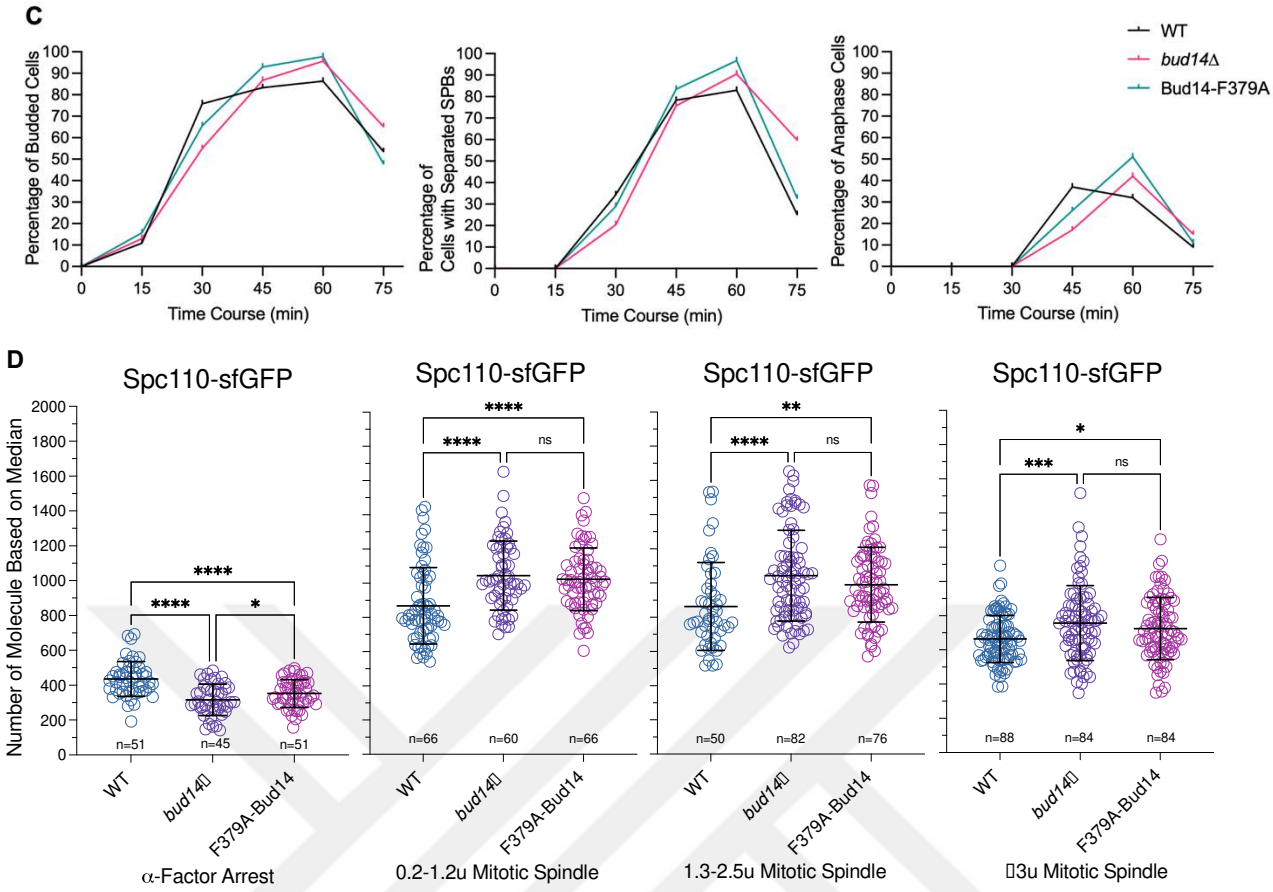

Figure 3.6.1: The Spc110 phenotype of *bud14*Δ emerges after SPB separation.

A. Experimental design of sample collection over 2 hours are depicted. Each collected sample was fixated by 8% PFA solution. B. Fluorescence microscopy representative images of Spc110-sfGFP in G1 arrested cells, cells with newly separated SPBs (0.2-1.2µ tubulin length), metaphase cells (1.3-2.5µ tubulin length), and anaphase cells (≥3µ tubulin length) of WT, *bud14*Δ, and F379A-Bud14 expressing strains. Scale bar: 3µ. C. Percentage of budded cells, percentage of cells with separated SPBs, and anaphase cell percentage in wild type and *bud14*Δ, and *bud14*Δ+Bud14-F379A strains over 75 minutes. D. SPB bound Spc110 molecule numbers measured in G1 arrested cells, cells with newly separated SPBs (0.2-1.2µ tubulin length), metaphase cells (1.3-2.5µ tubulin length), and anaphase cells (≥3µ tubulin length) of WT, *bud14*Δ, and *bud14*Δ+Bud14-F379A strains. Sample numbers of each data group are presented on graphs. For each graph, one-way ANOVA was conducted and p-values: **** $P < 0.0001$, ***$P < 0.001$, **$P < 0.01$, *$P < 0.05$.

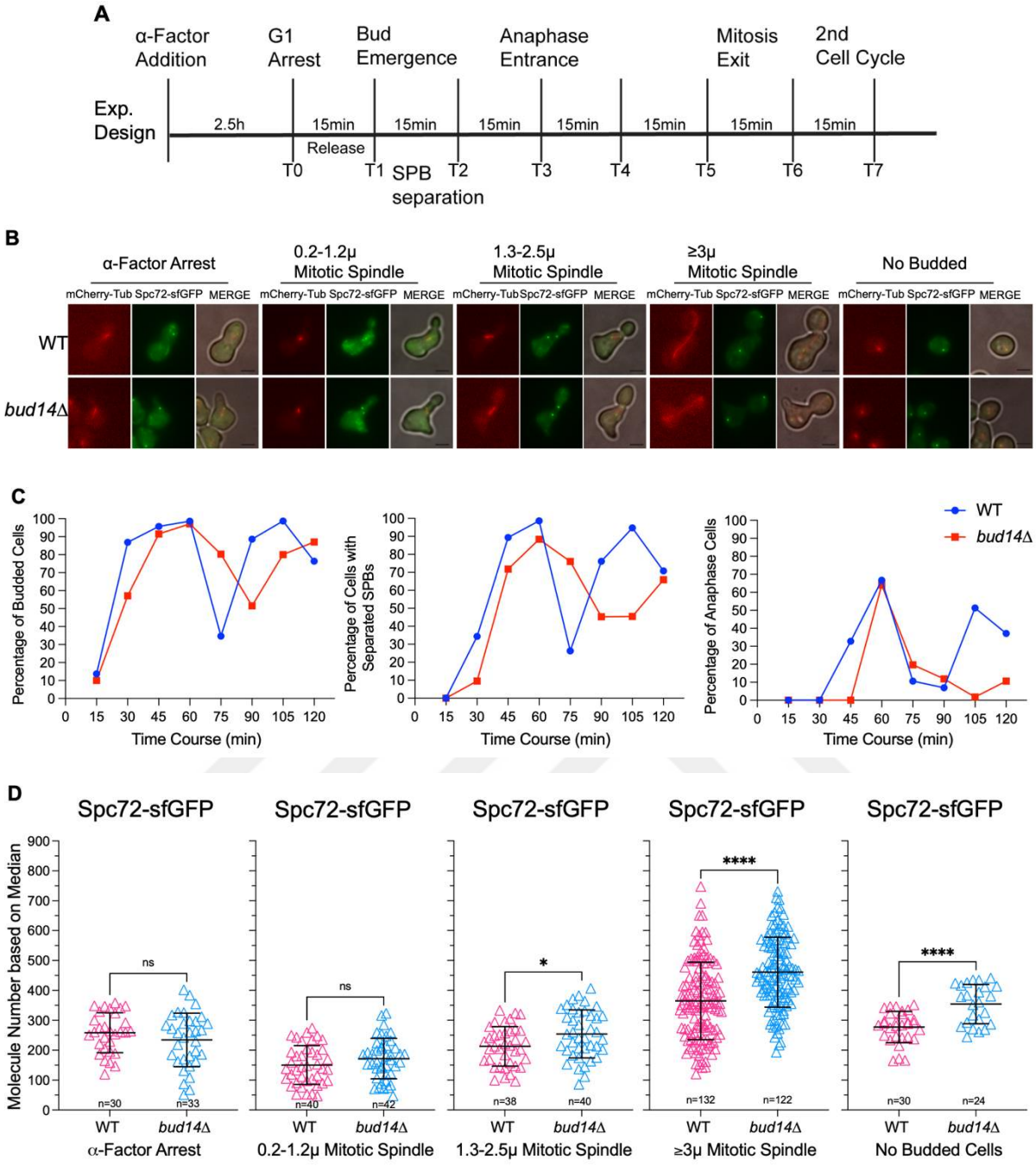

Figure 3.6.2: The Spc72 phenotype of *bud14*Δ of emerges in metaphase.

A. Experimental design of sample collection over 2 hours are depicted. Each collected sample was fixated by 8% PFA solution. B. Fluorescence microscopy representative images of Spc72-sfGFP in G1 arrested cells, cells with newly separated SPBs (0.2-1.2μ tubulin length), metaphase cells (1.3-2.5μ tubulin length), anaphase cells (≥3μ tubulin length), and the next cell cycle no budded cells of WT, and *bud14*Δ. Scale bar: 3μ. C. Percentage of budded cells, percentage of cells with separated SPBs, and anaphase cell percentage in wild type and *bud14*Δ

populations over 2 hours. D. SPB bound Spc72 molecule numbers measured in G1 arrested cells, cells with newly separated SPBs (0.2-1.2μ tubulin length), metaphase cells (1.3-2.5μ tubulin length), anaphase cells (≥3μ tubulin length), and the next cell cycle no budded cells of WT, and *bud14*Δ. Sample numbers of each data group are presented on graphs. For each comparison, t-test was performed and p-values: **** $P < 0.0001$, ***$P < 0.001$, **$P < 0.01$, *$P < 0.05$.

*3.7 Absence of functional Cdc14 does not abolish the Spc72 phenotype of bud14*Δ

Cdc14 regulates the MEN components at SPBs to execute mitotic exit. Cdc14 localizes to the SPB upon its release from the nucleolus during early metaphase (Pereira et al., 2002). Idil Kirdok from our lab demonstrated that while in WT cells Cdc14 localizes to SBPs at the anaphase onset and stays there till telophase, in *bud14*Δ cells, Cdc14 localization to the SPBs persists also in the next G1 (Kirdok, submitted MSc. thesis, 2022). Since absence of *BUD14* changes Cdc14 localization pattern at the SPBs, involvement of Cdc14 in the *bud14*Δ SPB size phenotype was investigated. For this purpose, Cdc14 temperature sensitive mutant (*cdc14-ts*) was utilized. First, strains were arrested at G1, then shifted to the restrictive temperature for *cdc14-ts.* pFA fixated samples were collected 15 minutes apart starting from G1 arrest (see Figure3.7 for experimental design). Pole to pole distance was used as a cell cycle indicator. Based on this distance, anaphase percentage of populations were calculated over 2 hours (Figure 3.7.1 C.). Spc72-sfGFP levels of WT, *bud14*Δ, *cdc14-ts*, *cdc14-ts*/*bud14*Δ were equalized at the G1 arrested SPBs. After 1 hour of release, (T4), cell populations experienced first anaphase. At anaphase the Spc72 phenotype of *bud14*Δ was observed (WT vs *bud14*Δ in Figure 3.7.1 E.). Unfunctional Cdc14 caused noticeable but unsignificant increase in WT Spc72-sfGFP level (Figure 3.7.1). *BUD14* absence in *cdc14-ts* cells led a significant upsurge in Spc72-sfGFP FI compared to other 3 strains (Figure 3.7.1). This suggests that Cdc14 loss of function in mitosis does not interfere with the increased Spc72 levels in *bud14*Δ.

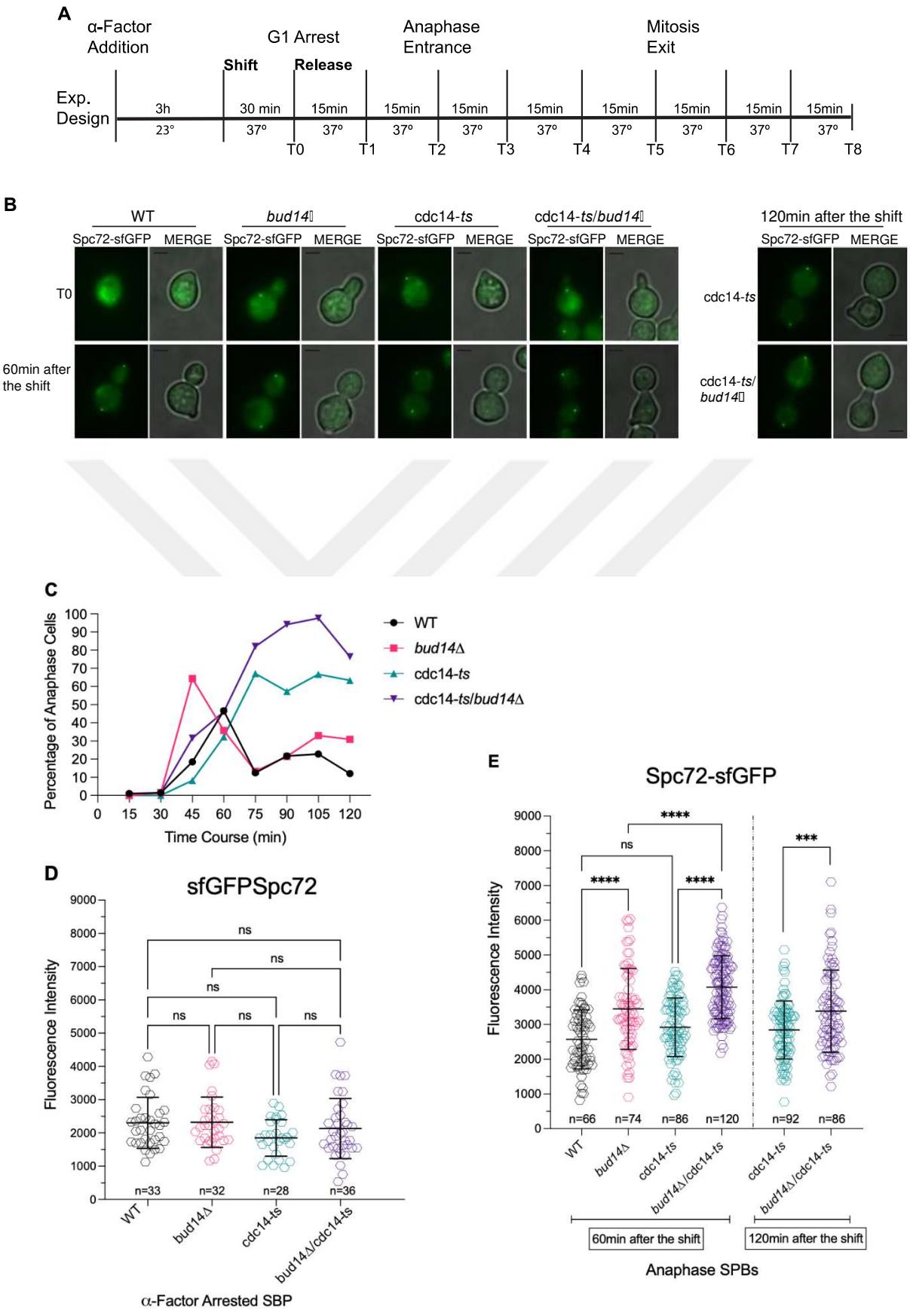
A
α-Factor Addition
G1 Arrest
Anaphase Entrance
Mitosis Exit
Shift
Release
Exp. Design
3h
30 min
15min
15min
15min
15min
15min
15min
15min
23°
37°
37°
37°
37°
37°
37°
37°
37°
T0
T1
T2
T3
T4
T5
T6
T7
T8
B
WT
bud14Δ
cdc14-ts
cdc14-ts/bud14Δ
120min after the shift
Spc72-sfGFP
MERGE
T0
60min after the shift
cdc14-ts
cdc14-ts/bud14Δ
C
Percentage of Anaphase Cells
Time Course (min)
WT
bud14Δ
cdc14-ts
cdc14-ts/bud14Δ
D
sfGFPSpc72
Fluorescence Intensity
ns
n=33
n=32
n=28
n=36
WT
bud14Δ
cdc14-ts
bud14Δ/cdc14-ts
α-Factor Arrested SBP
E
Spc72-sfGFP
Fluorescence Intensity
****
ns
***
n=66
n=74
n=86
n=120
n=92
n=86
60min after the shift
120min after the shift
Anaphase SPBs

Figure 3.7.1: Loss of Cdc14 function in mitosis does not abolish the Spc72 phenotype of *bud14*Δ.

A. Experimental design of sample collection over 2 hours are depicted. Each collected sample was fixated by 8% PFA solution. B. Fluorescence microscopy representative images of Spc72-sfGFP in G1 arrested cells (T0), T4 anaphase cells (0.2-1.2µ pole-to-pole distance), and anaphase arrested cells (≥3µ pole-to-pole distance). Scale bar: 3µ. C. Percentage anaphase cells in WT, *bud14*Δ, *cdc14-ts*, and *cdc14-ts/bud14*Δ strains over 2 hours. D. SPB bound Spc72 levels measured in G1 arrested cells of WT, *bud14*Δ, *cdc14-ts*, and *cdc14-ts/bud14*Δ. D. Spc72 levels measured at T4 anaphase SPBs of WT, *bud14*Δ, *cdc14-ts*, and *cdc14-ts/bud14*Δ and at T8 anaphase arrested cells of *cdc14-ts*, and *cdc14-ts/bud14*Δ. Sample numbers of each data group are presented on graphs. In each graph, one-way ANOVA was performed and p-values: **** $P < 0.0001$, ***$P < 0.001$, **$P < 0.01$, *$P < 0.05$.

3.8 Absence of Cdc14 function in G1 rescues the effect of bud14Δ on Spc72

Previously, we showed that the Spc72 phenotype of *bud14*Δ was eminent during *cdc14-ts* mediated anaphase arrest. Our experiment set-up however could not rule out any potential Cd14 role in the early stages of the cell cycle. We sought to analyze effect of early Cdc14 function on *bud14*Δ by forcing anaphase arrested cells enter to the next cell cycle. Therefore, we utilized overexpression of undegradable *SIC1* (Cross et al., 2007).

Firstly, log phase cultures *cdc14-ts* and *cdc14-ts/bud14*Δ bearing Gal1-*SIC1* plasmid were shifted to the restrictive temperature. This was done in raffinose containing media to avoid Gal1 induction. In line with the previous result, *cdc14-2/bud14*Δ cells had more SPB bound Spc72 levels at this time point (Figure 3.8.1, T0). Then galactose was added to anaphase arrested cultures to induce *SIC1* overexpression. Overexpression of *SIC1* decreases mitotic CDK activity, bypassing the Cdc14 requirement for mitotic exit of cells (Elserafy et al., 2014). Cells exited mitosis and started re-budding 30 min after galactose addition. Nonetheless, at a later time point they got arrested as a large budded cells with single SBP (Elserafy et al., 2014) (Figure 3.8.1 B). Remarkably, forceful entry to G1 via *SIC1* overexpression abolished the Spc72 phenotype of *bud14*Δ in *cdc14-ts* cells at restrictive temperature (Figure 3.8.1). Of importance, this was Cdc14-dependent, as stable *SIC1* overexpression did not affect the Spc72 phenotype of *bud14*Δ cells with functional Cdc14 (Figure 3.8.1 E).

This result suggests that increased Spc72 levels observed in *bud14*Δ cells requires that a functional Cdc14 in G1. Therefore, persistent Cdc14 SPB localization in *bud14*Δ cells may account for the raise in Spc72 levels in *bud14*Δ cells.

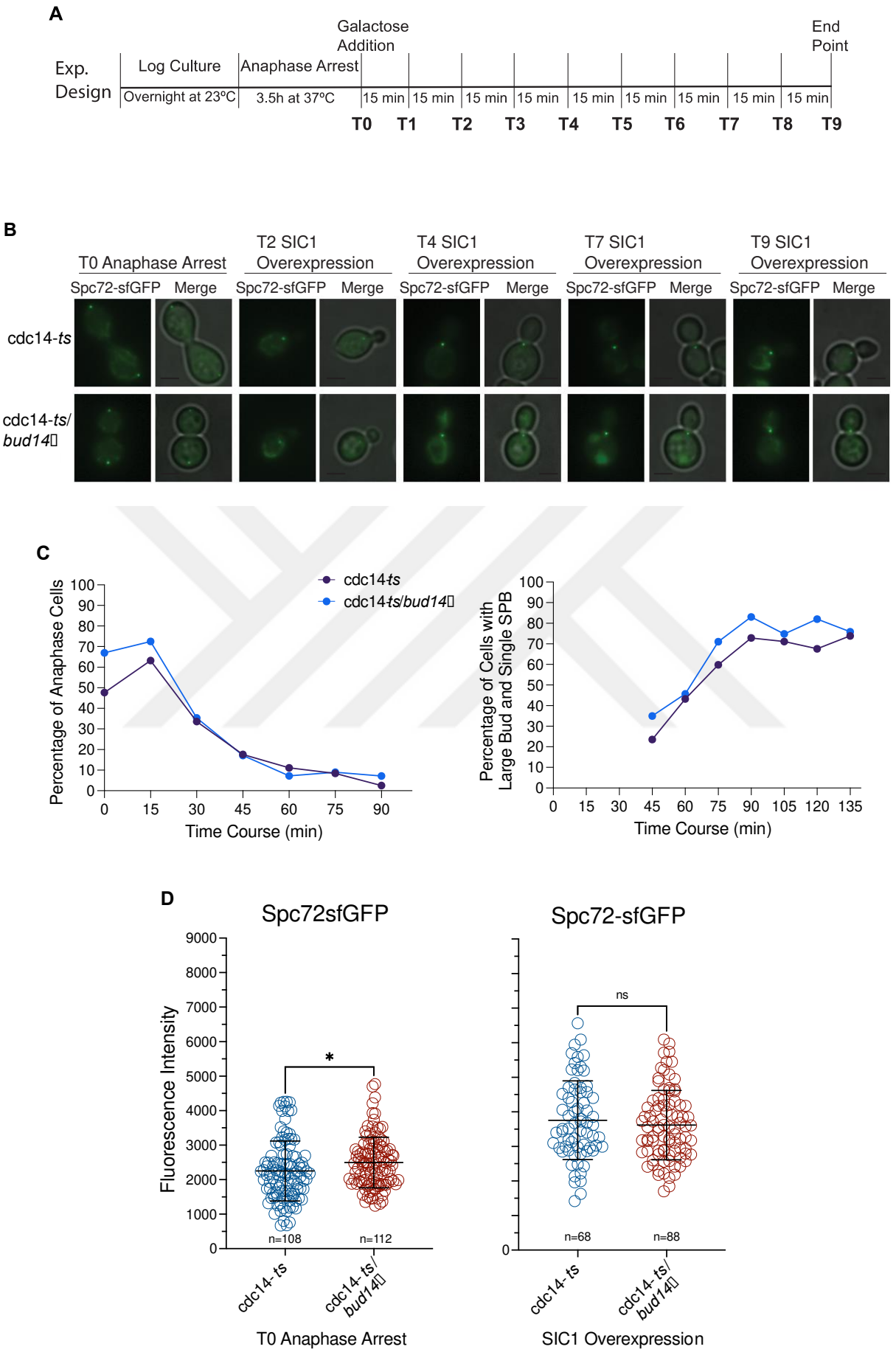
A
Galactose Addition
End Point
Exp. Design
Log Culture
Anaphase Arrest
Overnight at 23ºC
3.5h at 37ºC
15 min
T0 T1 T2 T3 T4 T5 T6 T7 T8 T9
B
T0 Anaphase Arrest
T2 SIC1 Overexpression
T4 SIC1 Overexpression
T7 SIC1 Overexpression
T9 SIC1 Overexpression
Spc72-sfGFP Merge
cdc14-ts
cdc14-ts/bud14Δ
C
cdc14ts
cdc14ts/bud14Δ
Percentage of Anaphase Cells
Time Course (min)
Percentage of Cells with Large Bud and Single SPB
Time Course (min)
D
Spc72sfGFP
Spc72-sfGFP
Fluorescence Intensity
*
ns
n=108
n=112
n=68
n=88
cdc14-ts
cdc14-ts/bud14Δ
T0 Anaphase Arrest
SIC1 Overexpression

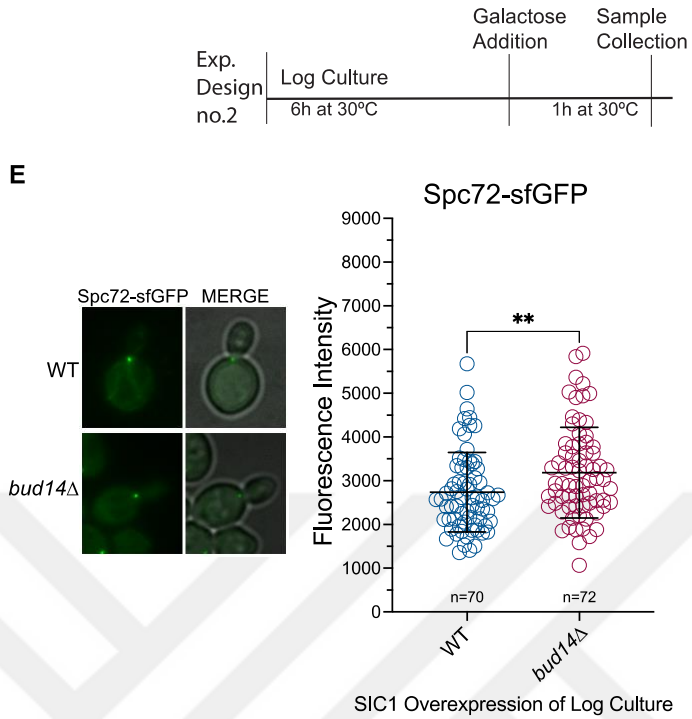

Figure 3.8.1: Forceful entry into G1 with unfunctional Cdc14 abolishes Spc72 phenotype of *bud14*Δ.

A. Experimental design of sample collection over 2 hours is depicted. Each collected sample was fixated by 8% PFA solution. B. Fluorescence microscopy representative images of Spc72-sfGFP in *cdc14-ts*, and *cdc14-ts/bud14*Δ cells at T0, T2, T4, T7, and T9. Scale bar: 3µ. C. Percentage anaphase cells and percentage of cells with large bud and single nuclei in *cdc14-ts*, and *cdc14-ts/bud14*Δ populations. D. SPB bound Spc72 levels measured in anaphase arrested cells (T0) and *SIC1* overexpressing (large bud with single nuclei) cells of *cdc14-ts*, and *cdc14-ts/bud14*Δ. E. For comparison purpose, *SIC1* was overexpressed in log cultures of WT and *bud14*Δ and samples were fixated by 8% PFA solution. Experimental set-up is represented at the top of part E. Representative microscopy image and Spc72-sfGFP levels in *SIC1* overexpressing cells of WT and *bud14*Δ are displayed at the bottom of the figure. Sample numbers of each data group are presented on graphs. For each comparison, t-test was performed and p-values: **** $P < 0.0001$, ***$P < 0.001$, **$P < 0.01$, *$P < 0.05$.

3.9 Absence of Cdc14 function during mitosis rescues the Spc110 phenotype observed in bud14Δ cells

Next, we investigated Cdc14 effect on altered Spc110 levels at the SPBs of *bud14*Δ cells. First, *cdc14-ts* and *cdc14-ts/bud14*Δ cells were arrested in G1 via α-factor and then they were released from the arrest. As in previous experiment, α-factor mediated G1 arrest resulted in Spc110 decrease in *cdc14-ts*/*bud14*Δ strain. Nonetheless, *cdc14-ts*/*bud14*Δ cells displayed similar Spc110 levels as *cdc14-ts* cells during the cell cycle until late anaphase. This result indicates that in the Bud14 absence, cell requires functional Cdc14 for Spc110 size maintenance. Altogether, our research suggests that Cdc14 and Bud14 may work in the same pathway in SPB size maintenance.

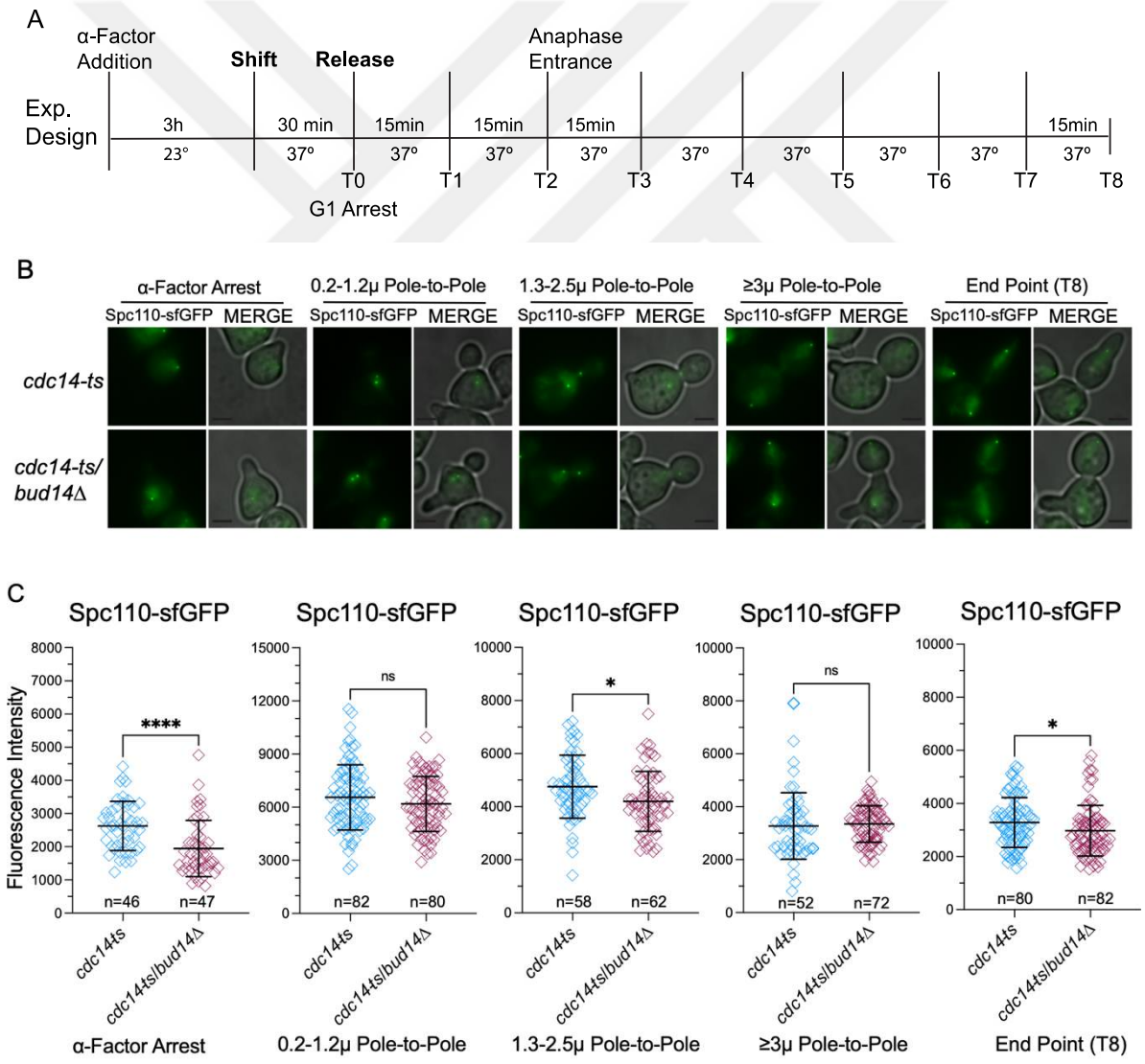

Figure 3.9.1: Lack of functional Cdc14 rescues the Spc110 phenotype observed in *bud14*Δ cells during mitosis.

A. Experimental design of sample collection over 135 minutes is depicted. Each collected sample was fixated by 8% PFA solution. B. Fluorescence microscopy representative images of Spc110-sfGFP in G1 arrested cells, cells with newly separated SPBs (0.2-1.2µ pole-to-pole distance), metaphase cells (1.3-2.5µ pole-to-pole distance), anaphase cells (≥3µ pole-to-pole distance), and anaphase arrested cells, at T8, of *cdc14-ts*, and *cdc14-ts/bud14*Δ strains. Scale bar: 3µ. C. SPB bound Spc110 levels measured in G1 arrested cells, cells with newly s separated SPBs (0.2-1.2µ pole-to-pole distance), metaphase cells (1.3-2.5µ pole-to-pole distance), anaphase cells (≥3µ pole-to-pole distance), and anaphase arrested cells, at T8, of *cdc14-ts*, and *cdc14-ts/bud14*Δ strains. Sample numbers of each data group are presented on graphs. For each comparison, t-test was performed and p-values: **** $P < 0.0001$, ***$P < 0.001$, **$P < 0.01$, *$P < 0.05$.

*3.10 The Spc110 phenotype of bud14*Δ *is independent from impaired Kelch-Bud14 function*

Bud14 forms a stoichiometric complex with two conserved Kelch proteins: Kel1 and Kel2 (Gould et al., 2014) (Figure 3.10.1 A). In several organisms, Kelch proteins are responsible for the cell morphogenesis. Bud14-Kel1-Kel2 complex prevents actin depolymerization via Bud14 modulated Bnr1 inactivation (Gould et al., 2014). Impaired Kelch-Bud14 complex causes malfunctions in cytokinesis and secretory vesicle trafficking (Gould et al., 2014). To evaluate Kelch-Bud14 role in SPB size maintenance, Spc110-sfGFP levels were measured in three strains: WT, *bud14*Δ and *kel1*Δ*kel2*Δ. Spc110-sfGFP levels are measured in various circumstances: α-factor mediated G1 arrest, nocodozole driven metaphase arrest, and anaphase of log culture. If Kelch-Bud14 is crucial for Spc110 level regulation by Bud14, we would except *kel1*Δ*kel2*Δ to phenocopy *bud14*Δ.

Whereas deletion of *KEL1*and *KEL2* did not change Spc110 FI levels in any condition (Figure 3.10.1). Altogether, we conclude that Bud14 is involved in maintenance of Spc110 levels at the SPBs independently from its function in actin regulation but dependently on Glc7 (Figure 3.2.1).

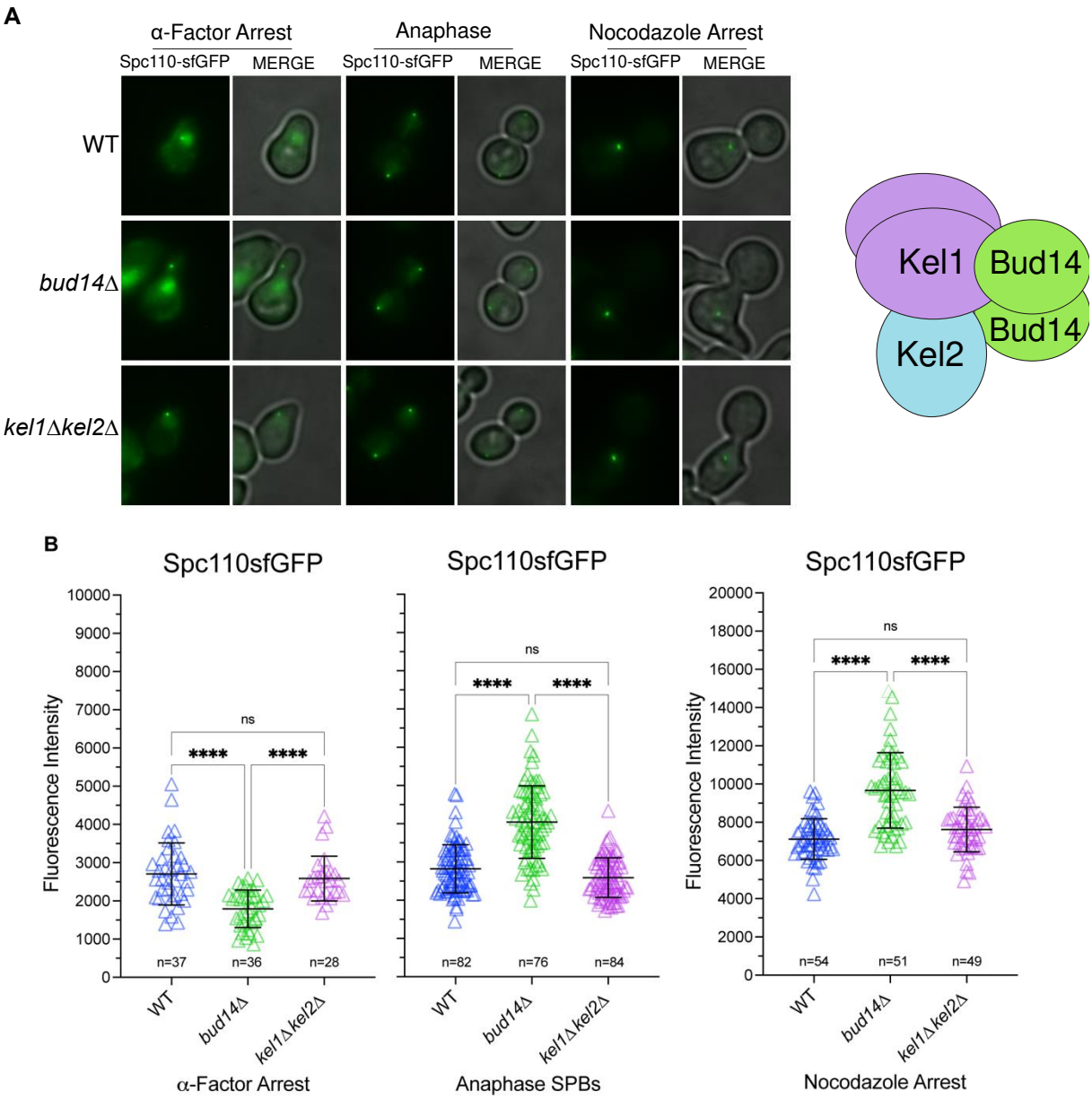

Figure 3.10.1: The Spc110 phenotype of *bud14*Δ is independent from impaired Kelch-Bud14 function.

A. Fluorescence microscopy representative images of Spc110-sfGFP in G1 arrested cells, anaphase cells (≥3µ tubulin length), and nocodazole mediated metaphase arrested cells of WT, *bud14*Δ, *kel1*Δ*kel2*Δ. Scale bar: 3µ. Right panel of A. Kelch-Bud14 complex is schematically represented. B. SPB bound Spc110 levels measured in G1 arrested cells, anaphase cells (≥3µ tubulin length), and nocodazole mediated metaphase arrested cells of WT, *bud14*Δ, *kel1*Δ*kel2*Δ. Sample numbers of each data group are presented on graphs. For each comparison, one-way ANOVA was performed and p-values: **** $P < 0.0001$, ***$P < 0.001$, **$P < 0.01$, *$P < 0.05$.

3.11 Enrichment of Bud14 at cytoplasmic site of SPB increased Spc110 level whereas Spc72 level remained unchanged

Thus far, we showed that Bud14 is required for size maintenance of following SPB structural proteins: Spc42, Spc29, Spc110, Spc72, Spc97, Nud1 and Spc110. Bud14 mediated this observed effect on the SPB partially via Glc7 except for Spc72. Furthermore, nonfunctional Cdc14 abolished Spc110 and Spc72 phenotype of *bud14*Δ at metaphase and at G1, respectively. Then we wondered about other possible molecules that can function in the SPB size maintenance. To answer this question, several experiments utilizing GBP-GFP system was conducted (see Materials and Methods).

Firstly, we investigated Spc72 and Spc110 levels when Bud14 was localized to Spc42-GBP corresponding cytoplasmic site of the SPB (see Fig.3.11.1 for experimental design). Spc72 level remained unchanged according to the measurement done in anaphase. In contrast, Spc110 level significantly increased when Bud14 was in proximity with Spc42. This phenocopies the observed increasement of SPB bound Spc110 in *bud14*Δ.

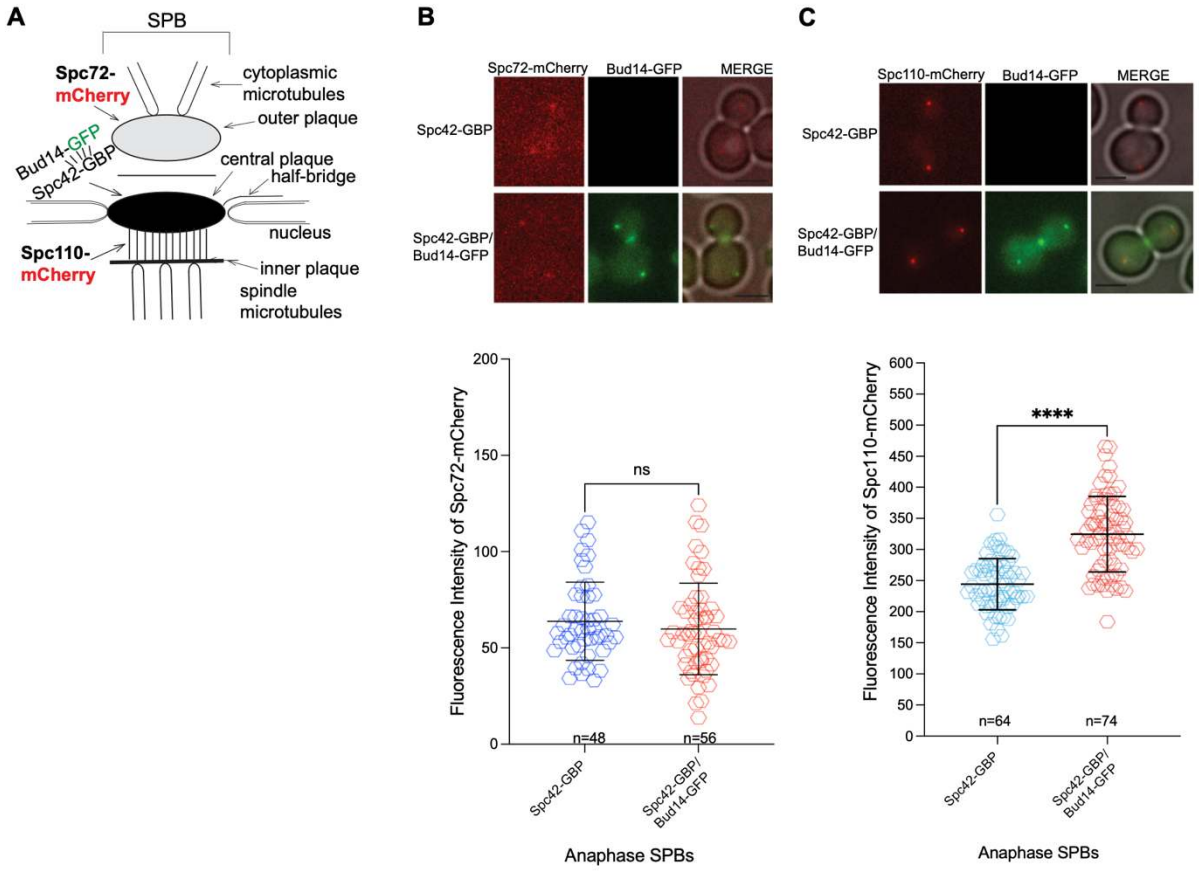

Figure 3.11.1: Bud14 localization to cytoplasmic face of the SPB increases SPB bound Spc110 levels in anaphase.

A. Representative scheme of experimental set up is depicted. Design is valid for both Spc72 and Spc110 measurements. B. Representative image of fluorescence imaging of Spc72-mCherry is shown at the top. Scale bar:3µ. B. bottom, SPB-bound Spc72 levels in anaphase cells of Spc42-GBP expressing and cells with constitutively expressing Bud14 at CP. C. Representative image of fluorescence imaging of Spc110-mCherry. Scale bar:3µ. At the bottom, SPB-bound Spc110 levels in anaphase cells of Spc42-GBP expressing and cells with constitutively expressing Bud14 at CP of SPB. Sample numbers of each data group are presented in the graphs. For each comparison, t-test was performed and p-values: **** $P < 0.0001$, ***$P < 0.001$, **$P < 0.01$, *$P < 0.05$.

3.12 Constitutively targeting of Cdc14 at inner plaque of the SPB had opposing effect on the Spc72 and Spc110 levels.

Cdc14 is the major phosphatase which drives cells out of the mitosis in the budding yeast (Azzam et al., 2004). Cdc14 is sequestered as inactive in nucleolus until anaphase onset. Upon its release, Cdc14 localizes to SPBs (Azzam et al., 2004). Idil Kirdok from our lab demonstrated that absence of Bud14 prolongs Cdc14 localization at SPB. Previously, we demonstrated that unfunctional Cdc14 abolishes the Spc72 phenotype at the G1, and the Spc110 phenotype at the metaphase cells of *bud14*Δ.

We enriched Cdc14 localization at the nuclear site of the SPB to investigate its possible effects on anaphase SPBs. For both measurements, Cdc14 was tagged with GFP to target Spc29-GBP (see Figure 3.12.1 A). dSPB bound Spc72 levels were measured in anaphase due to experimental bottleneck (Spc72 levels were too low at the SPB). mCherry has a longer maturation period compared to GFP which renders dSPB brighter (Guerra et al., 2022). This mCherry mediated constraint was inflated by moderate Spc72 protein level at SPB. Therefore, distinguishing Spc72-mCherry signal at mSPB was intractable. Only dSPB bound Spc72 levels were measured in control sample for the sake of reliable comparison (Figure 3.12.1 B). We measured Spc110 levels in anaphase cells having constitutively localized Cdc14 at the Spc29. Spc110 assembles onto Spc29 during SPB duplication (Rüthnick & Schiebel, 2018).

Forceful Cdc14 localization at the SPB nuclear site via Spc29 interaction had opposing effects on Spc72 and Spc110 levels at anaphase SPBs. Cdc14 enrichment in the nucleus induced significantly elevated levels of Spc72 at the dSPB. This increase can be interpreted as phenocopy of *bud14*Δ for Spc72. In contrast, enforced Cdc14 localization at nuclear site of

SPB, significantly decreased SPB bound Spc110 levels. We hypothesize that antagonistic effects of the constitutive Cdc14 expression at nuclear SPB site on the Spc72 and Spc110 were derived from their spatial difference hence Spc110 resides at nuclear site whereas Spc72 reside at the cytoplasm. Altogether, this data implies that Cdc14 has a role in SPB size maintenance (proven by Figure 3.8.1, 3.9.1, and 3.12.1) and Cdc14 localization might have opposing effects on SPB structural proteins based on the cellular site they reside on.

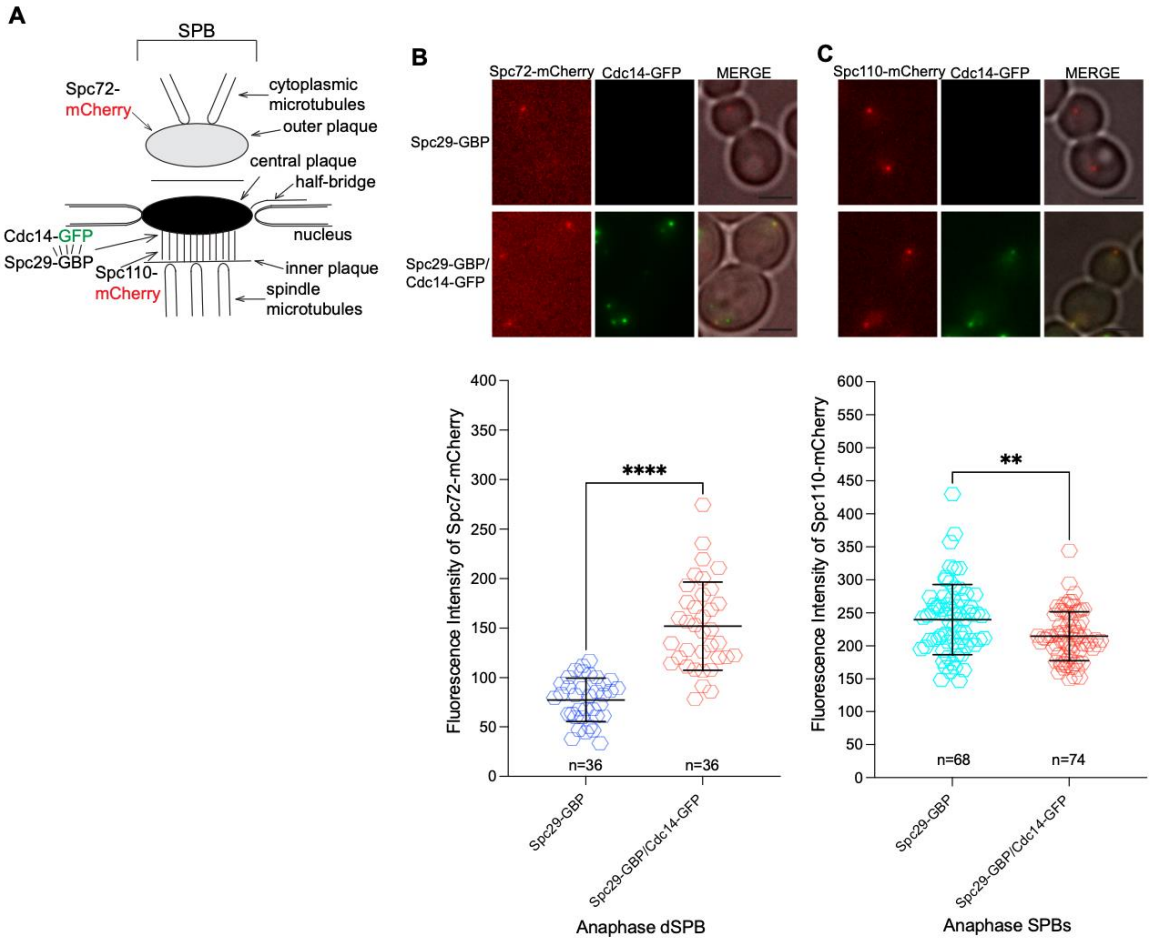

Figure 3.12.1: Enforced Cdc14 localization at inner plaque of SPB has opposing effect on SPB bound Spc110 and Spc72 levels in anaphase.

A. Representative scheme of experimental set up is shown. Design is valid for both Spc72 and Spc110 measurements. B. Representative image of fluorescence imaging of Spc72-mCherry is shown at the top. Scale bar:3µ. B. bottom, SPB-bound Spc72 levels in anaphase cells of Spc29-GBP expressing cells and cells with constitutive Cdc14 expression at IP. C. Representative image of fluorescence imaging of Spc110-mCherry. Scale bar:3µ. At bottom, SPB-bound Spc110 levels in anaphase cells of Spc29-GBP expressing cells and cells with constitutive Cdc14 expression at IP of SPB. Sample numbers of each data group are presented in the graphs.

For each comparison, t-test was performed and p-values: **** P < 0.0001, ***P < 0.001, **P < 0.01, *P < 0.05.

3.13 Constitutively expressing Cdc28 at outer plaque of the SPB had opposing effect on the Spc72 and Spc110 levels

Cdc28 is the single Cdk1 in the budding yeast. Several research indicated that Cdc28 phosphorylates SPB components like Spc110 and Nud1 in a cell cycle dependent manner (Geymonat et al., 2020; Lin et al., 2014). Nevertheless, its actions on SPB could not be elucidated detailly. Therefore, we enriched Cdc28 localization at the cytoplasmic site of the SPB to investigate its possible effects on anaphase SPBs. For Spc72 measurement, Cdc28 was tagged with GFP whereas Spc42 was tagged with GBP (Figure 3.13.1 A). As explained in section 3.12, only dSPB bound Spc72-mCherry levels were measured. For Spc110-Cherry measurements in anaphase cells Cdc28 was tagged with GFP, whereas Spc72 was tagged with GBP (Figure 3.13.1 B).

Forceful Cdc28 localization at the SPB cytoplasmic site generated opposing effects on Spc72 and Spc110 levels in anaphase. This result suggests that the constitutive expression of Cdc28 near Spc72 led to its enlargement in anaphase. In contrast, enforced Cdc28 localization to Spc72, significantly lowered SPB bound Spc110 levels. This decrease can be interpreted as phenocopy of *bud14*Δ for Spc110. We believe that observed antagonistic effects of the Cdc28 on the Spc72 and Spc110 were derived from their spatial difference hence Spc110 resides at nuclear site. These observations are very interesting and further work will enlighten the molecular mechanisms behind these phenotypes.

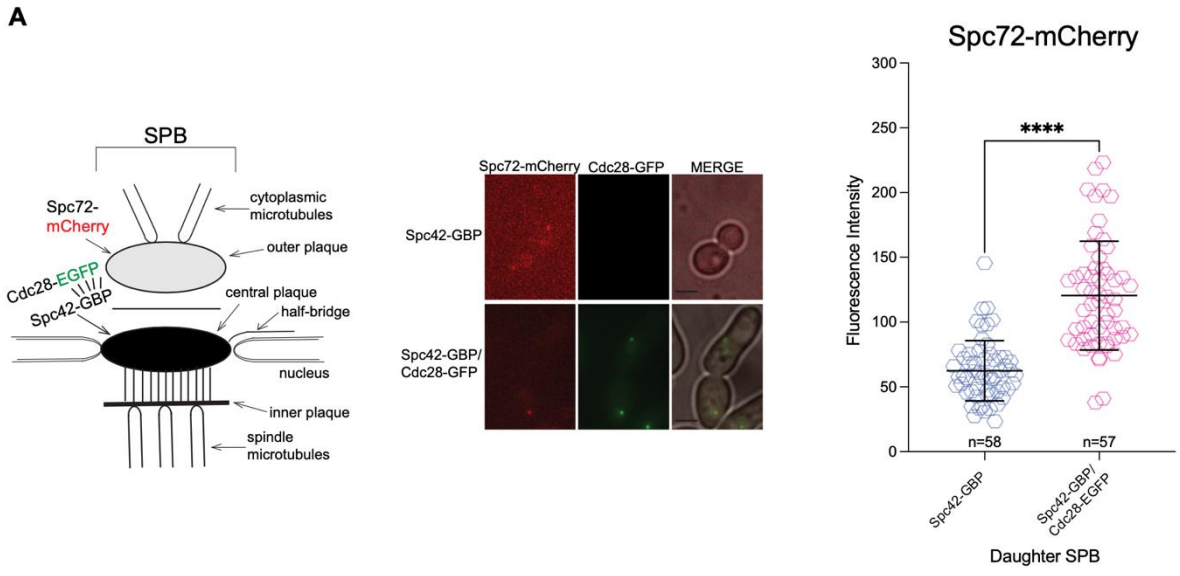

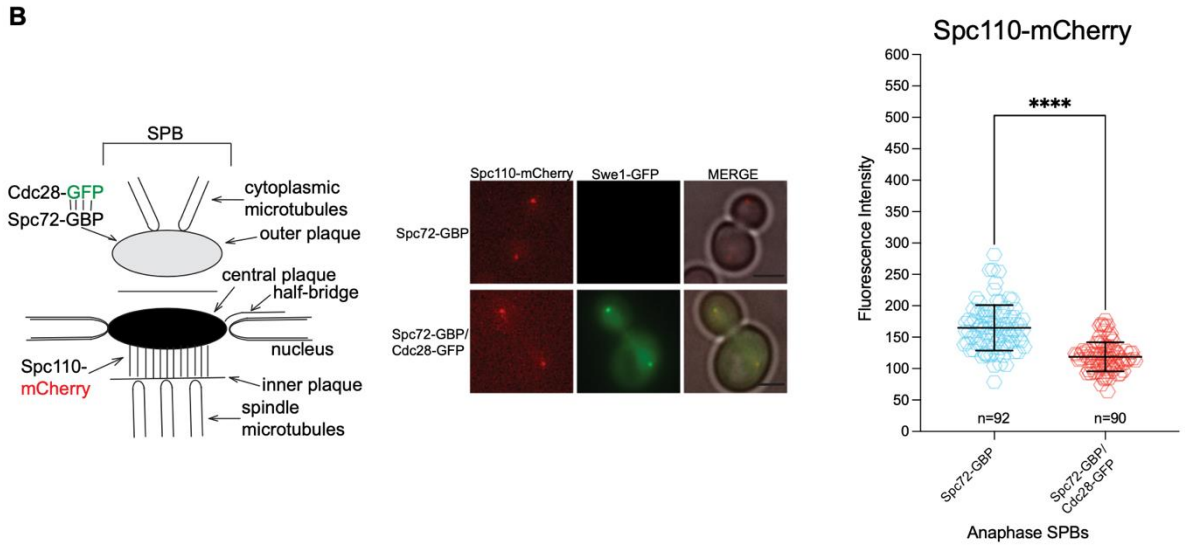

Figure 3.13.1: Constitutively expressing Cdc28 at outer plaque of the SPB had opposing effect on SPB bound Spc72 and Spc110 levels.

A. Representative scheme of experimental set up for Spc72-mCherry measurement is presented at the most left site of the panel. Representative image of fluorescence imaging of Spc72-mCherry is shown at middle of A. Scale bar:3µ. At the rightest side, SPB-bound Spc72 levels at anaphase dSPBs of Spc42-GBP expressing cells and cells with constitutive Cdc28 expression at cytoplasmic SPB face. B. Representative scheme of experimental set up for Spc110-mCherry measurement is presented at the most left. Representative image of fluorescence imaging of Spc110-mCherry is shown at middle of B. Scale bar:3µ. At the rightest side, SPB-bound Spc110 levels at anaphase SPBs of Spc72-GBP expressing cells and cells with constitutive Cdc28 expression at cytoplasmic SPB site. Sample numbers of each data group are presented in the graphs. For each comparison, t-test was performed and p-values: **** $P < 0.0001$, ***$P < 0.001$, **$P < 0.01$, *$P < 0.05$.

3.14 Constitutively localizing Cdc28 at Nud1 SPB scaffold protein resulted in similar phenotype on Spc72 and Spc110 levels

Then we investigated Spc72 and Spc110 levels in cells Cdc28 was constitutively expressed in Nud1. Enforced Cdc28 localization at Nud1 significantly intensified dSPB bound Spc72 levels. Cdc28 enrichment at Nud1 also increased Spc110-mCherry at anaphase SPBs. This was unanticipated result regarding previous result (Figure 3.12.1). Nud1 scaffold protein functions in two distinct events: cytoplasmic microtubule nucleation and mitotic exit (Gruneberg et al., 2000). Further Cdc28 phosphorylates Nud1 and induce Spc72 docking to Nud1 (Geymonat et

al., 2020). Therefore, this observed result cannot be interpreted based on solely SPB structure and size maintenance.

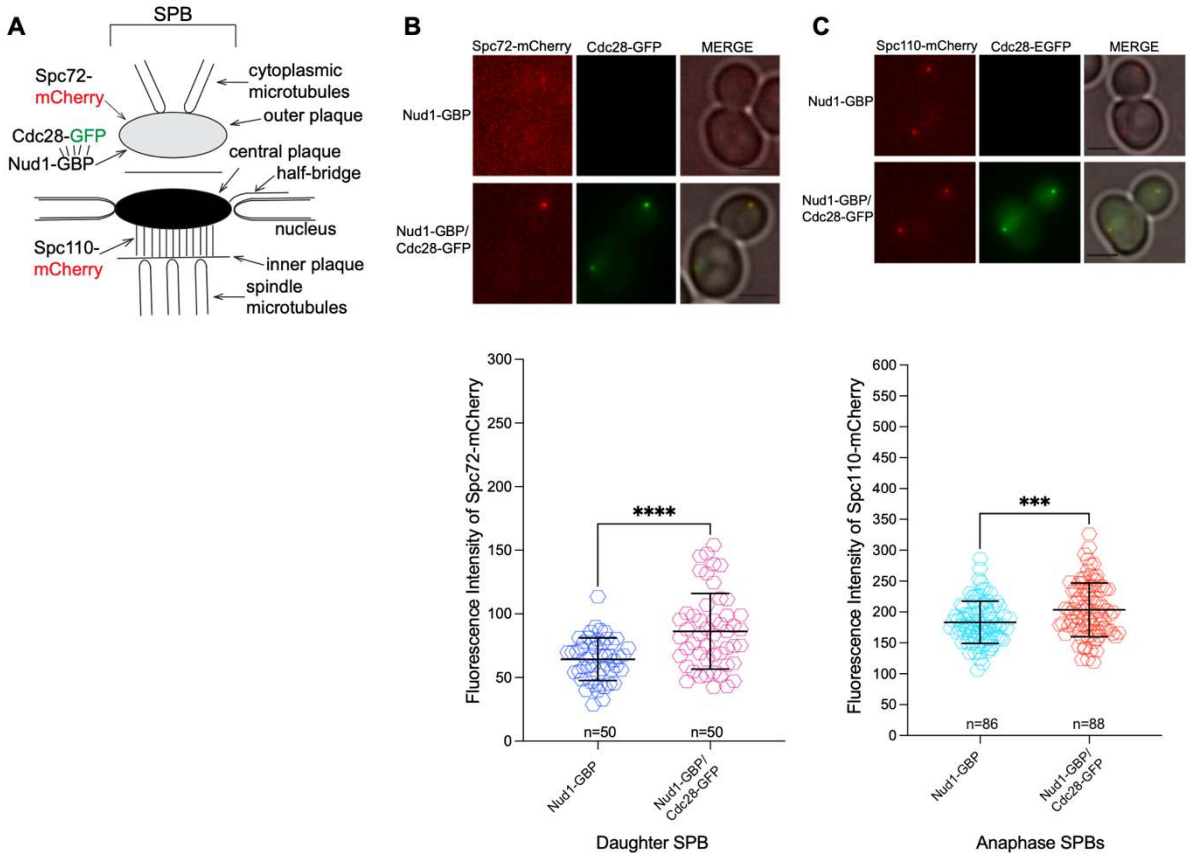

Figure 3.14.1: Constitutively localizing Cdc28 at Nud1 SPB scaffold protein have similar effect on SPB bound Spc72 and Spc110 levels.

A. Representative scheme of experimental set up is shown. Design is valid for both Spc72 and Spc110 measurements. B. Representative image of fluorescence imaging of Spc72-mCherry is shown at the top. Scale bar:3µ. B. bottom, SPB-bound Spc72 levels at anaphase dSPBs of Nud1-GBP expressing cells and cells with constitutive Cdc28 expression at OP. C. Representative image of fluorescence imaging of Spc110-mCherry. Scale bar:3µ. At bottom, SPB-bound Spc110 levels at anaphase SPBs of Nud1-GBP expressing cells and cells with constitutive Cdc28 expression at OP. Sample numbers of each data group are presented in the graphs. For each comparison, t-test was performed and p-values: **** $P < 0.0001$, ***$P < 0.001$, **$P < 0.01$, *$P < 0.05$.

3.15 Constitutively expressing Mps1 and Swe1 at cytoplasmic site of the SPB did not change Spc110 level

Furthermore, we examined Spc110 levels in anaphase when Mps1 and Swe1 localizations was individually enforced to cytoplasmic site of the SPB. Mps1 is an essential kinase which phosphorylated Spc42 essential for Spc42 assembly during SPB duplication (Castillo et al., 2002; Schutz & Winey, 1998). Nonetheless, its constitute expression at Spc42 did not alter SPB-bound Spc110 levels in anaphase.

Clb2-Cdc28 is inhibited by direct binding of Swe1 thereby decreases Clb2-Cdc28 at the time of mitotic entry (Asano et al., 2005). Nevertheless, Swe1 constitutive expression at the cytoplasmic SPB component, Spc72, did not affect SPB bound Spc110 level in anaphase.

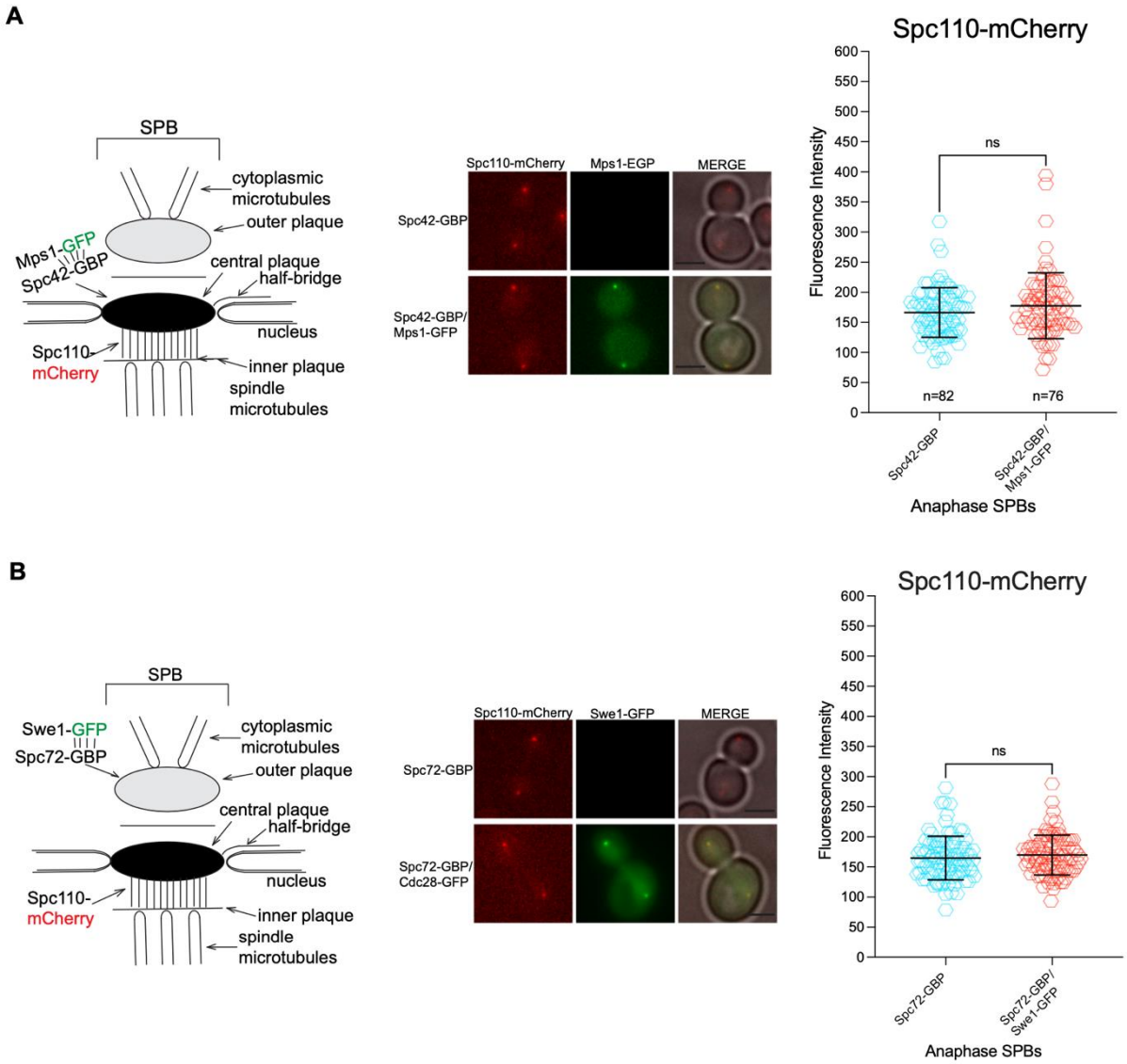

Figure 3.15.1: Constitutively expressing Mps1 and Swe1, separately, at cytoplasmic site of the SPB did not change SPB bound Spc110 levels.

A. Representative scheme of experimental set up for Spc110-mCherry measurement is presented at the most left site. Representative image of fluorescence imaging of Spc110-mCherry is shown at middle of A. Scale bar:3µ. At the rightest side, SPB-bound Spc110 levels at anaphase SPBs of Spc42-GBP expressing cells and cells with constitutive Mps1 expression at cytoplasmic SPB face. B. Representative scheme of experimental set up for Spc110-mCherry measurement is presented at the most left. Representative image of fluorescence imaging of Spc110-mCherry is shown at middle of B. Scale bar:3µ. At the rightest side, SPB-bound Spc110 levels at anaphase SPBs of Spc72-GBP expressing cells and cells with constitutive Swe1 expression at cytoplasmic SPB site. Sample numbers of each data group are presented in the graphs. For each comparison, t-test was performed and p-values: **** $P < 0.0001$, ***$P < 0.001$, **$P < 0.01$, *$P < 0.05$.

Chapter 4: DISCUSSION

S. cerevisiae is frequently utilized as model organism to elucidate fundamentals of the eukaryotic cell biology. The application of genetics coupled with molecular biology is notably effective for cell cycle studies with S. cerevisiae. The cell cycle is a conserved process, the fidelity of which is governed by various mechanisms. Cell division enables cells to reproduce and inherit their genomic DNA to progenies and thus constitutes multicellular life.
During cell division, various critical events like DNA duplication, chromosome, and organelle segregation occurs. Microtubule organizing centers (MTOCs) has significant role in managing accurate chromosome segregation and thus cell and the progeny viability. Nonetheless, how MTOCs duplicates and maintains its fidelity throughout the cell cycle are not fully elucidated. Spindle pole body (SPB) is functional equivalent of the eukaryotic MTOC, the centrosome. Many SPB component has homologs in the eukaryotic centrosomes. In this thesis, *S. cerevisiae* is utilized to study size maintenance of SPB.

SBP is composed of three major compartments: The inner and outer plaques face nucleoplasm and cytoplasm, respectively, and central plaque is embedded in the nuclear envelope (NE). Previously, SPB duplication was explained in the context of the conservative dispersive theory on macromolecules. SPB duplication was perceived as an example of conservative assembly model. Old SPB was consists of old components whereas new components made up new SPB. Nevertheless, several experimental results were cultivated over time to challenge the idea that cellular macromolecules are static once they are formed. Yoder et al. demonstrated that Spc110 assembly at SPB cannot be explained by neither of the assembly models. Furthermore, it has been proven that SPB components undergo extensive exchange and growth cycles.

Bud14 is regulatory subunit of Glc7, PP1. Kocakaplan et al. identified Bud14-Glc7 as a novel SPOC player. Spindle position checkpoint assures cells remain their genomic integrity. Further, it has been showed that absence of *BUD14* changed SPB bound Bfa1, Tem1 and Bub2 levels. To understand whether observed level changes derived from a global change at SPB, mean fluorescence intensities of SPB structural proteins measured. During anaphase, the SPB bound levels of all studied structural proteins of IP and OP were elevated in *bud14*Δ compared to wild type cells whereas the levels of the half bridge protein Sfi1 were not different.

In no budded cells (G1), outer plaque components Spc72, Nud1 and Spc97 exhibited increased levels upon *BUD14* deletion. In contrast, inner plaque components, Spc110 and Spc29, and half-bridge protein, Sfi1, levels remained unchanged in the Bud14 absence. Unanticipatedly, SPB bound Spc42 level drastically lowered in *bud14*Δ no budded cells. It is worth mentioning that sometimes the beginning of bud emergence is difficult to see in the brightfield images. Given that the deletion of *BUD14* influences budding, selection of no budded cells based on bright field images in our experimental set up maybe biased. Therefore, more experiments are required to make further conclusions on differences between anaphase and no-budded cell (G1) measurements. Nevertheless, increased amount of outer plaque components Spc72, Nud1 and Spc97 and unaffected levels of Sfi1 are consisted in both anaphase and no-budded cell measurements of *bud14*Δ cells. Thus, we can conclude the behavior of outer plaque observed in anaphase/telophase is maintained after cytokinesis (no budded).

SPB duplication starts with the bridge elongation through Sfi1 oligomerization in anaphase. Cdc14 mediated dephosphorylation of Sfi1 is required for this elongation and Cdk1 phosphorylation prevents it (Elserafy et al., 2014). Elongation is followed by the assembly of SPB satellite. Satellite assembly likely to occurs first by Spc42 deposition on the half bridge after mitotic exit, which is followed by first Spc29 and then by Nud1 and Cnm67 assembly (Burns et al., 2015). Satellite is then matured into the duplication plaque which is later inserted into the nuclear envelope. Only after insertion into the nuclear envelope Spc110 is recruited to the IP.

The observed divergence in level changes between outer and inner plaque might be derived from the timing of the OP and IP assembly during SPB duplication. In anaphase onset, increased Cdc14 activity leads dephosphorylation of Sfi1; thus, Sfi1 elongates into the bridge (Rüthnick & Schiebel, 2018). SPB precursor, the satellite, forms at the distal cytoplasmic end of the bridge in G1. Upon passing START point, satellite develops into duplication plaque (DP) via growth in size. After insertion of DP into nuclear envelope, nuclear SPB components, like Spc29 and Spc110, begin to SPB binding within the nucleus. IP and OP SPB structural proteins diverge in both their assembly and cellular localization might explain the differences in their *bud14*Δ caused phenotypes.

In addition, throughout cell cycle, protein functions are regulated by several mechanisms. One of those mechanisms is sequestering proteins to certain cellular areas. Oscillations in

localization of proteins which mediate effect on SPB might be another reason for the observed deviation between outer and inner plaque SPB proteins.

Since Spc72 and Spc110 function as a gamma tubulin receptor and nucleates cytoplasmic and nuclear microtubules, respectively, we wondered whether tubulin nucleation capacity of cells change upon Bud14 absence. To answer this *TUB1* was tagged N terminally with GFP. We measured tubulin intensity of 1.2-1.5μ mitotic spindle. Spc72 nucleates astral microtubules and help old SPB segregation to the bud. Therefore, we measured mean tubulin fluorescence intensity at poles of no budded and anaphase cells (see Figure 3.2.1 figure for measurement sites in cell). Tubulin mean intensity was significantly elevated upon Bud14 absence in three measurement approaches. This result is consistent with the previous result (Figure 3.1.1 and 3.1.2) and exemplifies physiological effect of Bud14 absence on cell structures like mitotic spindle.

Protein phosphatases govern extensive functions throughout the cell cycle. Since Bud14 is a regulatory subunit of the protein phosphatase 1, we questioned involvement of Bud14-Glc7 interaction in observed phenotypes (Figure 3.1.1 and 3.1.2). To investigate the role of Bud14-Glc7 interaction, we cloned endogenous Bud14, pSMG02, then introduced an amino acid substitution at F379A, pSMG03, to prevent Bud14 binding to Glc7 (Cannon, 2010).
Different from previous measurements, we utilized fluorescence ratio model to calculate molecule numbers of SPB structural proteins (see Materials and Methods for the details). Expression of endogenous Bud14 in *bud14*Δ cells restored molecule numbers of all: Spc29, Spc97, Spc42, Spc110, Nud1 and Spc72. This result verifies and emphasis our previous result that in the absence of *BUD14* levels of SPB structural proteins increases. For Spc42, Nud1 and Spc97, expression of Bud14-F379A in Bud14 knock-out cells phenocopied *bud14*Δ. This proves that Bud14-Glc7 interaction is required for the size maintenance for Nud1, Spc42 and Spc97 at SPB. Bud14-F379A expression in Bud14 knock-out cells resulted in partial rescue for Spc110 and Spc29 molecule numbers. Therefore, Bud14 relies on its interaction with Glc7 for the size maintenance of Spc29, Spc110, Nud1, Spc42 and Spc97 at anaphase SPBs. Thus, potential dephosphorylation of these SPB components by the Glc7-Bud14 complex may have role in SPB regulation.
Surprisingly Spc72 behaved differently. Expression of endogenous and mutant Bud14 in *bud14*Δ strain yielded similar molecular numbers which suggests that Bud14 might work independently from Glc7 to exert its effect on Spc72. Nevertheless, it should be discretely noted

that Spc72 molecule number in Bud14-F379A expressing cells was significantly higher than wild type cells. Therefore, Bud14-Glc7 interaction might have limited role in Spc72 size maintenance at SPBs.

To eliminate the possibility that *bud14*Δ phenotype on SPB caused by difference in cell cycle progression of WT and *bud14*Δ, we investigated Spc42, Nud1, Spc72 and Spc110 levels in cells of WT and *bud14*Δ, arrested separately by two agents: α-Factor and nocodazole. In α-Factor mediated G1 arrested WT and *bud14*Δ cells, SPB bound Spc42, Spc72 and Nud1 levels are equalized. Unanticipatedly, Spc110 levels were significantly lowered in *bud14*Δ cells upon G1 arrest. This might be explained by the action mechanism of α-Factor induced G1 arrest. According to proposed model, α-Factor binding its receptor, Ste1, induces MAPK (Breitkreutz & Tyers, 2002). This cascade promotes Far1 mediated Cdc28 inhibition. Since Spc110 levels are similar in G1 cells of WT and *bud14*Δ, sudden decrease in Cdc28 activity might be the reason behind lowered Spc110 levels in G1 arrested *bud14*Δ cells. In nocodazole induced metaphase arrested cells, Spc110, Spc72, and Nud1 levels remained significantly higher compared to WT. Surprisingly, Spc42 levels equalized in metaphase arrested cells of WT and *bud14*Δ. We hypothesize that significantly lowered SPB bound Spc42 level in *bud14*Δ no budded cells might be recovered through cell cycle since increased Spc42 level observed in anaphase *bud14*Δ cells. This might be the reason behind equalized levels in nocodazole mediated metaphase arrest which is the merging of two SPBs due to absence of microtubule polymerization (Wang & Burke, 1995). Altogether, we proved that *bud14*Δ phenotype of SPB (Figure 3.1.1 and 3.3.1) is independent from the possible cell cycle progression differences between wild type and *bud14*Δ cells.

Our research demonstrated that Bud14 exerts its effect on SPB structural components mostly via its interaction with Glc7 (see Figure 3.3.1for proteins). Therefore, we decided to investigate migration patterns of Spc72, Nud1 and Spc110 on SDS-PAGE for possible phosphorylation difference between wild type and *bud14*Δ cells. Nonetheless, no readily detectable migration difference was observed. We should carefully note that Spc110 had a light slow migrating smear in *bud14*Δ but not in wild type, which may indicate posttranslational modification differences. It is important to underline that this result does not rule out the possibility of differences in phosphorylation status of analyzed proteins. One site limited phosphorylation can change assembly and functionality of proteins (see Spc110 phosphorylation in Lin et al., 2014), but this

kind of post-translational modification is hard to detect on SDS-PAGE due to limited separation resolution; thus, more must be conducted to compare the phosphorylation status.

Time course assays of Spc110 and Spc72 demonstrated when the SPB phenotype in *bud14*Δ emerges (see Figure 3.6.1 for experimental design). After released from α-Factor induced G1 arrest, Spc110 molecule numbers in *bud14*Δ cells with newly segregated nuclei exceeded and remained significantly higher than wild type Spc110 molecule numbers. In contrast, Spc72 molecule number became significantly higher in metaphase compared to WT. The difference in when the *bud14*Δ phenotype emerges for Spc110 and Spc72 implies that the localization pattern of executive protein in the *bud14*Δ phenotype might be the underlying reason.

Later we wondered the Cdc14 effect on SPB in *bud14*Δ cells since Cdc14 localizes to the SPB upon its release and stays longer in *bud14*Δ cells (Submitted MS Thesis, Kirdok, 2022; Sullivan & Uhlmann, 2008). At restrictive temperature, 37°C, *cdc14-2* mutant, labeled as *cdc14-ts* in our experiments, cannot execute mitotic exit and cells arrested in anaphase (see Figure 3.7.1 B part). SPB bound Spc72 levels were similar in α-Factor induced G1 arrested cells of WT, *bud14*Δ, *cdc14-ts*, *cdc14-ts/bud14*Δ. After releasing cells into fresh media, Spc72 levels were measured at T3 for WT and *bud14*Δ and at T4 for *cdc14-ts*, *cdc14-ts/bud14*Δ, T3 and T4 correspond to time when cells entered anaphase the first time (see Figure 3.7.1 C for anaphase percentage of strains). Spc72 levels also measured in anaphase arrested cells of *cdc14-ts*, *cdc14-ts/bud14*Δ. Spc72 levels, however, remained high in the absence of *BUD14* compared to its control group.

We conducted a follow up experiment to explore effect of unfunctional Cdc14 on Spc72 in G1 cells. In this follow up experiment, *SIC1* was overexpressed to drive cells into G1 and arrest at this phase. Elserafy et al. illustrated that *SIC1* overexpression in *cdc14-2* cells arrest cells in G1 with one SPB (Elserafy et al., 2014). SPB bound Spc72 levels measured at anaphase arrested, T0, cells and *SIC1* overexpressed cells of *cdc14-ts*, *cdc14-ts/bud14*Δ. We proved that functional Cdc14 absence in G1 abolished *bud14*Δ phenotype of Spc72 levels (Figure 3.8.1 D). To exclude the possibility that *SIC1* overexpression mediates Spc72 level equalization in WT and *bud14*Δ cells (as in α-Factor treatment), *SIC1* was overexpressed and Spc72 levels were measured in WT and *bud14*Δ cells. SPB bound Spc72 level was significantly higher in Sic1 overexpressed *bud14*Δ cells compared to WT. Wild type cells mostly have two SPBs in contrast to *cdc14-2*

upon *SIC1* overexpression (Elserafy et al., 2014). Thus, this result suggest that it is either an event after SPB duplication or an event dependent on Cdc14 activity in G1 that causes the increased SPc72 levels in the absence of Cdc14.

Since Spc110 is nuclear functional equivalent of Spc72 both being γ-Tubulin receptor, we analyzed SPB bound Spc110 levels in *cdc14-ts*, *cdc14-ts/bud14*Δ cells at restrictive temperature over 2 hours (for experimental design see 3.9.1 A). Spc110 levels was significantly lower in G1 arrested *cdc14-ts/bud14*Δ cells, phenocopying *bud14*Δ Spc110 levels upon α-Factor treatment. Following the release, however, SPB bound Spc110 levels almost recovered after SPB separation. At metaphase and end point of experiment, T8, Spc110 levels were lowered in *cdc14-ts/bud14*Δ cells. Spc110 levels were completely equalized at same mean fluorescence intensity in *cdc14-ts*, *cdc14-ts/bud14*Δ anaphase cells. This result shows that Cdc14 functionality is required for the elevated Spc110 levels observed in *bud14*Δ. Collectively, our research suggests that Cdc14 and Bud14 may work in the same pathway of SPB size maintenance.

In literature, Bud14 interaction with Kelch proteins is well established. Bud14 forms complex with Kel1 and Kel2 with 2.2.1 stoichiometry (Gould et al., 2014). Kelch-Bud14 complex function in formin regulation thereby mediate actin structures which required for budding and division (Gould et al., 2014). To test whether *bud14*Δ phenotype of SPB structural proteins is dependent on Bud14-Kelch complex functioning, Spc110 levels are measured in cells of WT, *bud14*Δ, and *kel1*Δ*kel2*Δ strains at several cell cycle conditions: G1 arrest, anaphase, and nocodazole. Nonetheless, *kel1*Δ*kel2*Δ could not phenocopy *bud14*Δ of Spc110 in any measurements. This data concludes that *bud14*Δ phenotype of Spc110 is independent from its function with Kelch complex.

At this point, our research proved that Bud14 mediates SPB size partnering with Glc7 and Cdc14 in this regulating pathway. Since we showed that phosphatases Glc7 and Cdc14 have roles in the *bud14*Δ phenotype occurrence on SPB structural proteins, we speculated that there can be a counteracting kinase against Bud14-Glc7. Cdc28, Mps1 and Swe1 were determined as candidate kinases since they have established functions in regulation of SPB duplication and the cell cycle. Cdc28 is sole Cdk1 in the budding yeast and Cdc28 association with C1-C3 cyclins promotes SPB duplication by enlarging the satellite into a full SPB (Jaspersen et al., 2004). In addition, S phase Cdc28 activity mediates separation of new and old SPBs after

duplication (Lim et al., 1996). Later in cell cycle, mitotic Cdk1 activity of Cdc28 prevents SPB reduplication through unelucidated mechanism (Elserafy et al., 2014). Mps1 also mediates SPB duplication via phosphorylating Spc42 (Castillo et al., 2002). Swe1 is known Cdc28 inhibitory kinase (Asano et al., 2005).

One of the major challenges in cell biology is directly associating protein localization to its function (Y. hui Chen et al., 2017). One methodology to overcome this challenge is that artificially enhance localization of studied protein at a particular cellular site which followed by characterization and functional analysis. The GBP mediated targeting presents very effective method to associate cellular localization to function (Y. hui Chen et al., 2017).
GBP has a small size and binds to GFP with 1:1 stoichiometry which renders it widely applicable approach (Y. hui Chen et al., 2017). Therefore, GBP-GFP system was utilized to find possible functioning of candidate kinases in SBP size maintenance.
Nonetheless, when both Swe1 and Mps1 could not change Spc110 levels in anaphase when they separately enforced to localize cytoplasmic site of SPB (Figure 3.15.1). On contrary, constitutive Cdc28 expression at cytoplasmic site of SPB, had antagonizing effect on SPB bound Spc72 and Spc110 levels in anaphase. Cytoplasmic SPB component Spc72 levels increased whereas Spc110 levels significantly declined due to enforced Cdc28 localization to Spc42, and Spc72, respectively (Figure 3.13.1). Enforced localization of Cdc28 to Spc72, thereby lowered Cdc28 nuclear level, phenocopied Spc110 levels in G1 arrested *bud14*Δ cells upon α-Factor treatment (Figure 3.4.1). Surprisingly, enforced Cdc28 binding to Nud1, outer plaque component, resulted in increase of Spc72 and Spc110 levels in anaphase cells (3.14.1). Both enforced Cdc28 localization to cytoplasmic site of SPB significantly increased Spc72 levels in anaphase cells (Figure 3.13.1 D and 3.14.1 B). Unanticipatedly, Spc110 levels were affected differently by enforced Cdc28 localization to Spc72 and Nud1. This difference might be derived from Nud1 protein identity. Nud1 is a scaffold protein functions in Mitotic Exit Network (MEN) and binds with Spc72 (Geymonat et al., 2020). These distinct roles of Nud1 prevent interpretation of the result based on solely SPB structure and size maintenance.

Later, Cdc14 was constitutively expressed at nuclear site of SPB via Spc29 binding (see Figure 3.12.1 A for experimental design). Cdc14 enrichment at nuclear SPB face had opposing effect on Spc72 and Spc110 levels in anaphase. Spc72 level increased whereas Spc110 level declined significantly. This result suggests that size maintenance of Spc110 requires wild type Cdc14

levels in nucleus. Enriched Cdc14 levels in nucleus phenocopied *bud14*Δ phenotype of Spc72 in anaphase indicating that Bud14 and Cdc14 works in same SBP size maintenance pathway. Due to enrichment of Bud14 localization at the cytoplasmic face of SPB, SPB bound Spc72 level remained unchanged whereas Spc110 levels increased in anaphase cells. This is consistent with our previous finding that Bud14 absence significantly increases Spc110 and Spc72 levels in anaphase (Figure 3.1.1) hence enforced Bud14 localization to cytoplasm may be mimicking Bud14 absence for Spc110 size maintenance pathway.

All in all, our research established Bud14 functioning in SPB size maintenance for the first time. We established that Bud14 exerts its effect on SPB primarily via Glc7. Further we illustrated that Cdc14 and Bud14 functions on the same SPB size maintaining pathway. At the last part, we illustrated the effects of constitutive Cdc28 expression at cytoplasmic SPB site on Spc72 and Spc110 levels in anaphase. This indicates Cdc28 as a strong kinase candidate for antagonizing Cdc14 and Bud14-Glc7 functioning in SPB size maintenance.

Chapter 5: BIBLIOGRAPHY

Asano, S., Park, J. E., Sakchaisri, K., Yu, L. R., Song, S., Supavilai, P., Veenstra, T. D., & Lee, K. S. (2005). Concerted mechanism of Swe1/Wee1 regulation by multiple kinases in budding yeast. *EMBO Journal*, *24*(12), 2194–2204. https://doi.org/10.1038/sj.emboj.7600683

Azzam, R., Chen, S. L., Shou, W., Mah, A. S., Alexandru, G., Nasmyth, K., Annan, R. S., Carr, S. A., & Deshaies, R. J. (2004). Phosphorylation by cyclin B-Cdk underlies release of mitotic exit activator Cdc14 from the nucleolus. *Science*, *305*(5683), 516–519. https://doi.org/10.1126/science.1099402

Bloom, J., & Cross, F. R. (2007). Multiple levels of cyclin specificity in cell-cycle control. *Nature Reviews Molecular Cell Biology*, *8*(2), 149–160. https://doi.org/10.1038/nrm2105

Boleti, H., Karsenti, E., & Vernos, I. (1996). Xklp2, a novel Xenopus centrosomal kinesin-like protein required for centrosome separation during mitosis. *Cell*, *84*(1), 49. https://doi.org/10.1016/s0092-8674(00)80992-7

Breitkreutz, A., & Tyers, M. (2002). MAPK signaling specificity: It takes two to tango. *Trends in Cell Biology*, *12*(6), 254–257. https://doi.org/10.1016/S0962-8924(02)02284-5

Burns, S., Avena, J. S., Unruh, J. R., Yu, Z., Smith, S. E., Slaughter, B. D., Winey, M., & Jaspersen, S. L. (2015). Structured illumination with particle averaging reveals novel roles for yeast centrosome components during duplication. *ELife*, *4*(September2015), 1–27. https://doi.org/10.7554/eLife.08586

Cannon, J. F. (2010). Function of Protein Phosphatase-1, Glc7, in Saccharomyces cerevisiae. In *Advances in Applied Microbiology* (1st ed., Vol. 73, Issue C). Elsevier Inc. https://doi.org/10.1016/S0065-2164(10)73002-1

Castillo, A. R., Meehl, J. B., Morgan, G., Schutz-Geschwender, A., & Winey, M. (2002). The yeast protein kinase Mps1p is required for assembly of the integral spindle pole body component Spc42p. *Journal of Cell Biology*, *156*(3), 453–465. https://doi.org/10.1083/jcb.200111025

Caydasi, A. K., Lohel, M., Grünert, G., Dittrich, P., Pereira, G., & Ibrahim, B. (2012). A dynamical model of the spindle position checkpoint. *Molecular Systems Biology*, *8*(1), 582. https://doi.org/10.1038/MSB.2012.15

Cross, F. R., Schroeder, L., & Bean, J. M. (2007). Phosphorylation of the Sic1 inhibitor of B-type cyclins in Saccharomyces cerevisiae is not essential but contributes to cell cycle robustness. *Genetics*, *176*(3), 1541–1555. https://doi.org/10.1534/genetics.107.073494

Diffley, J. F. X. (1996). Once and only once upon a time: Specifying and regulating origins of DNA replication in eukaryotic cells. *Genes and Development*, *10*(22), 2819–2830. https://doi.org/10.1101/gad.10.22.2819

Elserafy, M., Šarić, M., Neuner, A., Lin, T. C., Zhang, W., Seybold, C., Sivashanmugam, L., & Schiebel, E. (2014). Molecular mechanisms that restrict yeast centrosome duplication to one event per cell cycle. *Current Biology*, *24*(13), 1456–1466. https://doi.org/10.1016/j.cub.2014.05.032

Fisher, D. L., & Nurse, P. (1996). A single fission yeast mitotic cyclin B p34cdc2 kinase promotes both S-phase and mitosis in the absence of G1 cyclins. *EMBO Journal*, *15*(4), 850–860. https://doi.org/10.1002/j.1460-2075.1996.tb00420.x

Geymonat, M., Peng, Q., Guo, Z., Yu, Z., Unruh, J. R., Jaspersen, S. L., & Segal, M. (2020). Orderly assembly underpinning built-in asymmetry in the yeast centrosome duplication cycle requires cyclin-dependent kinase. *ELife*, *9*, 1–29. https://doi.org/10.7554/ELIFE.59222

Gimeno, C. J., & Fink, G. R. (1992). The logic of cell division in the life cycle of yeast. *Science*, *257*(5070), 626. https://doi.org/10.1126/science.1496375

Gould, C. J., Chesarone-Cataldo, M., Alioto, S. L., Salin, B., Sagot, I., & Goode, B. L. (2014). Saccharomyces cerevisiae Kelch proteins and Bud14 protein form a stable 520-kDa formin regulatory complex that controls actin cable assembly and cell morphogenesis. *Journal of Biological Chemistry*, *289*(26), 18290–18301. https://doi.org/10.1074/jbc.M114.548719

Herskowitz, I. (1988). Life cycle of the budding yeast Saccharomyces cerevisiae. *Microbiological Reviews*, *52*(4), 536–553. https://doi.org/10.1128/mmbr.52.4.536-553.1988

Jaspersen, S. L., Huneycutt, B. J., Giddings, T. H., Resing, K. A., Ahn, N. G., & Winey, M. (2004). Cdc28/Cdk1 regulates spindle pole body duplication through phosphorylation of Spc42 and Mps1. *Developmental Cell*, *7*(2), 263–274. https://doi.org/10.1016/j.devcel.2004.07.006

Jaspersen, S. L., & Winey, M. (2004). The budding yeast spindle pole body: Structure, duplication, and function. *Annual Review of Cell and Developmental Biology*, *20*, 1–28. https://doi.org/10.1146/annurev.cellbio.20.022003.114106

Bell, S., Stillman, B. ATP-dependent recognition of eukaryotic origins of DNA replication by a multiprotein complex. Nature 357, 128–134 (1992). https://doi.org/10.1038/357128a0

Kocakaplan, D., Karabürk, H., Dilege, C., Kirdök, I., Bektas, S. N., & Caydasi, A. K. (2021). Protein phosphatase 1 in association with Bud14 inhibits mitotic exit in Saccharomyces

cerevisiae. *ELife*, *10*. https://doi.org/10.7554/ELIFE.72833

Lim, H. H., Goh, P.-Y., & Surana, U. (1996). Spindle Pole Body Separation in Saccharomyces cerevisiae Requires Dephosphorylation of the Tyrosine 19 Residue of Cdc28 . *Molecular and Cellular Biology*, *16*(11), 6385–6397. https://doi.org/10.1128/mcb.16.11.6385

Lin, T. C., Neuner, A., Schlosser, Y., Scharf, A., Weber, L., & Schiebel, E. (2014). Cell-cycle dependent phosphorylation of yeast pericentrin regulates γ-TUSC-mediated microtubule nucleation. *ELife*, *2014*(3), 1–29. https://doi.org/10.7554/eLife.02208

Morgan, D. O. (1995). Principles of CDK regulation. In *Nature* (Vol. 374, Issue 6518, pp. 131–134). https://doi.org/10.1038/374131a0

Nicklas, R. B. (1997). How cells get the right chromosomes. *Science*, *275*(5300). https://doi.org/10.1126/science.275.5300.632

Nurse, P. (2000). A long twentieth century of the cell cycle and beyond. *Cell*, *100*(1), 71–78. https://doi.org/10.1016/S0092-8674(00)81684-0

Pereira, G., Manson, C., Grindlay, J., & Schiebel, E. (2002). Regulation of the Bfa1p-Bub2p complex at spindle pole bodies by the cell cycle phosphatase Cdc14p. *Journal of Cell Biology*, *157*(3), 367–379. https://doi.org/10.1083/jcb.200112085

Rüthnick, D., & Schiebel, E. (2018). Duplication and nuclear envelope insertion of the yeast microtubule organizing centre, the spindle pole body. *Cells*, *7*(5). https://doi.org/10.3390/cells7050042

Schutz, A. R., & Winey, M. (1998). New alleles of the yeast MPS1 gene reveal multiple requirements in spindle pole body duplication. *Molecular Biology of the Cell*, *9*(4), 759–774. https://doi.org/10.1091/mbc.9.4.759

Schwob, E., & Nasmyth, K. (1993). CLB5 and CLB6, a new pair of B cyclins involved in DNA replication in Saccharomyces cerevisiae. *Genes and Development*, *7*(7 A), 1160–1175. https://doi.org/10.1101/gad.7.7a.1160

Shirayama, M., Tóth, A., Gálová, M., & Nasmyth, K. (1999). APC(Cdc20) promotes exit from mitosis by destroying the anaphase inhibitor Pds1 and cyclin Clb5. *Nature*, *402*(6758), 203–207. https://doi.org/10.1038/46080

Submitted, D. (2022). *Novel Mechanisms in Control of Mitotic Exit Novel Mechanisms in Control of Mitotic Exit*. *May*.

Sullivan, M., & Uhlmann, F. (2008). *Europe PMC Funders Group Europe PMC Funders Author Manuscripts A non-proteolytic function of separase links anaphase onset to mitotic exit*. *5*(3), 249–254. https://doi.org/10.1038/ncb940.A

Trans, D., Carpentier, J., Palade, G. E., Bruns, R. R., Chen, R., Waters, J. C., Salmon, E. D., &

Murray, A. W. (1996). *The spindle assembly checkpoint delays anaphase until all chromosomes are attached*. *274*(October).

Uhlmann, F., Lottspelch, F., & Nasmyth, K. (1999). Sister-chromatid separation at anaphase onset is promoted by cleavage of the cohesin subunit Scc1. *Nature*, *400*(6739), 37–42. https://doi.org/10.1038/21831

Verma, R., Annan, R. S., Huddleston, M. J., Carr, S. A., Reynard, G., & Deshaies, R. J. (1997). Phosphorylation of Sic1p by G1 Cdk required for its degradation and entry into S phase. *Science*, *278*(5337), 455–460. https://doi.org/10.1126/science.278.5337.455

Wang, Y., & Burke, D. J. (1995). Checkpoint Genes Required To Delay Cell Division in Response to Nocodazole Respond to Impaired Kinetochore Function in the Yeast Saccharomyces cerevisiae . *Molecular and Cellular Biology*, *15*(12), 6838–6844. https://doi.org/10.1128/mcb.15.12.6838

Yoder, T. J., Pearson, C. G., Bloom, K., & Davis, T. N. (2003). The Saccharomyces cerevisiae spindle pole body is a dynamic structure. *Molecular Biology of the Cell*, *14*(8), 3494–3505. https://doi.org/10.1091/mbc.E02-10-0655

Chapter 6: APPENDICES

6.1 Table of Strains

Table 6.1: Descriptions of the yeast strains used in this thesis are listed.

Strain Name	Description	Reference
ESM356-1	(Spore 2.1) MATa ura3-52 leu2Δ1 his3Δ200 trp1Δ63.	(Pereira & Schiebel, 2001)
YPH499	MATa ura3-52 lys2-801amber ade2-101ochre trp1Δ63 his3Δ200 leu2Δ1.	
SGY020-1	ESM356((Spore 2.1) MATa ura3-52 leu2Δ1 his3Δ200 trp1Δ63) transformed with Nud1-sfGFP-kan6MX cassette. Verification was done with fluorescence imaging.	This study
SGY021-1	ESM356((Spore 2.1) MATa ura3-52 leu2Δ1 his3Δ200 trp1Δ63) transformed with Spc42-sfGFP-kan6MX cassette. Verification was done with fluorescence imaging.	This study
SGY022-1	ESM356((Spore 2.1) MATa ura3-52 leu2Δ1 his3Δ200 trp1Δ63) transformed with Spc72-sfGFP-kan6MX cassette. Verification was done with fluorescence imaging.	This study
SGY023-1	ESM356((Spore 2.1) MATa ura3-52 leu2Δ1 his3Δ200 trp1Δ63) transformed with Spc110-sfGFP-kan6MX cassette. Verification was done with fluorescence imaging.	This study
SGY024-1	SGY021-1 mCherry-Tub1-URA3. Verification was done by fluorescence imaging.	This study
SGY025-1	SGY022-1 mCherry-Tub1-URA3. Verification was done by fluorescence imaging.	This study
SGY026-1	SGY023-1 mCherry-Tub1-URA3. Verification was done by fluorescence imaging.	This study

SGY027-1	SGY020-1 mCherry-Tub1-URA3. Verification was done by fluorescence imaging.	This study
SGY028-1	ESM356((Spore 2.1) MATa ura3-52 leu2Δ1 his3Δ200 trp1Δ63) transformed with Spc29-sfGFP-kan6MX cassette. Verification was done with fluorescence imaging.	This study
SGY029-1	ESM356((Spore 2.1) MATa ura3-52 leu2Δ1 his3Δ200 trp1Δ63) transformed with Spc97-sfGFP-kan6MX cassette. Verification was done with fluorescence imaging.	This study
SGY031-1	SGY028-1 mCherry-Tub1-URA3. Confirmed by fluorescence microscopy.	This study
SGY032-1	SGY029-1 mCherry-Tub1-URA3. Confirmed by fluorescence microscopy.	This study
SGY034-1	ESM356 Nud1-sfGFP-kan6MX *bud14*Δ*::klTRP1* Deletion confirmed by colony PCR.	This study
SGY037-1	SGY026 *bud14*Δ*::klTRP1*. Deletion confirmed by colony PCR.	
SGY038-1	SGY031-1 *bud14*Δ*::klTRP1*. Deletion confirmed by colony PCR.	
SGY039-1	SGY032-1 *bud14*Δ*::klTRP1*. Deletion confirmed by colony PCR.	
SGY045-1	ESM356 is transformed with Sfi1-sfGFP-kan6MX. Verification done via fluorescence cell image.	This study
SGY046-1	SGY045-1 mCherry-Tub1-URA3. Verification done via fluorescence cell image.	This study
SGY048-1	ESM356 Spc42-sfGFP-kan6MX *Bud14*Δ*::klTRP1* Deletion confirmed by colony PCR.	This study
SGY050-1	ESM356 Spc72-sfGFP-kan6MX *Bud14*Δ*::klTRP1* Deletion confirmed by colony PCR.	This study
SGY052-1	ESM356 transformed with Nuf2-sfGFP-kan6MX cassettes. Verified by fluorescence imaging.	This study

SGY053-1	ESM356 *Bud14*Δ*::klTRP1* Deletion confirmed by colony PCR.	This study
SGY054-1	ESM356 Spc110-sfGFP-kan6MX Tub1-mCherry-URA3 Bud14-6HA-hphNT. Verified by western blotting.	This study
SGY057-1	ESM356 *bud14*Δ*::klTRP1* mCherry-Tub1-URA3.	
SGY058-1	ESM356 *bud14*Δ*::klTRP1* mCherry-Tub1-URA3 Sfi1-sfGFP-kan6MX.	This study
SGY064-1	ESM356 Spc29-sfGFP-kan6MX *bud14*Δ*::klTRP1* pRS405-BUD14-LEU.	This study
SGY65-1	ESM356 Spc97-sfGFP-kan6MX *bud14*Δ*::klTRP1* pRS405-BUD14-LEU.	This study
SGY066-1	ESM356 Spc97-sfGFP-kan6MX *bud14*Δ*::klTRP1* pRS405-BUD14-F379A-LEU.	This study
SGY067-1	ESM356 Nud1-sfGFP-kan6MX *bud14*Δ*::klTRP1* strain is transformed with HpaI linearized pRS405.	This study
SGY070-1	ESM356 Spc72-sfGFP-kan6MX *bud14*Δ*::klTRP1* strain is transformed with HpaI linearized pRS405.	This study
SGY073-1	YPH499 Spc72-sfGFP-kan6MX.	This study
SGY074-1	YPH499 *bud14*Δ*::klTRP3* Spc72-sfGFP-kan6MX.	This study
SGY075-1	YPH499 cdc14-2 pUG120 (CDC14-pRS316)) *bud14*Δ*::klTRP3*) Spc72-sfGFP-kan6MX. It has been plated on YPD for 2 days at 23 degrees. Then it has been plated onto FOA and then incubated at 23 degrees for 3 days.	This study
SGY080-1	ESM356 Spc29-sfGFP-kan6MX *bud14*Δ*::klTRP1* pRS405-BUD14-LEU.	This study
SGY086-1	GPY491-1 Spc72-sfGFP-kan6MX.	This study
SGY087-1	ESM356 *kel1*Δ*::HIS6X*. Verified by colony PCR and chromosomal DNA PCR.	This study
SGY099-1	SGY087-1 *kel2*Δ (backbone is pKS133). Verified by colony PCR.	This study

SGY113-1	SGY057 pRS405-BUD14-LEU Spc110-sfGFP-kan6MX.	This study
SGY114-1	SGY057 pRS405-BUD14F379A-LEU Spc110-sfGFP-kan6MX.	This study
SGY115-1	SGY057-1 linearized pRS405 Spc42-sfGFP-kan6MX.	This study
SGY117-1	SGY057-1 pRS405-BUD14-LEU.	This study
SGY118-1	SGY057-1 pRS405-BUD14-LEU Spc72-sfGFP-kan6MX.	This study
SGY119-1	SGY057 pRS405-BUD14F379A-LEU Spc42-sfGFP-kan6MX	This study
SGY120-1	SGY071-1 is transformed with cut Sic1 plasmid (stable version). Plates are grown at 23 degrees. Verification done by plating them on YP-Raf/Gal plate. The ones who are not grown picked and frozen. + control used to compare growth on YP-Raf/Gal plates.	This study
SGY121-1	SGY073-1 is transformed with cut Sic1 plasmid (stable version). Plates are grown at 23 degrees. Verification done by plating them on YP-Raf/Gal plate. The ones who are not grown picked and frozen. + control used to compare growth on YP-Raf/Gal plates.	This study
SGY122-1	SGY075-1 is transformed with cut Sic1 plasmid (stable version). Plates are grown at 23 degrees. Verification done by plating them on YP-Raf/Gal plate. The ones who are not grown picked and frozen. + control used to compare growth on YP-Raf/Gal plates.	This study
SGY123-1	SGY086-1(#3201) is transformed with cut Sic1 plasmid (stable version). Plates are grown at 23 degrees. Verification done by plating them on YP-Raf/Gal plate. The ones who are not grown picked	This study

	and frozen. + control used to compare growth on YP-Raf/Gal plates.	
SGY124-1	SGY057 pRS405-BUD14F379A-LEU.	This study
SGY125-1	ESM356 GFP-Tub1-Ura.	This study
SGY126-1	ESM356 *bud14*Δ*::klTRP1* GFP-Tub1-Ura.	This study
SGY127-1	SGY124-2 Nud1-sfGFP-kan6MX. Verification was done by microscopy.	This study
SGY132-1	HAY48-2 Spc72-mCherry-natNT2. Verified by microscopy.	This study
SGY133-1	DKY173 Spc72-mCherry-natNT2. Verified by microscopy.	This study
SGY139-1	GPY491-1 Spc110-sfGFP-kan6MX.	This study
SGY140-1	DKY057-1 Spc110-sfGFP-kan6MX.	This study
SGY141-1	HAY48-2 Spc110-mCherry-natNT2. Verified by microscopy.	This study
SGY142-1	DKY173-1 Spc110-mCherry-natNT2. Verified by microscopy.	This study
SGY143-1	SGY057 pRS405-BUD14-LEU Nud1-sfGFP-kan6MX. Bud14 levels are verified by Western Blot.	This study
SGY144-1	SGY124-1 Spc72-sfGFP-kan6MX. Verified by fluorescence imaging.	This study
SGY146-1	HKY148-1 Swe1-GFP-HIS6X. Verified by microscopy.	This study
SGY147-1	HKY149-1 is transformed with Cdc28-GFP-HIS6X. Verified by microscopy.	This study
SGY149-1	ESM356 Spc42-6HA-hphNT1.	This study
SGY150-1	ESM356 Spc110-6HA-hphNT1.	This study
SGY151-1	ESM356 *bud14*Δ*::klTRP1* Spc110-6HA-hphNT1.	This study
SGY152-1	HKY148-1 Spc110-mCherry-natNT2.	This study
SGY145-1	HKY148 Cdc28-GFP-HIS6X	
SGY153-1	SGY145-1 Spc110-mCherry-natNT2.	This study
SGY154-1	HKY149-1 Spc110-mCherry-natNT2.	This study

SGY155-1	SGY147-1 Spc110-mCherry-natNT2.	This study
SGY158-1	SGY145-1 Spc72-mCherry-natNT2.	This study
SGY159-1	SGY132 Cdc14-GFP-klTRP1.	This study
SGY160-1	SGY132 Cdc28-GFP-klTRP1.	This study
HKY148-1	ESM356 Nud1-GBP-kITRP1 (After Bud14-GFP transformation, it was confirmed).	This study
HKY149-1	ESM356 72-GBP-kITRP1 (After Bud14-GFP transformation, it was confirmed).	This study
AKY4044-1	ESM356 SPC72-6HA-klTRP1. Confirmed by WB. Band runs above 75 kDa with hypershift.	
AKY4045-1	DKY068 (ESM356 bud14Δ::HIS) SPC72-6HA-klTRP1. Confirmed by WB. Band runs about 100 with hypershift.	
AKY4042-1	ESM356 NUD1-6HA-klTRP1. Confirmed by WB. Band runs about 100 with hypershift.	
AKY4043-1	DKY068 (ESM356 *bud14Δ::HIS*) NUD1-6HA-klTRP1. Confirmed by WB. Band runs above 100 kDa with hypershift.	

6.2 Table of Primers

Table 6.2: Name and sequences of the primers employed by this thesis are listed.

Primer Name	**Primer Sequence**
Bud14-T-rv	CTGACTCGAGCTTGCAAGGAAGAGGTCATC
Bud14-P-fw	GATCAGATCTCCAACCGTCTTACCTCAAAG
Bud14-col2-fow A	CACGACTAAGTAGTTGTCG
Bud14-col1 rev	GCAAGAGTCAGACTGACTCG
Bud14-S1	GTGAAATACACGTAGTTTTTAGATAACATTCTCTGCTTGGT AAGAGAATGCGTACGCTGCAGGTCGAC
Bud14-S2	AAGTTCGTTGGATGAGAAAAAGACCAGGCTTTATTGTAAG GACAATATCAATCGATGAATTCGAGCTCG

Bud14-S3	TTGACAGAATGGATGTGTTGATGAAACAATTGGATGAAATTATTCGTAAACGTACGCTGCAGGTCGAC
Bud14-S4	TCCTTGACACCACTTGCGGAAGTCTCATCAACATGCTCTTCCTTATTACTCATCGATGAATTCTCTGTCG
Bud14-F379A-rev	ACCGACAACATCATTGGCACTAACAGATTTGTT
Bud14-F379A-fw	AACAAATCTGTTAGTGCCAATGATGTTGTCGGT
Spc110 new S2	GTCGATGTACATACGAGAAATATGATGATAGAGTAAGCGATACTAATCGATGAATTCGAGCTCGTT
Spc110 new S3	ATACTAAGAGATAGAATTGAGAGTAGCAGCGGGCGTATATCTTGGCGTACGCTGCAGGTCGACGG
Spc29-S2	TAGTTTTAGTTACGATTATGCTGGTATTATTTAGTTAAGTACTTAATTCAATCGATGAATTCGAGCTCG
Spc29-S3	ATGAAAGTACGGAGGATATACTAAAAATATTGTCTTCGTCTTTTCACAATCGTACGCTGCAGGTCGAC
Spc72-S2	GTGACTGAGTGTTACATTAAATATATTTATATATAAACGTATGATATTTAATCGATGAATTCGAGCTCG
Spc72-S3	GAAAATGAGTCATTGAGATCGAAACTTTTCAACCTATCAATCAACAATCCCCGTACGCTGCAGGTCGAC
Spc97-S2	CCACTTTCCGCAAGTTGGTGCACGTCGTTAGTGACATAACGCCGCGTTCAATCGATGAATTCGAGCTCG
Spc97-S3	TTCTTTACTCTATAGTACCTCCTCGCTCAGCATCTGCTTCTTCCCAAAGACGTACGCTGCAGGTCGAC
Spc42-S2	AGAACGCTTTAAGAATGCGCCATACTCCTTAACTGCTTTTTAAATCATCAATCGATGAATTCGAGCTCG
Spc42-S3	CTGAAAATAATATGTCAGAAACATTCGCAACTCCCACTCCCAATAATCGACGTACGCTGCAGGTCGAC
Nud1-S2	ACTAATTACATACATTTTTAGTACTGCGTACGGGTATAGTTATGGGGTTAATCGATGAATTCGAGCTCG
Nud1-S3	TGGCGACCCTCTGGTTAGATGACACTCCTGCCCCAACTGCCACGAATCTGCGTACGCTGCAGGTCGAC
Sfi1-S2	GGTTACGACTACATATGCACACATACATACGTACATAATATATATATCTAATCGATGAATTCGAGCTCG

Sfi1-S3	TGGATTATATAAGAGAGCATGATAAATCCCCGTTAAGTCGT AAACGTCAACGTACGCTGCAGGTCGAC
CDC14-S2	TAAGTTTTTTTATTATATGATATATATATATATATAAAAATGAAAT AAATTAATCGATGAATTCGAGCTCG
CDC14-S3	CTACAAGCGCCGCCGGTGGTATAAGAAAAATAAGTGGCTC CATCAAGAAACGTACGCTGCAGGTCGAC
CDC28-S2	ACAGTGCAGTAGCATTTGTAATATAATAGCGAAATAGATTAT AATGCTTAATCGATGAATTCGAGCTCG
CDC28-S3	ACCGGATTAGCGCCAGAAGAGCAGCCATCCACCCCTACTT CCAAGAATCACGTACGCTGCAGGTCGAC
Swe1-S2	TGTGGGAAAAAGTATGTAAATAAAACAAGGTTTTTGTTCC ATTTATCAATCGATGAATTCGAGCTCG
Swe1-S3	GTGCTATTATCCAGGAAGACGACTTTGGACCTAAGCCAAA ATTTTTTATACGTACGCTGCAGGTCGAC
Mps1-S3	5'- TCAATGATGTGGTAGACACTGTTTTAAGGAAATTTGCAGAT TACAAAATTCGTACGCTGCAGGTCGAC-3'
Mps1-S2	5'- ATTTATGTTCATAACTGGCACATGCTTTTCTTCCTTATGCGG CTCTTCTAATCGATGAATTCGAGCTCG-3'

6.3 Table of Plasmids

Table 6.3: Utilized plasmids in this research are listed.

Plasmid Name	Description	Reference
pBLa	pFA6a-sfGFP-KanMX	
pBK002-1	GBP-klTRP1. GBP (GFP binding protein) from BamHI and BssHII digested pHA29 is subcloned into BamhI and BssHII digested pYM26.	From K. Nasmyth

	Tested by control digestion with BamHI and BssHII.	
pYM16	6HA-hphNT1.	From M. Knop.
pAK011	pRS306-mCherry-TUB1. NotI/KpnI mCherry-TUB1 fragment from pAK010-1 was subcloned in NotI/KpnI pRS306. Digest with ApaI for integration into URA3 locus.	From Khmelinskii et al., 2007.
pAFS125-GFP-TUB1	pAFS125-GFP-TUB1. URA3; TUB1 promoter-GFP-TUB1. Integration plasmid. Cut with StuI in URA3 to integrate.	From A. Murray.
pD361	Yiplac211-Gal1-SIC1T5V, T33V, S76A-HA. URA3-based integration plasmid with SIC1-HA triple mutant (V5, V33, A76) behind the Gal1 promoter. Cut with EcoRV to integrate at the URA3 locus. Most stabilized version.	From E. Schwob.
pSMG02-1	*BUD14* is amplified by Bud14-P-fw and Bud14-T-rv then cut by XhoI and BglII. Backbone pRS405 cut with BamHI and XhoI. After ligation rxn, isolated plasmid confirmed by PCR with Bud14-P-fw and Bud14-T-rv. Furthermore, confirmed	This study.

	plasmids cut with XhoI and StuI. Functionality established by SPOC analysis.	
pSMG06-1	pSMG02-1 is manipulated by site directed mutagenesis PCR to introduce aminoacid substitution on 379 aa where phenylalanine converted into alanine. With this subsitution Bud14 protein will not be able to bind Glc7. Verification is done by sequencing with 2 different primer sets.	This study.

6.4 Table of Buffers, Reagents and Chemicals

Table 6.4: Table lists all the reagents, chemicals and buffers used in this thesis.

Name	Description
TY agar with selective antibiotics (Ampicillin or Kanamycin)	5 g of NaCl (Merck, #106498), 5 g of Yeast Extract (Conda, #1702), 10 g of Tryptone (Biolife, #4122902), 20 g of Agar (Carl Roth, #5210.2), ddH2O up to 1000 mL. 100 µg/mL Ampicillin or 50 Kanamycin µg/mL
10X PCR Buffer	500mM Tris-HCl pH: 9.2 (Sigma, #T1503), 160mM (NH4)2SO4,

	17.5mM MgCl2 (Fisher BioReagents, #BP214)
1X Blotting Buffer	25mM Tris, 190mM Glycine (AppliChem, #A1067), 0.025% SDS (Sigma, #75746), 20% methanol (Sigma, #32213)
1X PBS	137mM NaCl, 2.7mM KCl (Merck, #104936), 10mM Na2HPO4 (Merck, #106575), 1.76mM KH2PO4 (Fisher BioReagents, #BP362). Adjust pH to 7.2-7.4
1X PBS-T	137mM NaCl, 2.7mM KCl, 10mM Na2HPO4, 1.76mM KH2PO4. Adjust pH to 7.2-7.4 and add Tween-20 in final concentration of 0.02% (AppliChem, #A4974)
1X TAE Buffer	4.84 g of Tris, 1.14 mL of Glacial acetic acid (Isolab, #901016), 2 mL of 0.5M EDTA pH:8.0 (Sigma, #E5134), ddH2O up to 1000 mL.
2mM dNTPs mix	20 µL of dATP (100 mM), 20 µL dCTP (100 mM), 20 µL dTTP (100

	mM) and 20 µL dGTP (100 mM), 920 µL ddH2O
P1 Buffer	50mM Tris-HCl pH:8.0, 10mM EDTA pH 8.0, 0.1 mg/mL RNase A
P2 Buffer	200mM NaOH, 1% SDS
P3 Buffer	3M KAc pH: 5.5
Ponceau S	0.2% (w/w) Ponceau S (Sigma #P3504) 3% (w/w) TCA in ddH2O
LiSORB	100mM Lithium Acetate (LiOAc), 10mM Tris pH: 8.0, 1mM EDTA pH: 8.0, 1M Sorbitol (Merck, #107758), ddH2O to complete the desired volume. Filter sterilized.
LiPEG	100mM LiOAc (Sigma, #L6883), 10mM Tris pH: 8.0, 1mM EDTA pH 8.0, 40% PEG3350 (Sigma, #P4338) ddH2O to complete the desired volume. Filter sterilized.
HU-DTT	8M Urea (MP Biomedicals, #823048), 5% SDS, 200mM Tris- HCl pH: 6.8, 0.1mM EDTA, Bromophenol blue,

	100mM 15 mg/mL DTT (Fisher BioReagnets, #BP172)
Homemade ECL Solutions	Solution 1: 20 mL of 1M Tris-HCl pH: 8.5, 2 mL of 250mM Luminol (in DMSO, Sigma # A-8511), 889 µL of 90mM p-Coumaric acid (in DMSO, Sigma # C-9008), 178 mL of ddH2O Solution 2: 20 mL of 1M Tris-HCl pH: 8.5, 180 mL of ddH2O, 123 µL of 30% Hydrogen peroxide (H2O2, Sigma # H-1009)
SC-X (X= URA, LEU, HIS or TRP)	3.4 g of Bacto Yeast Nitrogen Base (YNB) without amino acids with ammonium sulfate, 1 g of SC-X dropout amino acid mix, 10 g of D-(+)-Glucose, 0.05 g of Adenine hemisulfate salt (Sigma # A9126), ddH2O up to 500 mL
TY agar	5 g of NaCl, 5 g of Yeast Extract, 10 g of Tryptone, 20 g of Agar, ddH2O up to 1000 mL

YPAD	5 g of Yeast Extract, 10 g of Peptone (Conda, #1616), 10 g of D- (+)-Glucose, 0.05 g of Adenine hemisulfate salt, ddH2O up to 500 mL
YPD with selective antibiotics (Geneticin, Nourseothricin, or Hygromycin)	10 g of Yeast Extract, 20 g of Peptone, 20 g of D-(+)-Glucose, 20 g of Agar, ddH2O up to 1000 mL. 200 mg/L G418, 100 mg/L Nourseothricin or 300 mg/L Hygromycin in autoclaved agar
YPAD for nocodazole arres	5 g of Yeast Extract, 10 g of Peptone (Thermo, #211820), 10 g of D-(+)-Glucose, 0.05 g of Adenine hemisulfate salt, ddH2O up to 500 mL
TY medium	5 g of NaCl, 5 g of Yeast Extract, 10 g of Tryptone, ddH2O up to 1000 mL
TY medium with selective antibiotics (Ampicillin or Kanamycin)	5 g of NaCl, 5 g of Yeast Extract, 10 g of Tryptone, ddH2O up to 1000 mL. 100 µg/mL Ampicillin or 50 Kanamycin µg/mL